CAPITAL UNIVERSITY OF SCIENCE AND TECHNOLOGY, ISLAMABAD

Coverage Analysis of Dense Heterogeneous Cellular Networks using Dual-Slope Path Loss Model

by

Khurram Shehzad

A thesis submitted in partial fulfillment for the degree of Doctor of Philosophy

in the

Faculty of Engineering
Department of Electrical Engineering

2021

Coverage Analysis of Dense Heterogeneous Cellular Networks using Dual-Slope Path Loss Model

By

Khurram Shehzad

(PE141001)

Dr. Rodica Ramer, Professor

University of New South Wales, NSW, Australia

Foreign Evaluator 1

Dr. Raziq Yaqoob, Associate Professor

Alabama Agriculture & Mech University, USA

Foreign Evaluator 2

Dr. Noor Muhammad Khan

(Thesis Supervisor)

Dr. Noor Muhammad Khan

(Head, Department of Electrical Engineering)

Dr. Imtiaz Ahmed Taj

(Dean, Faculty of Engineering)

DEPARTMENT OF ELECTRICAL ENGINEERING

CAPITAL UNIVERSITY OF SCIENCE AND TECHNOLOGY

ISLAMABAD

2021

I dedicate this thesis to my family.

CAPITAL UNIVERSITY OF SCIENCE & TECHNOLOGY ISLAMABAD

Expressway, Kahuta Road, Zone-V, Islamabad
Phone:+92-51-111-555-666 Fax: +92-51-4486705
Email: info@cust.edu.pk Website: https://www.cust.edu.pk

CERTIFICATE OF APPROVAL

This is to certify that the research work presented in the thesis, entitled "**Coverage Analysis of Dense Heterogeneous Cellular Networks using Dual-Slope Path Loss Model**" was conducted under the supervision of **Dr. Noor Muhammad Khan**. No part of this thesis has been submitted anywhere else for any other degree. This thesis is submitted to the **Department of Electrical Engineering, Capital University of Science and Technology** in partial fulfillment of the requirements for the degree of Doctor in Philosophy in the field of **Electrical Engineering.** The open defence of the thesis was conducted on **August 05, 2021.**

Student Name : Khurram Shehzad (PE-141001)

The Examination Committee unanimously agrees to award PhD degree in the mentioned field.

Examination Committee :

(a) External Examiner 1: Dr. Adeel Akram
Professor
UET, Taxila

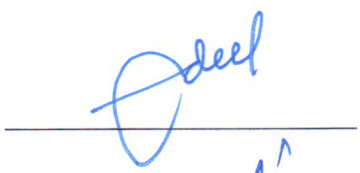

(b) External Examiner 2: Dr. Zia ul Haq Abbas
Associate Professor
GIKI, Topi, Swabi, KPK

(c) Internal Examiner : Dr. Imtiaz Ahmad Taj
Professor
CUST, Islamabad

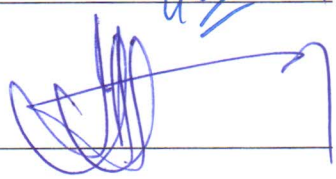

Supervisor Name : Dr. Noor Muhammad Khan
Professor
CUST, Islamabad

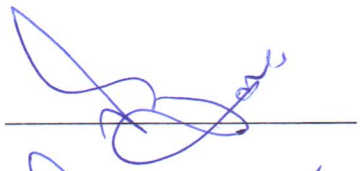

Name of HoD : Dr. Noor Muhammad Khan
Professor
CUST, Islamabad

Name of Dean : Dr. Imtiaz Ahmad Taj
Professor
CUST, Islamabad

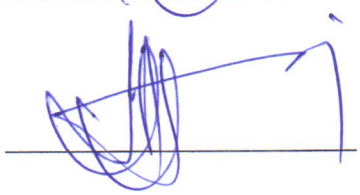

AUTHOR'S DECLARATION

I, **Khurram Shehzad (Registration No. PE-141001)**, hereby state that my PhD thesis titled, "**Coverage Analysis of Dense Heterogeneous Cellular Networks using Dual-Slope Path Loss Model**" is my own work and has not been submitted previously by me for taking any degree from Capital University of Science and Technology, Islamabad or anywhere else in the country/ world.

At any time, if my statement is found to be incorrect even after my graduation, the University has the right to withdraw my PhD Degree.

(**Khurram Shehzad**)

Dated: August, 2021

Registration No : PE-141001

PLAGIARISM UNDERTAKING

I solemnly declare that research work presented in the thesis titled "**Coverage Analysis of Dense Heterogeneous Cellular Networks using Dual-Slope Path Loss Model**" is solely my research work with no significant contribution from any other person. Small contribution/ help wherever taken has been duly acknowledged and that complete thesis has been written by me.

I understand the zero tolerance policy of the HEC and Capital University of Science and Technology towards plagiarism. Therefore, I as an author of the above titled thesis declare that no portion of my thesis has been plagiarized and any material used as reference is properly referred/ cited.

I undertake that if I am found guilty of any formal plagiarism in the above titled thesis even after award of PhD Degree, the University reserves the right to withdraw/ revoke my PhD degree and that HEC and the University have the right to publish my name on the HEC/ University Website on which names of students are placed who submitted plagiarized thesis.

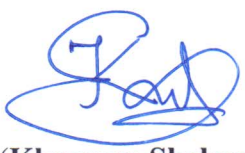

(**Khurram Shehzad**)

Dated: August, 2021

Registration No : PE-141001

List of Publications

It is certified that following publication(s) have been made out of the research work that has been carried out for this thesis:-

1. **K. Shehzad**, N. M. Khan, and J. Ahmed, "Impact of frequency reuse and flexible cell association on the performance of dense heterogeneous cellular networks using dual-slope path loss model," *IEEE Access*, vol. 7, pp. 166214-166234, 2019.

2. **K. Shehzad**, N. M. Khan, and J. Ahmed, "Performance analysis of coverage-centric heterogeneous cellular networks using dual-slope path loss model," *Computer Networks*, vol. 185, pp. 107672, 2020.

Khurram Shehzad
(PE141001)

Acknowledgement

In the name of Allah, The Most Gracious, The Most Merciful. Firstly, I thank Allah SWT for granting me with the opportunity, strength, and perseverance to pursue my doctoral studies. I also extend my deepest greetings to the Holy Prophet Muhammad (PBUH), the last messenger of Allah SWT, whose life is the perfect model for all humans and whose teachings are the source of guidance in all disciplines of life.

I am indebted to all of my teachers whose teachings have brought me to this stage. I am highly grateful to my PhD supervisor, Prof. Dr. Noor M Khan, for his unending support and thorough guidance throughout my degree program. His kind efforts contributed greatly to my knowledge, understanding, and enthusiasm for this research. I have not only learned from his insight, deep technical knowledge, and practical experience, but a lot of things from him as a person as well. It has been a real honor for me to work under his supervision and to attend his lectures and talks. I would also like to express my gratitude to Dr. Junaid Ahmed for his valuable guidance, and suggestions, which he was always ready to offer. His constructive comments and suggestions throughout my research phase helped a lot in the completion of my research work. I am sincerely grateful to Dr. Syed Safwan Khalid for being a friend and a mentor. He always appreciated me and encouraged me which in turn kept me motivated throughout the research work. I am thankful to Dr. M. Mansoor Ahmed and Dr. Fazal-ur-Rehman for giving me the opportunity to present my research work in their research groups. I am grateful to my office colleagues and friends whose valuable company always kept me focused and motivated. Especially, I recognize the valuable support from Mr. Syed Bilal Javed, Mr. Noman Riaz, Dr. Rizwan Azam, and Dr. Ali Arshad.

Last, but not the least, I wish to thank my family, whom I always took for granted but they have always stood by my side and supported me through the good and bad times. It is to them that I owe my success in life. My sincerest acknowledgments go to my proud parents whose prayers and best wishes were always with me. I am also thankful to them for inculcating in me the values responsible for making me

the person, I am today. I am thankful to my wife for supporting me during odd times and compromising on family life due to my PhD. Moreover, I am thankful to my siblings for their constant support and encouragement throughout my graduate studies. I am grateful to my kids Salaar and Muaaz for keeping me cheerful and refreshed during my studies.

Khurram Shehzad

Abstract

Densifying the cellular networks has been largely considered as a promising solution in meeting the capacity demands of emerging cellular networks that have expeditiously transformed from voice-oriented to data-oriented. Owing to the disparity in transmit power of the base station (BS) tiers, proactive offloading of users is extensively required to ensure a balance in the user load amongst different BS tiers. Meanwhile, it is equally essential to utilize efficient interference management schemes to account for the excessively-increasing interference in the densely deployed cellular networks. There is extensive literature available on the performance analysis of dense multi-tier networks that undertake various load-balancing and interference management mechanisms, but it is strictly limited to the usage of the single-slope (SS) path loss model (PLM). Nonetheless, it is also well-known in the literature that the usage of SS-PLM leads to inaccuracies in evaluating the performance of dense networks. Therefore, the primary objective of this research is to use dual-slope (DS)-PLM in analyzing the downlink performance of dense heterogeneous cellular networks (HCNs) and investigate its impact on the utility/pitfall of the commonly employed load balancing and interference management strategies.

In the first part of the thesis, the downlink performance of uniformly distributed two-tier HCNs is analyzed while jointly considering the load balancing and interference management mechanisms. The adopted load balancing strategy is based on the range extension of small BSs (SBSs), whereas a simple interference management scheme based on the static frequency reuse mechanism is considered. Analytical expressions for the tier association and coverage probability are derived for a randomly chosen user using the tools from stochastic geometry and validated through the Monte Carlo simulations. Owing to the better accuracy of DS-PLM in estimating the path loss in dense deployment scenarios, the results obtained precisely demonstrate the benefits and detriments of densifying SBSs, while employing the load balancing and interference management mechanisms. Meanwhile, a thorough comparison of the evaluated network performance using

both SS-PLM and DS-PLM is also performed for the tier association and network coverage probabilities. The comparative analysis verifies the limitation of SS-PLM in dense cellular network scenarios. For instance, it is observed that the usage of SS-PLM not only overestimates the user offloading to smaller BS tier, but it also results in the overestimation of network coverage.

In a two-tier uniform HCN with BSs having disparity in transmit powers, deployed densities and critical distances, the SBSs located in the immediate vicinity of macro BSs (MBSs) have negligible coverage areas and therefore act as the strong interference sources and cause degradation of the network coverage. This shortcoming of the uniform HCNs is addressed in the second part of the thesis, where deactivation of the SBSs located in the near vicinity of MBSs is proposed. This selective muting of SBSs introduces a partial spatial correlation between the BS locations of both tiers that transforms the network into a non-uniform HCN. This network transformation ensures that the macro associated users within the near proximity of cell-center region of their respective MBSs experience reduced inter-tier interference. In order to further enhance the performance of these non-uniform HCNs, the above-mentioned load balancing and interference abating strategies are jointly adopted as well. Using stochastic geometry, the mathematical expressions for tier association and coverage probability are derived for a randomly chosen user and validated through the Monte Carlo simulations. A comparison of the estimated network performance using both SS-PLM and DS-PLM is also carried out for the above-mentioned performance metrics. The results highlight that the usage of SS-PLM causes underestimation of the benefits associated with SBS densification, load balancing and interference management in non-uniform HCNs.

The research work thus concludes that the choice of PLM greatly impacts the performance prediction of the dense cellular networks and leads to valuable design insights that are vital in determining the optimal parametric values for cellular planning.

Contents

List of Figures

List of Tables

Abbreviations

3GPP	Third Generation Partnership Project
ASAPPP	Approximate SIR analysis based on the Poisson point process
bps	bits per second
BS	Base station
CCDF	Complementary cumulative distribution function
CDF	Cumulative distribution function
CoMP	Coordinated multipoint
CRE	Cell range extension
DS	Dual-slope
DUDe	Decoupled uplink downlink access
FBS	Femto base station
HCN	Heterogeneous cellular network
iid	Independent and identically distributed
LTE	Long-term evolution
LTE-A	Long-term evolution-Advanced
MBS	Macro base station
MIMO	Multiple-input multiple-output
mm-wave	Millimeter wave
NuHCN	Non-uniform HCN
PBS	Pico base station
PDF	Probability distribution function
PGFL	Probability generating functional
PLM	Path loss model
PLE	Path loss exponent

PPP	Poisson point process
RATs	Radio access technologies
SBS	Small base station
SS	Single-slope
SINR	Signal to interference plus noise ratio
T-UE	Typical User equipment
UE	User equipment
UE-AS	User equipment association strategy
WiMAX	Worldwide Interoperability for Microwave Access

Symbols

ϕ_M, ϕ_S, ϕ_{UE}	PPPs of MBSs, SBSs and UEs
α_0, α_1	Pre-critical and post-critical PLEs
B_S, B_M	SBS and MBS biasing factor
λ_S, λ_M, λ_{UE}	SBS, MBS and UE densities
P_M, P_S	Transmit powers of MBSs and SBSs
${P_r}^M$	Received power from the nearest MBS
${P_r}^S$	Received power from the nearest SBS
R_{C_M}	Macro tier critical distance
R_{C_S}	Small tier critical distance
η_M, η_S	Continuity constants
x_0, L_0	Reference distance and its path-loss
τ	SINR threshold
σ^2	Noise power
N	Frequency reuse factor
h_X	Rayleigh fading gain
$l(x_i)$	Generic path loss
Γ	Instantaneous received SINR
ϖ, ϱ, ς, υ	Likelihood of association regions R-I, R-II, R-III, R-IV
X_M, X_S	T-UE distance from MBS and SBS
$f_{X_M}(x_M)$, $f_{X_S}(x_S)$	PDF of the T-UE distance from the MBSs and SBSs
$f_{X_M\|X_M>R_{CM}}(x_M)$, $f_{X_M\|X_M<R_{CM}}(x_M)$	PDF of T-UE distance $> R_{CM}$

	and $< R_{CM}$ from the serving MBS
$f_{X_S \mid X_S > R_{CS}}(x_S)$, $f_{X_S \mid X_S < R_{CS}}(x_S)$	PDF of the T-UE distance $> R_{CS}$
	and $< R_{CS}$ from the serving SBS
$\mathcal{A}_{\mathcal{M}}$, $\mathcal{A}_{\mathcal{S}}$	Total macro and small T-AP
$\mathcal{A}_{\mathcal{M},\mathcal{R}-\mathcal{I}}$ to $\mathcal{A}_{\mathcal{M},\mathcal{R}-\mathcal{IV}}$	Joint macro T-AP in R-I to R-IV
$\mathcal{A}_{\mathcal{S},\mathcal{R}-\mathcal{I}}$ to $\mathcal{A}_{\mathcal{S},\mathcal{R}-\mathcal{IV}}$	Joint small T-AP in R-I to R-IV
$\mathbb{P}[\Gamma_{X_M \mid X_M > R_{CM}}(x_M) > \tau]$	CCDF conditioned on $X_M > R_{CM}$
$\mathbb{P}[\Gamma_{X_M \mid X_M < R_{CM}}(x_M) > \tau]$	CCDF conditioned on $X_M < R_{CM}$
$\mathbb{P}[\Gamma_{X_S \mid X_S > R_{CS}}(x_S) > \tau]$	CCDF conditioned on $X_S > R_{CS}$
$\mathbb{P}[\Gamma_{X_S \mid X_S < R_{CS}}(x_S) > \tau]$	CCDF conditioned on $X_S < R_{CS}$
$\mathcal{L}_{\mathcal{I}_{\mathcal{M}}}$, $\mathcal{L}_{\mathcal{I}_{\mathcal{S}}}$	Laplace transform of interference
	from MBSs and SBSs
$\mathrm{C_P}$	Network coverage probability
$\mathrm{C_{P_{M \mid X_M > R_{CM}}}}$	Macro coverage for distances $> R_{CM}$
$\mathrm{C_{P_{M \mid X_M < R_{CM}}}}$	Macro coverage for distances $< R_{CM}$
$\mathrm{C_{P_{S \mid X_S > R_{CS}}}}$	Small coverage for distances $> R_{CS}$
$\mathrm{C_{P_{S \mid X_S < R_{CS}}}}$	Small coverage for distances $< R_{CS}$

Chapter 1

Introduction

This chapter introduces the thesis, provides the basic motivation for carrying out this research work and highlights its importance. The chapter is divided into seven sections. In section 1.1, a brief summary on the rapidly increasing mobile traffic demands is presented. The limited suitability of conventional cellular networks in handling the excessive data deluge is highlighted in section 1.2. Moreover, the commonly employed strategies to resolve the capacity crunch faced by cellular networks is also presented in the same section. A brief introduction on the theory of path loss modeling is presented in section 1.3. In section 1.4, the challenges commonly faced in the dense deployment of low power base stations in the already deployed macro based cellular networks are described. The research objectives are presented in section 1.5 while the organization of the rest of the thesis is described in section 1.6. Lastly, the concluding remarks on the contents covered in this chapter are presented in section 1.7.

1.1 Overview

The past decade has witnessed an exponential increase in mobile data traffic, owing primarily to the drastic rise in the demand for high-end devices that support numerous high data rate applications. According to the mobility report published by

Ericsson, the mobile data traffic is predicted to reach a mammoth 131 exabytes/-month by the year 2024, wherein the video traffic alone is expected to account for a significant 74% of the total traffic [1]. The report also predicts that by the end of year 2024, approximately 45% of world's population would be under 5G coverage while around 35% of data traffic would be carried by 5G networks. Interestingly, the cellular networks were originally designed for voice-oriented applications, but with the popularity of high-tech devices, the trend has clearly shifted towards data-hungry applications like high-definition video conferencing, telehealth, mobile television, interactive gaming, augmented/virtual reality and many others [2]. Hence, this two-pronged growth requires substantial increase not only in the peak data rates (bps) but also in data rate density (bps/km^2). Fig 1.1 illustrates the continual dominance of video traffic over other application categories as foreseen in [1].

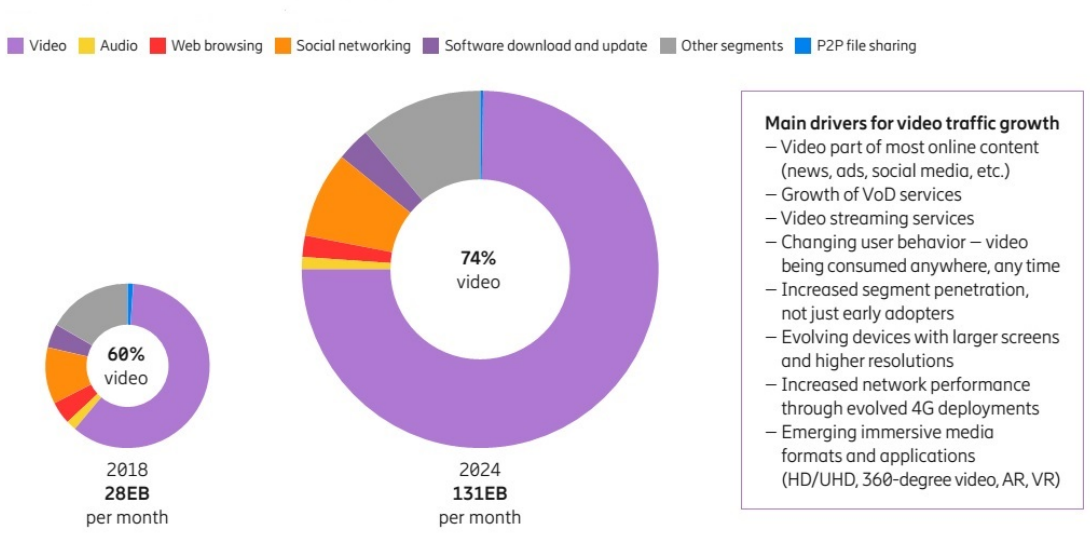

FIGURE 1.1: Video traffic dominating other application categories and the data traffic forecast (Ericsson Mobility Report, June 2019)

.

1.2 Cellular Networks and the Capacity Crunch

In order to meet the rapidly increasing traffic demands, the mobile cellular networks must realize the gains on the order of 1000 times increase in transmission

capacity [3]. The feasible options in achieving improved peak link rates include enhancing the spectrum efficiency, and/or utilizing larger bandwidths. Meanwhile, augmenting the data rate density requires aggressive reuse of the available spectrum within near-vicinity of user equipment (UE) by densifying the network infrastructures. Thus, it is getting progressively challenging for the traditional cellular networks in coping up with this drastic increase in the data demand, as the single base station (BS) tier based cellular networks have nearly reached their optimum capacity limits as governed by the principles of information theory [4]. Therefore, in order to support the traditional high power macro BSs (MBSs), the addition of economical and low-power BSs has been recommended by the Third Generation Partnership Project (3GPP) to be a viable solution in addressing this data deluge [5].

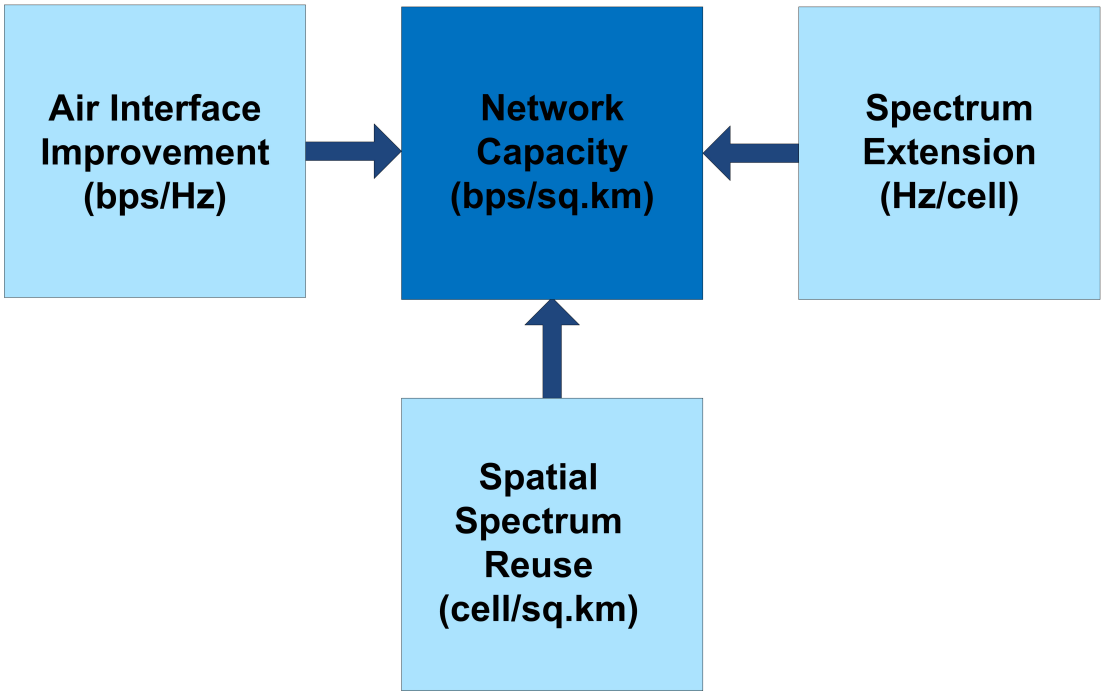

FIGURE 1.2: Possible paths leading to the network capacity improvements.

From year 1950 to 2000, the capacity of wireless networks has increased by a million fold and it has been primarily achieved through the reusing of available spectrum, while spectral efficiency improvements and the extension in spectrum have also played their parts [6]. However, as of now, employing better modulation and coding schemes offer a scanty improvement in the efficiency of wireless links.

This is because, these schemes have nearly reached their optimum capacity limits as governed by the principles of information theory [7, 8]. Similarly, multiple input multiple output (MIMO) systems which are used in the renowned wireless standards like WiMAX and LTE-A, also do not offer significant improvement in spectral efficiency owing to the limited number of antennas available at each BS [9]. Thus, these techniques do not meet the hallmark of increasing the network capacity by 1000×. Fig. 1.2 mentions the possible paths that have historically lead to improvements in the network capacity of cellular networks.

Nonetheless, massive MIMO offers a favorable solution as it has the capability of serving tens to hundreds of users concurrently in a single resource block by using hundreds or even thousands of antennas embedded on a single BS [10–13]. In order to pack a large number of antennas on a BS, their size needs to be as small as possible and the configuration of tiny antennas looks most suitable. Consequently, it has resulted in an increased interest in millimeter wave (mm-wave) based massive MIMO systems [14–17]. The mm-wave massive MIMO systems operate at 30-300 GHz frequency spectrum and due to the abundance availability, low-cost and no-congestion in that frequency range, it offers a unique opportunity to address the excessive data deluge [18, 19]. However, signal propagation characteristics in this extremely high frequency range are vastly different from the operational frequencies of current cellular networks; for instance, path loss, object diffraction and building blockage, atmospheric absorption, rain attenuation, and vegetation effects [20–23]. This variation in characteristics poses new challenges not only in the system design but also in the architectures of various hardware infrastructures involved [24–27].

The capacity offered by the conventional cellular networks is certainly not enough to meet the drastically increasing traffic demands. Hence, in order to meet such a momentous target, it is necessary to densify the deployed networks. Moreover, it is pertinent to mention that over the last two decades, the increase in cellular networks capacity has largely been achieved by reducing the cell sizes and reusing the available spectrum efficiently. For instance, in 3G cellular networks, the MBSs were densified to ensure improved coverage and transmission rates in urban areas

while the density of MBSs was around 4-5 BSs/km^2 [28]. However, coping up with the increasing traffic requirements urged a much higher MBS densification, especially when compared with the era prior to smart-phone boom and penetration. Contrarily, densifying MBSs required prohibitively high deployment costs along with other limitations including the unavailability of cell-sites, and dedicated and faster backhaul in dense urban areas.

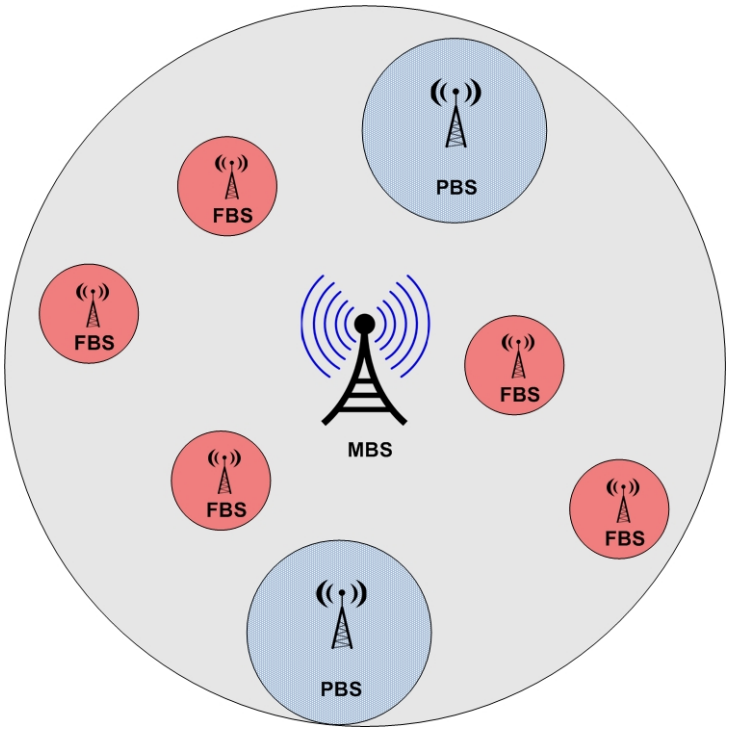

FIGURE 1.3: A Heterogeneous Cellular Network comprising of three BS tiers.

Keeping in view the limited feasibility of MBS densification, the popularity of low-powered BSs i.e., small cells (SBSs) erupted [29]. In contrast to the MBS densification, the SBSs are less costly and can be readily deployed to assist the macro-cellular network especially in highly dense urban areas to meet the desired data demands. It is for the same reason that 4G cellular networks, like LTE-A, deploy abundant SBSs to complement the MBSs in addressing the explosive data deluge [30, 31]. Hence, transforming the conventional cellular networks into dense and irregular networks, i.e., heterogeneous cellular networks (HCNs) [5]. Fig. 1.3 depicts a section of HCN coverage area, where multiple Pico BSs (PBSs) and Femto BSs (FBSs) are deployed in the surrounding area of a MBS. With the

assistance of SBSs (PBSs and FBSs), low coverage areas associated with MBSs can be eliminated and capacity can be improved in hot-spots. Furthermore, the relay BSs boost flexibility in backhaul especially in areas where the wired backhaul is either costly or unavailable [32]. Moreover, HCNs offer notable improvements in the overall network performance by coping up with intense data rate requirements using intelligent combination of technologies, network architectures, disparity in cell sizes, and/or frequency bands [4, 33].

1.3 Introduction of Path Loss Modeling

The wireless communication systems, over the past five decades, have traversed through five generations while supporting highly diverse applications ranging from voice-only to extremely data demanding. Hence, a wide range of frequency bands ranging from 800 MHz to 100 GHz has been allocated to account for the ever-growing data rate demands of the wireless systems [34]. With the widespread usage of high-end user devices capable of supporting numerous data-hungry applications, the data demand from the users to the service providers has significantly increased. Therefore, to accommodate these demands, the cellular operators are bound to improve the connectivity between the deployed network infrastructures and user devices. Meanwhile, it is important to mention here that the benefits associated with any radio communication system cannot be fully harvested without understanding the prorogation mechanisms of the radio waves through different environments. The wired channels are commonly assumed to be stationary and predictable; however, the wireless channels are extremely random and as a result they do not lead to easy analysis. The modeling of wireless channel plays an extremely vital role in the performance evaluation of any wireless communication system, as it permits the network planners to optimize the distribution of BSs, and set their transmit powers for achieving the desired service level requirements for a given environment profile or the frequency band [35]. Comprehensive surveys related to standardization and evolution of path loss models from 1G to 5G cellular networks are presented in [34] and the references therein.

Radio propagation models are commonly employed to characterize the attenuation experienced by the radio wave as it traverses through the wireless channel. Generally, the signal attenuation is a function of the operating frequency (carrier), heights of the BSs and UEs, nature of environment i.e., urban/suburban/rural, and the distance between the transmitting and receiving stations. The attenuation of the received signal due to the distance between BS and UE is termed as the path loss, and it is a large scale fading parameter. It has been reported in [36] that the average received power decays logarithmically with the distance in both indoor and outdoor environments, while the signal attenuation rate is further dictated by the path loss exponent (PLE). Meanwhile, it is well-known in the literature that the PLE value is sensitive to the environment profile, i.e., the value of the PLE increases when obstacles are present in the communicating path. This PLE is also termed as the slope of the decay rate of the signal strength in logarithmic scale. The simplest of the path loss models (PLMs) is the single-slope (SS) PLM, in which it is assumed that the received signal strength decays with a constant rate i.e., independent of the distance between transmitter and receiver stations. Contrarily, in case of the dual-slope (DS) PLM, the signal attenuates with two different rates separated by a critical or breakpoint distance. For example, if the distance between the communicating stations is smaller than the critical distance then the received signal attenuates with α_0 otherwise it falls-off with α_1, where both α_0 and α_1 are the far-field PLEs and $2{<}\alpha_0{\leq}\ \alpha_1$. Lastly, it is also well-known in the literature that the value of critical distance depends primarily on the heights of the communicating stations [37].

For a fixed link distance between the BS and UE, the fluctuations in the received signal strength due to the natural and man-made objects like mountains, buildings, forests, tunnels etcetera, are characterized by shadow fading which results in the degradation of signal strength of up to 10 dB around the mean value i.e., path loss. The shadow fading is further sensitive to the carrier frequency and the geometry of obstacles around the communicating stations. The PLMs are usually developed from large datasets that are collected from measurements in a particular environment, and hence their suitability is limited for those environments only.

1.4 Challenges in Dense HCNs

Traditionally, the conventional (homogeneous) networks involved only macro cells in which MBSs transmitted with equal power, while their locations were also planned. On average, this schematic strategy of regular placement and uniform power transmission not only restricted the inter-cell interference from affecting system performance but it also guaranteed a balanced load on all BSs [38]. Moreover, it was generally assumed in macro-cellular networks that the MBSs were positioned on a regular-grid and their performance was mostly analyzed by exhaustive Monté Carlo simulations. Contrarily, the ongoing evolution of cellular networks into dense and irregular networks have introduced multiple disparities, and as a result, it makes them significantly different from the macro-cellular networks. For instance, HCNs feature multiple BSs of varying cell sizes, transmission powers, backhaul capabilities, signal-to-interference plus noise ratio (SINR) thresholds, spatial densities, path loss exponents (PLEs) and carried traffic loads [32, 39]. Hence, the heterogeneity associated with these multi-tier cellular networks emphasize the need for revamping the conventional strategies of cellular planning and deployment.

Though deploying densified SBSs in support of MBSs has been one of the primary driving forces in meeting the staggering user demands [40, 41], but their consideration brings along new technical challenges as well that need special attention prior to the successful rollout and operation of HCNs. For instance, the possible challenges can be divided into these major categories: hardware expenses associated with new SBS deployments, utilization of radio resources, need for subtle user association strategies within the deployed BS tiers, management of interference, network topologies, coexistence with other radio access technologies (RATs) [42–45].

In addition to the above issues, it is equally important to employ suitable propagation path loss models (PLMs) as they play a pivotal role in the designing of cellular systems. For any given environment, the PLMs help in specifying important parameters such as transmit power of BSs, the antenna heights, location and

density of BSs, frequency etceteras. The PLMs dedicated for the macro-cellular systems were usually based on the antenna heights of the communicating stations and frequency, while building heights, orientation and width of the streets were the prime parameters in the PLMs of micro-cellular systems [35, 36]. The performance of cellular networks is greatly influenced by the choice of PLM because interference estimates are based directly on it, and a balance must be struck between financial feasibility and the quality of services offered [46, 47]. Hence, for designing a cellular system that comprises of BSs with disparate transmit powers and coverage areas, it is important to select an appropriate PLM.

This thesis is mainly focused on the interference management, load balancing between BS tiers and random deployments/positioning of SBSs in HCNs. The addition of SBSs in the overlaid macro-cellular network is like a *double-edged sword*, it brings the network resource in close proximity to UEs but the excessive interference also has a detrimental impact on the performance of dense HCNs. Moreover, it is the disparity in transmit powers of BS tiers which is the root-cause for the load imbalance between the BS tiers, as UEs mostly receive better signal strength from MBSs. Thus, it is of paramount importance to address this disparity of UEs association to avail maximum potential of these multi-tier HCNs. Similarly, due to random SBS deployments and transmit power disparity, the services received by cell-edge UEs could be well below the desired quality levels or those experienced by cell-center UEs. Thus, degrading the overall network capacity.

1.5 Research Objectives

With the increasing popularity and penetration of high-tech devices capable of supporting numerous data-hungry applications, the cellular networks are expeditiously transforming from voice-oriented to data-oriented. Hence, there is an urgent need to analyze the performance of these emerging wireless networks and devising strategies to increase their network capacity. Densifying SBSs is one of those strategies that is widely considered to be a promising solution in meeting

the intensive capacity demands. Although the distance between users and the deployed network decreases with the increasing SBS density, it also alters the regular/schematic geometry of BS distribution that is commonly associated with the macro-cellular networks. Consequently, highlighting the need for devising more dynamic network modeling strategies.

It is interesting to note that the performance analysis of dense HCNs mostly involves the usage of SS-PLM, which is generally well-suited for less dense and regular network deployment scenarios. Moreover, SS-PLM fails to precisely capture the dependence of PLE on the link distance in many practical deployment scenarios involving disparate link distances, e.g., dense cellular networks. Contrarily, the HCNs are bound to be more irregular due to the ad hoc and random deployment of SBSs. Hence, its usage can result in a significant difference in the values of average received and interference powers, and thus, may lead to incorrect estimation of the benefits/drawbacks associated with load balancing and interference management schemes. Therefore, the primary objective of this research is to use DS-PLM in analyzing the downlink performance of dense HCNs and investigate its impact on the utility/pitfall of the commonly employed load balancing and interference management strategies.

1.6 Thesis Organization

Chapter 2 begins with a detailed account of the work related to the modeling of cellular networks using stochastic geometry and the ease it brings in analyzing the performance of emerging cellular networks. A comprehensive literature survey on the performance analysis of uniform and non-uniform HCNs using stochastic geometry is also presented in this chapter which helps in identifying the research openings and formulation of the problem statement. The research methodology adopted in this thesis for analyzing the downlink coverage performance of dense HCNs is also described, while the chapter finally concludes with the contribution of thesis.

In chapter 3, DS-PLM is employed to study and analyze the downlink performance of a two-tier dense HCN with uniformly distributed BS tiers having disparity in transmit powers and infrastructure densities. Analytical expressions for the tier association and coverage probability are derived for a randomly chosen user using the tools from stochastic geometry and validated through simulations. Finally, with the help of numerical results, a thorough comparison of the estimated network performance using both SS-PLM and DS-PLM is also carried out. The comparative results highlight a critical limitation associated with the usage of SS-PLM in evaluating the network performance of densely deployed cellular networks.

Chapter 4 extends the work presented in chapter 3, wherein it was highlighted that DS-PLM is well-suited for analyzing the performance of dense HCNs owing to its better accuracy in estimating the strength of signals in disparate link distances. Moreover, it was noticed that the UEs mostly prefer associating with macro tier, whenever the distance between UE and its nearest MBS is smaller than the critical distance. Consequently, a correlation needs to be introduced between the positioning of MBSs and SBSs to better avail the potential of dense deployments of SBSs. Hence, a coverage-centric SBS deployment strategy i.e., muting the SBSs that exist at distances smaller than the critical distance from each MBS, is adopted in this chapter. In order to investigate the performance of non-uniform HCNs (NuHCNs) using DS-PLM, and for carrying out a thorough comparison, the estimated results for each of the performance metric using both SS-PLM and DS-PLM are compared as well.

Chapter 5 concludes the research work presented in this dissertation and suggests possible extensions of this research work.

1.7 Conclusion

The primary motivation for carrying out this research work has been presented in this chapter. Keeping in view the need for dense deployment of the network

infrastructures, the importance of selecting appropriate PLMs has also been highlighted in this chapter. Meanwhile, the challenges faced in the successful roll-out of the HCNs have been discussed as well.

Chapter 2

Literature Survey, Problem Formulation, and the Proposed Research Methodology

In this chapter, a comprehensive literature review of the works related to the acceptability of stochastic geometry modeling in cellular networks, and the performance analyses of uniform and non-uniform cellular networks are presented in section 2.1. The chapter also describes gap analysis and problem statement in sections 2.2 and 2.3 respectively. The proposed research methodology adopted in this thesis to address the identified problems is discussed in section 2.4. The thesis contributions are given in the section 2.5, while the concluding remarks on this chapter are given in section 2.6

2.1 Literature Survey

In order to provide readers with better visibility, the presented literature review is divided into three parts i.e., stochastic geometry and cellular networks, and the performance analyses of uniformly and non-uniformly distributed HCNs, which are presented in the subsequent subsections.

2.1.1 Stochastic Geometry and Cellular Networks

In the conventional cellular networks, the randomness associated with the positioning of MBSs was minimal, as the MBSs were positioned after careful planning on the basis of traffic density and/or coverage issues in the deployment area. However, the studies and designs of traditional cellular networks have inclined towards two extremes. For the sake of maintaining tractability during analysis, simpler models have been employed while complicated simulation based models have been used in the industry for gaining design insights. Numerous baseline models focusing on BS locations have been proposed in the literature to analyze the performance of cellular networks [48, 49]. However, given their simplicity which is additionally coupled with some unrealistic assumptions, analyzing the performance of conventional cellular networks using them is not suitable.

The derived SINR expression from the renowned hexagonal grid model for a simple MBS based cellular network is complicated and intractable. Thus, it requires numerical evaluation, which is equivalent to simulating the network deployment [48]. Similarly, the Wyner model suffers from the simplistic assumptions (i.e., fixed location of UEs, deterministic interference intensity, predefined channel gains between UEs and interfering BSs) which can result in an inaccurate estimation of the downlink performance especially in netwrok scenarios involving single or multiple strong interfering BSs [49]. In order to analyze such models, system-level simulations need to be performed which are not only extremely time consuming and error-prone but also require exhaustive repetitions to account for randomness [50, 51].

In these models when the densification is needed, the complexity of the cellular networks increases significantly and as a result, it limits the utility of system-level simulations due to the increasing number of simulation scenarios. These limitations highlight the need for employing tractable models which in turn signify the importance of the spatial stochastic models owing to their superior tractability. The BS locations in spatial stochastic models are assumed to be distributed using a particular probability distribution that captures the inherent spatial randomness

of the radio networks. Besides this, the spatial stochastic models can successfully grab other sources of randomness (like channel uncertainties) associated with various types of wireless networks as well [52].

In the recent past, various types of wireless networks have been modeled using stochastic geometry that provides a unified mathematical modeling to thoroughly understand the behavior of wireless networks [53–56]. Furthermore, the performance analysis carried out through the use of stochastic geometry can result in closed-form expressions for some special cases as well. These derived expressions not only facilitate in understanding the operation of the network but also provide easily the critical design insights, which cannot be obtained from the system-level simulations owing to their excessive computational complexities [57]. Typically, the Poisson point process (PPP) based models were mostly used to represent node locations in unplanned networks like Ad-Hoc networks [53, 56] or femto cells [58–61] due to the ease of random deployments in any specific area. In PPP, a collection of nodes is randomly and independently distributed in an infinite region while the number of points in any region follows a Poisson distribution. A PPP is known to be a homogeneous PPP when the density of nodes remains fixed in the entire region. On the contrary, the cellular networks were largely considered to be deployed in a relatively arranged or schematic manner, for instance hexagonal grid. Owing to the unprecedented success in characterizing unplanned networks using stochastic geometry, numerous attempts were made to utilize this concept in cellular networks as well [62].

A major breakthrough was reported in [63–65], when it was observed that the cellular networks exhibit random topology and variant behavior in different geographical locations. It was shown in [63] that the accuracy of stochastic geometry based model is comparable to that of an ideal grid based model, because the SINR received by UEs in a simulation environment with actual BS positions is lower-bounded by the random deployments of BSs and upper-bounded by idealized grid based BS deployments. Though both models provide similar tight bounds (pessimistic and optimistic); however the stochastic geometry oriented model is preferred owing to its remarkable tractability. Similarly, Andrews *et al.* in their

seminal work proposed a mathematical framework based on stochastic geometry and observed that the received SINR in case of real deployment can be approximated by stochastic geometry based model under general assumptions [64]. Meanwhile, the authors further observed that the exclusion of shadowing mechanism helps in improving the analytical tractability of the derived expressions without compromising on the accuracy of the analysis. The authors in [65] observed that for a shadowing environment, the SINR received by UEs in grid based network conforms to that received in stochastic geometry based model. Hence in the following subsections of the literature review, the locations of the BSs are modeled using appropriate point process models and stochastic geometry tools are employed to analyze the performance of dense cellular networks as depicted in the Fig. 2.1.

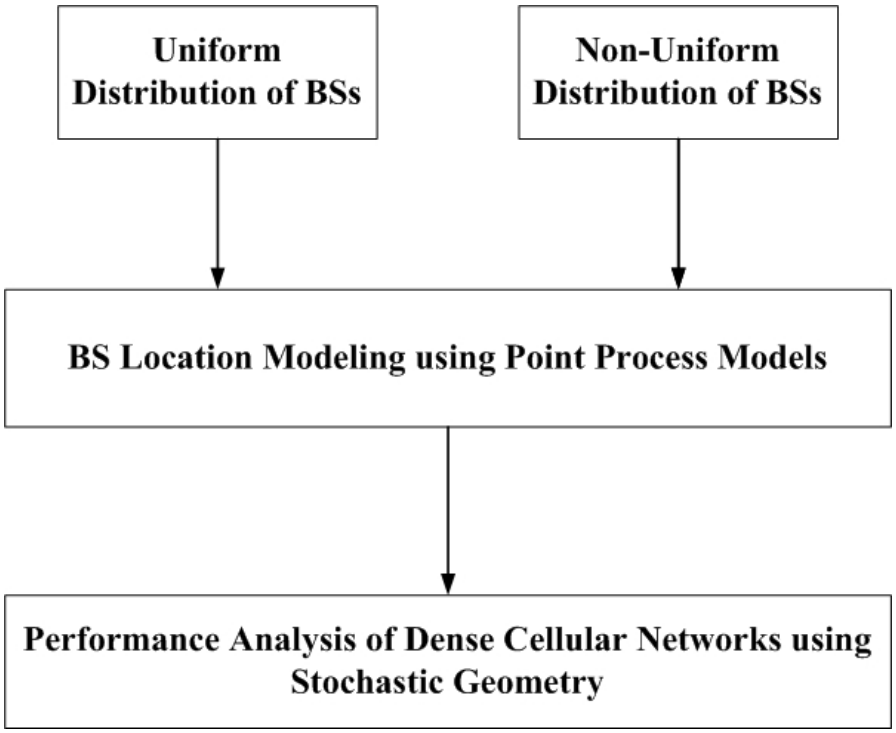

FIGURE 2.1: Main theme of the literature review

2.1.2 Performance Analysis of Uniformly Distributed HCNs

By taking advantage from the analytical tractability of stochastic geometry, Dhillon *et al.* extended the mathematical framework of a single-tier cellular network (presented in [64]) to a generic multi-tier HCN, where all the BS tiers were assumed

to be distributed through independent PPPs [66]. Expressions for the coverage probability and mean transmission rate were determined, while considering disparity in the transmit power of the BSs, BS density and data rate. In addition to the tractability, their proposed model effectively captures the placement of dense BSs which is a premier feature of HCNs. However, being a baseline model for analyzing the performance of HCNs, its applicability is limited in many aspects. For instance, the analysis is defined for SINR thresholds greater than 0 dB while it is assumed that only a single BS amongst the contending BSs of all tiers can meet this SINR threshold. Similarly, for a UE-AS based on highest instantaneous received SINR, the authors in [67] relaxed the SINR threshold condition of 0 dB considered in [66] and determined the CCDF of SINR for the nearest BSs of each tier. Moreover, the authors were also successful in determining the closed-form expressions for SINR distribution and UE association probability for Rayleigh fading assumption. The presented works in [66, 67] did not consider any strategies for interference management and steering of UEs to lightly loaded tiers. In order to resolve the issue of transmit power disparity between the MBS and SBSs, the 3GPP has recommended employing the cell range extension strategy. The cell range extension strategy which is also called as SBS biasing is implemented practically by increasing the cell selection offset of the SBSs.

An improved mathematical model was proposed in [68] that permitted flexible cell association to UEs using a UE-AS based on the average biased received power. Besides accounting for the ping-pong handovers that were inherent in the highest instantaneous received SINR based UE-AS, their proposed approach was helpful in providing valuable insights on important performance metrics like tier association probability, average load per tier, and per-tier coverage probabilities. Moreover, it has also been highlighted that although biasing helps in reducing the UE access load from macro tier but this feature is achieved at the cost of degraded network performance i.e., decrease in the coverage probability. Likewise, it has also been shown that the coverage area of SBSs is sensitive to the distance from their proximate MBSs. In [69], Singh *et al.* analyzed the impact of UE offloading using

flexible cell association in a multi-tier HCN supporting multiple radio access technologies (RATs) and observed that the optimum rate coverage can be achieved by steering a certain percentage of traffic to the other tiers with less load. Similarly in [70], the authors derived an expression for the rate distribution of a two-tier co-channel HCN for a joint incorporation of both load balancing and resource partitioning.

Nevertheless, load balancing in HCNs is directly related to the tier association of a user, which is a non-trivial problem [71]. Moreover, the UE-AS based on the nearest BS which has been extensively adopted in analyzing single-tier cellular networks is not valid in case of multi-tier cellular networks. For instance, a UE might be located in the near vicinity of any BS but due to the disparity in transmit power, it receives better signal strength from a relatively far located BS and thus, prefers association with that BS. Similarly, the irregularities associated with cell coverage areas (footprints) due to disparity in transmit power of tier BSs not only affect the composition of interference in densified HCNs but also cause highly diverse loads to be served by the BSs. In [72], Dhillon *et al.* observed that the disparity in transmit power and density of deployed BS tiers resulted in the overburdening of certain BSs while significant number of the BSs remained idle as well. Thus, the contribution of SBSs in the interference received by UEs is overestimated which results in pessimistic coverage. By incorporating dependent thinning of idle SBSs, the authors determined the expression for coverage probability and observed an increase in the network coverage due to increasing density of SBSs. In [73], the authors scrutinized numerous UE offloading schemes and observed that the UE association is primarily dependent upon the network density.

The cellular networks have transformed from their voice-oriented pattern to always-available and uninterrupted mobile broadband data networks. Generally in cellular networks, the speed and bandwidth requirements were driven by the downlink; however, the uplink also gained significant importance in the recent past owing to the applications that require symmetric data traffic. The commonly employed cell

association strategies in HCNs can be broadly categorized into coupled and decoupled. Traditionally, in the cellular networks both the uplink and downlink have been coupled i.e., the mobile terminals are forced to associate with a single BS for both links. The exponential upsurge in mobile data usage and recent trends in network densification have resulted in an increased interest in the decoupled association [74]. With the evolution of heterogeneity in the cellular networks, a device can access the deployed infrastructure through various BSs and may thus choose to associate with one BS for its uplink and any other for downlink. This amenity of choosing amongst multiple BSs for uplink and downlink is termed as the downlink-uplink decoupled (DUDe) access and its usage can potentially improve the overall network performance [75, 76]. In [77], the authors have compared the performance of coupled and decoupled UE association strategies in terms of the UE offloading to small tier while employing DS-PLM and observed the advantages of DUDe over non-DUDe or the coupled association scheme.

A comprehensive analytical framework for the uplink is complicated as compared to that for the downlink. Essential modifications in the system model are required for the uplink analysis when compared with the downlink. The random/regular locations of BSs contribute to the interference in the downlink, while in uplink, the source of interference is the randomness in the locations of UEs. Furthermore, the choice of transmit power in uplink is critical as well, owing to the battery-life limitation associated with user devices. Thus, the analysis of uplink becomes very difficult by using the conventional approaches. To manage the uplink interference in HCNs, power control is used as one of the approaches recommended by 3GPP [78–80]. For a detailed study on the power control, the reader may consult to [81] and the references therein. In order to determining accurately the basic performance metric (i.e., SINR distribution) of the uplink, the authors presented a tractable model using stochastic geometry [82]. Achieving maximum benefit of HCNs requires proactive offloading of users onto BSs with low loads. Mostly, offloading has been studied for downlink only under the assumption that offloaded users will have both the uplink and downlink from the BS having low load. Knowing that the uplink rate is better achieved with minimum path loss association,

the authors in [83] modeled the rate distribution and uplink SINR in a multi-tier HCN on the basis of power control parameters and association rules.

Due to the limited wireless spectrum availability, its aggressive reuse in co-existing BS tiers of HCNs has been extremely helpful in achieving improved network capacity; however, it leads to increased interference [29, 84]. In HCNs where SBSs and MBSs are co-existing, the interference received by the users in the downlink comes from both inter-tier and co-tier BSs respectively. As interference is a primary performance limiting parameter, therefore, it needs to be managed in an effective way. A comprehensive survey of various strategies adopted in combating interference is presented in [85]. In an another work focusing on urban environment, mathematical expressions for coverage probability and area spectral efficiency have been determined which lead to vital design insights [86]. The reported results explicitly highlight the need for employing spectrally-efficient interference management strategies to compensate for the excessive interference received by outdoor users due to densified SBS deployments.

It is pertinent to mention that the incorporation of frequency reuse mechanism introduces dependency on BS locations, since the neighboring BSs are bound to operate in different frequency bands and this affects the tractability of PPP. In [64], Andrews *et al.* addressed this dependency problem by considering static frequency reuse (worst-case) in a single-tier cellular network and observed its impact on the coverage and average achieved rate of the network. The authors have assumed that amongst the available frequency sub-bands, each BS randomly selects a frequency sub-band. Owing to this independent thinning, the tractability associated with PPP is retained. By using the same interference management strategy, Giambene *et al.* proposed prioritizing small tier association over macro tier in order to achieve load balancing amongst the BS tiers [87]. The joint incorporation of both load balancing and interference management mechanisms resulted in a pronounced improvement in the overall performance of the HCNs.

Another technique commonly employed in the literature to improve the received SINR of the cell-edge users (particularly) is based on fractional frequency reuse

(FFR) [88]. Dissimilar to the traditional frequency reuse mechanism, in FFR the coverage area of a cell is divided into cell-center and cell-edge regions by assigning different frequency sub-bands. The impact of FFR incorporation in a single-tier and multi-tier cellular network have been thoroughly studied in [89] and [90], respectively. In an another work, the potential of employing FFR in conjunction with UE offloading was investigated and a substantial enhancement in the network performance was reported [91]. In order to reduce the excessive cross-tier interference received by users, Ijaz *et al.* presented a strategy based on reversing the transmission direction of interfering BSs. On the basis of this reverse frequency allocation (RFA), they achieved a remarkable improvement in the received SINR and data rate [92]. Though these frequency reuse mechanisms help in reducing the interference experienced by users; however, this interference reduction is achieved at the cost of reduced spectral efficiency per unit area.

TABLE 2.1: Downlink coverage performance of densely deployed Uniform cellular networks using various PLMs.

Association Criteria		**Network Scope**		**Interference Management**					**Load Balancing**		**Path Loss Model**					**Reference**
Instant. Power	Average Power	Single-Tier	Multi-tier	Traditional FR	Universal FR	Fractional FR	Soft FR	Reverse FR	Cell Range Extension	None	Unbounded-SS	Bounded-SS	Unbounded-MS	Bounded-MS	3GPP	Author/s and Year
✓		✓		✓						✓	✓					[64]
✓		✓			✓					✓			✓			[93]
✓		✓			✓					✓				✓		[94]
✓			✓		✓					✓	✓					[66]
✓			✓		✓					✓	✓					[67]
✓			✓		✓				✓		✓					[69]
✓			✓		✓				✓						✓	[86]
✓			✓	✓					✓		✓					[87]
	✓	✓			✓					✓					✓	[95]
	✓	✓			✓					✓		✓				[96]
	✓	✓			✓					✓				✓		[97]
	✓	✓			✓					✓					✓	[98]
	✓		✓			✓			✓						✓	[91]
	✓		✓		✓				✓		✓					[68]

It is interesting to note that although the authors have assumed different UE-ASs in [66–69, 72, 87] but the derived expressions for SINR distributions were found to be almost similar in terms of their independency on the network density in interference dominant and fully loaded HCNs. One of the major reasons for this

insignificance of SBS densification, i.e., no improvement in coverage probability, is the increase in interference at those regions of MBS coverage areas where UEs are already receiving desired quality levels [99]. Similarly, it was also observed that the random deployment of SBSs not only reduces their coverage areas in the near vicinity of MBSs, but also degrades the efficiency of SBS biasing [68]. Thus, in nutshell, densifying SBSs limits the performance of uniform HCNs. This observation explicitly highlights the need for exploring selective or non-uniform densification option for SBSs. A qualitative summary of the coverage performance of densely deployed cellular networks with uniform distribution over varying PLMs is available in Table 2.1.

2.1.3 Performance Analysis of Non-Uniformly Distributed HCNs

In multi-tier cellular networks, the BSs of different tiers are commonly assumed to be deployed using independent PPPs; however, this strategy is not helpful in enhancing the network coverage of the dense HCNs. Owing to the uniform distribution of SBSs, the UEs associated with macro tier receive excessive interference from their nearby SBSs [100]; while on the other hand, the UEs which are offloaded to small tier using SBS biasing also face excessive interference from MBSs due to their higher transmit powers [101]. Nevertheless, as far as the practical BS deployments are concerned, it would also be unrealistic to assume no spatial correlation between the BSs of the different tiers. Similarly, it is also well-known in the literature that the traditional BSs are usually deployed in a planned manner and there is a little likelihood that any two BSs would be deployed in the close proximity of each other [102]. Consequently, the spatial stochastic models that permit repulsion between BS positions (both inter-tier and intra-tier) are well-suited in estimating the BS locations [103–106].

To ensure improved capacity and coverage of the deployed HCNs, a simplified non-uniform deployment of SBSs was considered in [107] by muting the SBSs within a specific distance from the MBSs. This spatial separation among the

MBSs and SBSs has two main advantages, 1) it protects the UEs located within the exclusion regions (i.e., MBS cell-center region) from excessive interference of nearby co-channel SBSs and 2) it increases the coverage region of SBSs. Hence, this results in a noteworthy improvement in the network coverage and throughput as compared to the uniform SBS deployment scenario without incurring any extra expenses. It is worth mentioning here that this selective muting/thinning of SBSs forms a Poisson hole process (PHP); however, the interference field is usually characterized by PPP, owing to its remarkable tractability [108, 109].

In [110], Deng *et al.* proposed adding dependencies between the locations of the MBSs and SBSs in order to improve the coverage performance. These dependencies include deploying SBSs only in those regions which are not completely covered by MBSs or in the regions that are relatively far-away from the MBSs. The desired locations of the SBSs were characterized using PHP and tier-wise outage probabilities were determined. The authors also studied the impact of the spatial correlation between the locations of BSs within a tier by modeling them with Matern cluster process (MCP) and determined the expressions for the outage probability and the spectral efficiency per unit area. In [111], the authors approximated the per-tier signal-to-interference ratio (SIR) distribution for interference-limited HCNs exploiting the spatial dependence between the locations of the BSs in real deployments using approximate SIR analysis based on PPP (ASAPPP) and mean SIR based gain schemes. In [112], the authors have used PHP to characterize the spatial interactions between active transmitters in cognitive and device-to-device (D2D) networks.

It is usually though that in order to accommodate the extremely high mobile data traffic requirements, the network operators need to deploy SBSs in abundance and employ advanced inter-cell interference mitigation techniques. This is because the available spectrum is scarce, and augmenting the network capacity extensively requires improvement in the spectral efficiency of the available spectrum or else it would result in a severely interference-limited network [113]. Xia *et al.* presented a coordinated multi-point (CoMP) based model to reduce the inter-cell interference in HCNs and achieved improved data rate and throughput in the cell-edge

region [114]. Guo *et al.* extended the work in [114] by proposing a location aware cooperation scheme that jointly achieves load balancing and eliminates excessive inter-tier interference in a two-tier HCN [115]. A comprehensive survey highlighting the weaknesses and strengths of the state-of-the-art CoMP clustering schemes is presented in [116], and the references therein.

Muhammad *et al.* extended the non-uniform SBS distribution model proposed in [107] by inculcating the load balancing perspective on the basis of SBS biasing [117]. This load balancing exhibited a considerable improvement in the UEs offloading to small tier and at the macro cell-edge regions which in turn improved the utilization of the network resources and resulted in capacity enhancement of non-uniform HCNs (NuHCNs). In [118], the authors enhanced the NuHCN model presented in [117] by considering an interference management strategy based on RFA. They observed that the RFA employment in NuHCNs yields better coverage and rate performance when compared to the uniformly distributed HCNs with or without RFA consideration. Similarly, Haroon *et al.* investigated the impact of soft frequency reuse (SFR) in conjunction with a power control factor on the performance of NuHCNs [119]. They also compared the obtained results with those of the uniform HCNs and observed significant improvement in the overall network coverage.

In the cases of PPP tweaked non-uniform deployment of SBSs [107, 117–119], it is usually observed that the SBSs in a multi-tier cellular network are generally distributed using independent PPPs. Thus, to inhibit the SBS services with in the near-vicinity of the MBSs, a fixed-sized exclusion region is considered around them. Nonetheless, another approach available in the literature for the non-uniform and selective SBS deployments is based on Stienen's model [120]. In this strategy, the coverage area of an MBS is divided into two disjoint regions, i.e. MBS cell-center and boundary regions. In this model, the MBSs and UEs are distributed using independent PPPs while the SBSs are deployed only in the outer region of macro coverage areas exploiting the PHP. This selective deployment of the SBSs assists in ensuring reduced interference within the MBS cell-center region, and thus leads to an improved performance of the deployed network [121]. Exploiting

the same Stienen's model, Sajid *et al.* jointly considered the SBS biasing and interference abating strategies, and investigated their impact on the performance of cell-edge users [122, 123]. A comprehensive survey of the estimated network performance of the densely deployed non-uniform cellular networks using various PLMs is summarized in Table 2.2.

TABLE 2.2: Downlink coverage performance of densely deployed non-uniform cellular networks using various PLMs.

Association Criteria		**Network Scope**		**Interference Management**					**Load Balancing**		**Path Loss Model**					**Reference**
Instant. Power	Average Power	Single-Tier	Multi-tier	Traditional FR	Universal FR	Fractional FR	Soft FR	Reverse FR	Cell Range Ext.	None	Unbounded-SS	Bounded-SS	Unbounded-MS	Bounded-MS	3GPP	Author/s and Year
✓		✓								✓	✓					[112]
✓			✓		✓				✓		✓					[72]
✓			✓		✓					✓	✓					[110]
	✓		✓		✓				✓		✓					[117]
	✓		✓					✓	✓		✓					[118]
	✓		✓				✓		✓		✓					[119]
	✓		✓		✓					✓	✓					[111]
	✓		✓		✓					✓	✓					[107]
	✓		✓		✓					✓	✓					[121]
	✓		✓						✓	✓	✓					[122]
	✓		✓						✓	✓	✓					[123]

2.2 Gap Analysis

The emerging cellular networks are bound to be dense, especially when their astounding success in meeting the high capacity demands over the last few years is considered. The densification of SBSs in an overlaid network is like a double-edged sword; it on one hand brings the deployed network resource in the close proximity of the users and helps in achieving the desired data rates but on the other hand, it results in excessive interference [124]. There is extensive literature available on the performance analysis of dense multi-tier networks that undertake various load-balancing and interference management mechanisms; however, such literature is strictly limited to the usage of SS-PLM. The estimation of path loss using SS-PLM is based on a simplified approach, i.e., the decay rate of a signal is assumed to be uniform over all ranges of the link distance. Due to this assumption, SS-PLM fails

to precisely capture the dependence of the value of path loss exponent on the range of link distance in dense cellular networks. Nevertheless, the signal attenuation generally increases with the distance in practical networks due to the presence of numerous obstacles in the path between UEs and BSs [93, 95, 125].

Using SS-PLM, it has been reported in numerous works [64, 66–69, 72, 73, 87, 126] that the expression for the coverage probability is independent of the network density in a fully-loaded and interference-limited cellular network. This independence of SINR distribution infers that the cellular operators may freely densify their infrastructures, as the increase in the interference is counterbalanced by the improved received power at the UEs owing to the decrease in link distances. In uniform HCNs, this observation of the SINR invariance to SBS densification has come under rigorous scrutiny. It has been shown in numerous recent works employing more realistic path loss models that the network coverage is sensitive to SBS densification [93, 95, 96, 127]. It was even reported recently that the ultra-densification of SBSs degrades the network performance significantly [94, 97, 128–130]. This contrasting behavior of uniform dense HCNs appears largely due to the usage of SS-PLM, which fails to precisely estimate the path loss in densely deployed cellular networks. The SS-PLM works on a '*one-size-fits-all approach*' and its usage leads to severe differences in estimating the strength of the desired and interfering signals. Since, the emerging cellular networks are bound to have varying distances of the desired and interfering links; hence, the analyses of such cellular networks is not recommended on the basis of SS-PLM.

There has already been a growing interest in replacing the SS-PLM by multi-slope PLMs due to their innate ability to account for extensive variations in the distances of the desired and interfering links. Meanwhile, it is well-known in the literature that the critical distance where the received/interfering signal decay rate changes is primarily dependent on the antenna heights of the transmitting and receiving stations [37, 131]. Similarly, it was observed in [98, 132–134] that the antenna height at the BS significantly affects the downlink performance of both single-tier and multi-tier cellular networks. As the available literature on the coverage performance analysis of dense HCNs is solely based on the usage of SS-PLM, which

leads to incorrect estimation of the benefits associated with various load balancing and interference management mechanisms. Therefore, it is of utmost importance to employ more accurate PLMs especially in the dense deployment scenarios to better estimate the network performance.

2.3 Problem Statement

As discussed in the earlier sections, the available literature on the downlink performance analysis of uniform HCNs and coverage-oriented HCNs considering various load balancing and/or interference management schemes is solely based on the usage of SS-PLM. Meanwhile, it is also well-known in the literature that employing SS-PLM leads to significant inaccuracies in evaluating the performance of dense networks. Nevertheless, it is important to note that the occurrence of disparate link distances is a usual phenomenon in dense cellular networks; hence, it is highly desirable to use more realistic PLMs in analyzing the downlink coverage performance of the dense multi-tier cellular networks. Although, DS-PLM is well-known to be fairly accurate in approximating the path loss in dense networks, the downlink performance analysis of densely deployed multi-tier cellular networks using DS-PLM still needs to be explored. Therefore, in this thesis, DS-PLM is employed to analyze the downlink coverage performance of dense HCNs considering both uniform and nonuniform distribution of SBSs. Meanwhile, the impact of DS-PLM consideration on the utility/pitfall of the commonly employed load balancing and interference management strategies is also investigated.

2.4 Research Methodology

From the perspective of modeling the locations of BSs and UEs, it is commonly accepted in the literature that the locations of UEs are random, while the locations of BSs are relatively fixed and regular. However, with the dense deployment of SBSs in the overlaid network, the randomness associated with the BS positions

also increases. Consequently, this increased randomness in the location of BSs necessitates adopting more tractable network modeling strategies that can circumvent the limitations of existing approaches [39]. The authors in [64, 66] have shown that the BS locations in both the conventional (single-tier) and multi-tier cellular networks can be precisely modeled by the point process models, e.g, PPP in their cases. Dissimilar to the previous models (i.e., Wyner and regular grid-based models), employing point process models permit mathematical derivation of SINR distribution which leads to important design insights. Moreover, owing to the translational and rotational invariant properties of the homogeneous PPP, the estimated network performance using PPP is location independent. Hence, this thesis assumes that the BSs and UEs are distributed in a service area using distinct PPPs.

Keeping in view the random distance-separation between the BSs and UEs which is additionally coupled with the random gains of the fading channel, parametric statistics of both the desired and interfering signals received by the UEs are highly random. Consequently, the received SINR is also random and highly sensitive to any variation in these factors. A number of techniques are available in the literature to analyze the downlink performance (i.e., coverage probability, average data rate, throughput etceteras) of cellular networks. However, due to the non-existence of a closed-form expression for the probability density function of aggregate interference, Rayleigh fading impairment is commonly considered on the reference link [135]. Based on this assumption, the exact expression for the SINR distribution can be determined using the Laplace transform of the aggregate interference experienced by the user devices [49, 64, 66–69, 72, 89, 90, 136, 137]. It is important to note that the Rayleigh fading assumption can be removed by considering any arbitrary fading, but in order to keep the analytical tractability, this thesis assumes that the reference link under investigation undergoes Rayleigh fading impairment, while ignoring shadowing.

As far as the performance evaluation strategy is concerned, the prime focus of this thesis is to investigate the impact of employing DS-PLM on the estimated downlink performance of dense cellular networks that jointly consider CRE-based

load balancing and traditional frequency reuse mechanism using stochastic geometry approach. By using DS-PLM, the coverage area of a BS is divided into two non-overlapping regions separated by a critical distance and this special distance is well-known to be dependent on the antenna heights of the communicating stations [37, 98, 132, 134]. In this thesis, it is also assumed that the UEs are free to associate with any tier, but their association with any BS is primarily based on the maximum average biased received power. Moreover, a fully-loaded HCN is assumed, i.e., the density of UEs is significantly greater than the density of BSs and every BS has always some data for at least a single UE.

In order to validate the accuracy of the derived expressions for both the uniform and non-uniform deployment scenarios, the mathematical expressions for each network layout are evaluated numerically and compared with the Monté Carlo simulations. The simulation setup involves placing a typical user device at the origin for each network realization while the locations of BSs of both the tiers are generated using independent PPPs. It is pertinent to mention here that the received interference and SINR are bound to vary in each network realization owing to the randomness associated with the selected point process model. Therefore, in order to effectively characterize the important performance metrics, average is commonly taken over very large number of simulation iterations to account for all the possible network realizations.

2.5 Thesis Contributions

The prime focus of this thesis is to employ DS-PLM to analyze the downlink coverage performance of dense HCNs considering both uniform and non-uniform distribution of SBSs. The novelty of the presented work lies in the derived expressions and the ease with which critical design insights can be obtained. As discussed earlier, the traditional approaches of obtaining the network design insights heavily relied on performing field experiments or using highly complicated system level simulations.

Thus, the two major contributions of this thesis can be briefly summarized as follows:

1. **Coverage performance of the uniformly distributed cellular networks using DS-PLM**

   In the first thesis contribution, a two-tier HCN has been considered in which the locations of BSs and UEs are modeled using independent PPPs. Contrary to SS-PLM usage, the consideration of DS-PLM ensures that the desired and interfering signals experience a more-realistic distance dependent path loss. Hence, DS-PLM is employed to study and analyze the performance of a two-tier dense cellular network that permits flexible user association using SBS biasing in conjunction with a simple frequency reuse mechanism. A thorough comparison of SS-PLM with DS-PLM is performed for the tier association probability (T-AP) and coverage probability, which outrightly shows that there is a significant difference in the estimated overall network performance using both PLMs. Thus, owing to the better accuracy of DS-PLM in path loss estimation in dense deployment scenarios, the impact of load balancing and/or interference avoiding strategies on the downlink performance of a two-tier HCN is better estimated by DS-PLM. A brief detail of the studied effects is described below:

   - New macro T-AP expression of T-UE is derived using DS-PLM which is found to be a function of critical distance of both tiers. Dissimilar to the SS-PLM where SBS biasing and densification always lead to aggressive offloading of UEs to small tier, DS-PLM expression explicitly highlights the MBS association regions wherein both SBS biasing and densification are not effective in UE steering. Thus, highlighting the overestimation of UE offloading to smaller tier in SS-PLM.
   - Conditioned on T-UE association with either of the BS tiers for link distance greater and smaller than their respective critical distances, novel coverage probability expressions are derived using DS-PLM. Unlike SS-PLM, it has been shown that the network coverage is sensitive

to both the density of BSs and their critical distances. In addition to this, it also highlights the overestimation of coverage degradation due to offloading of UEs to smaller tier using SS-PLM.

The above contribution has lead to the following research publication: **K. Shehzad**, N. M. Khan, and J. Ahmed, "Impact of frequency reuse and flexible cell association on the performance of dense heterogeneous cellular networks using dual-slope path loss model," IEEE Access, vol. 7, pp. 166214–166234, 2019.

2. **Coverage performance of the coverage-oriented cellular networks using DS-PLM**

   For a two-tier uniform HCN in which BSs of both tiers are randomly deployed using two independent PPPs, the SBSs that exist at distances smaller than the critical distance of each MBS are deactivated to form a non-uniform HCN i.e., NuHCN. This selective SBS deactivation ensures that most of the SBSs are deployed at locations where MBSs have weaker coverage. Moreover, the UEs that are located within the critical distance of any MBS are bound to associate with that MBS only. This is because when the UEs exist at distances smaller than the critical distance of any MBS, then owing to the disparity in transmit power of MBSs and SBSs, the UEs mostly receive a stronger signal from MBS as compared to the nearest SBS. Similar to the previous contribution, DS-PLM is employed to analyze the downlink performance of a two-tier NuHCN while considering load balancing and interference management strategies. An extensive performance comparison using both SS-PLM and DS-PLM is also carried out for both T-AP and coverage probability, which highlights that the usage of SS-PLM underestimates the benefits associated with load balancing and interference management schemes in NuHCNs. A brief detail of the studied effects is described below:

   - Novel expression for the macro association of a random UE is determined for the two-tier NuHCNs. The derived expression clearly highlights the important parameters of UE association with macro tier BSs.

Furthermore, it sheds light on the improved efficiency of SBS biasing in MBS outside region (post critical distance), as the UEs are proactively offloaded to SBSs in that region which reduces the load from macro tier.

- New expression for the network coverage probability is derived for the two-tier NuHCNs using DS-PLM, which highlights the dependency of network coverage on BS densities and critical distances of both tiers. Contrary to uniform HCNs, NuHCNs can ensure the same coverage performance with far lesser SBS deployments, owing to the reduction in interference due to selective SBS deployments. Moreover, the coverage performance of NuHCNs also highlights the perks of utilizing load balancing mechanism in conjunction with simple frequency reuse, as the network coverage provided by NuHCNs is significantly greater than the uniform HCNs.

The above contribution has lead to the following research publication:

K. Shehzad, N. M. Khan, and J. Ahmed,"Performance analysis of coverage-centric heterogeneous cellular networks using dual-slope path loss model," Computer Network, pp-107672, 2020.

2.6 Conclusion

In this chapter, a thorough study on the stochastic geometry modeling of cellular networks has been presented. Although the cellular networks have rapidly transformed from voice-only to data-centric over the past decade, it has been observed that the stochastic geometry modeling leads to tractable analyses in many practical scenarios. Meanwhile, the gap analysis, problem statement and the adopted research methodology have also been presented in this chapter.

Chapter 3

Coverage Analysis of Uniform HCNs using DS-PLM

Densifying low-powered BSs in support of the overlaid MBSs is getting significant consideration as a viable solution for meeting the rapidly increasing capacity demands of emerging wireless networks. Contrarily, this ongoing evolution of cellular networks into dense and irregular networks has introduced multiple disparities, which makes them significantly different from the macro-cellular networks. Nonetheless, it is worth mentioning that the analysis of conventional cellular networks is generally carried out using the standard SS-PLM. Contrarily, it is also well-known in the literature that the usage of SS-PLM leads to inaccuracies in evaluating the performance of dense networks. Thus, in this chapter, DS-PLM has been employed to study and analyze the downlink performance of dense HCNs with randomly distributed BS tiers. Meanwhile, the impact of DS-PLM consideration on the effectiveness of load balancing and interference management schemes is also investigated in this chapter.

Remaining parts of the chapter are organized in the following manner: Section 3.1 provides a brief introduction to the problem. System model is presented in section 3.2, which is followed by section 3.3 that presents the analysis for macro T-AP and statistical distance distributions for communicating distances greater and smaller

than the R_{CM}. In Section 3.4, the derivation of network coverage expression is presented for the two-tier HCNs. Numerical results are discussed in section 3.5, and the chapter is concluded in section 3.6.

3.1 Introduction

The last decade has witnessed an exponential increase in the mobile data traffic, owing primarily to the drastic rise in the demand of smart devices supporting numerous data hungry applications. This exponential rise in the demand of wireless data has lead to an evolution of cellular networks into a stage where MBS-based system has reached its optimum capacity limits, as governed by the principles of information theory. Deploying abundant low-powered BSs to complement the conventional MBSs has been considered a feasible approach to address the explosive data deluge [4]. Hence, transforming the conventional cellular networks into dense and irregular networks, i.e., HCNs [5]. The heterogeneity associated with HCNs necessitates revising the traditional strategies of cellular planning and deployment as it features multiple BSs of varying cell sizes, transmission powers, SINR thresholds, spatial densities, PLEs and carried traffic load [32].

The conventional (homogeneous) networks involved only macro cells in which MBSs usually transmitted with equal power while their locations were also relatively regular, thus restricting interference from affecting system performance. Moreover, this schematic strategy of regular placement and uniform power transmission also ensured equal load on all BSs, and hence, load balancing was not required explicitly. Contrarily, the disparity in transmit power of BS tiers in HCNs overburdens the macro tier, as the UEs mostly receive better strength of received signal from their nearest MBSs, and thus prefer association with the macro tier. To exploit maximum potential of HCNs, it is vital to address the issue of load balancing at cell association stage [138], [69]. Offloading UEs to lightly loaded tiers is highly desirable and numerous techniques targeting various perspectives have been reported in the literature to effectively offload UEs to smaller tiers [126, 139, 140].

The most commonly adopted strategy is based on the static cell biasing in which UEs are steered towards lightly loaded BS tiers with the help of biased received signals. With the consideration of cell biasing, the cell-range of the lightly loaded BS tiers is increased.

Besides inter-tier load balancing problem in HCNs, the densification of SBSs also leads to an excessive increase in the network interference which significantly impacts the user experience [141], [142]. The interference in HCNs has been extensively studied in literature [143–148], and references therein. The conventional cellular systems generally encountered two types of interference, i.e., co-channel and adjacent channel. Dealing with inter-cell interference mostly required controlling the usage of frequencies over various channels in a network. On the contrary in HCNs, besides co-channel and adjacent channel interference, random deployment of densified SBSs and their access strategies also play their part in making it a non-trivial problem. The inter-tier interference can be removed by dedicating frequency channels for SBSs but given limited spectrum and its effective utilization, the cellular operators prefer sharing over partitioning of the spectrum [149–152].

The future wireless networks are expected to be dense, and thus the transmission distances are more likely to be small. Given its simplicity, the SS-PLM fails to accurately capture path loss for such small distances, as it assumes homogeneous attenuation from all distance ranges. Contrarily, in real networks, signal attenuation increases with the distance due to numerous obstacles present in the path between UEs and BSs. Therefore, by analyzing the performance of dense HCNs while ignoring the disparity in path loss for varying link and interfering distance would lead to severe inaccuracies [125] and [124]. Consequently, there has been a growing interest in replacing SS-PLM by multi-slope PLMs due to their innate ability to account for extensive variations in communicating and interfering links. The critical distance where the received/interfering signal decay rate changes is primarily dependent on the antenna heights of communicating stations [131], while it has been shown in [98, 132, 134] that the antenna heights at transmitter end significantly affect the downlink performance of cellular networks.

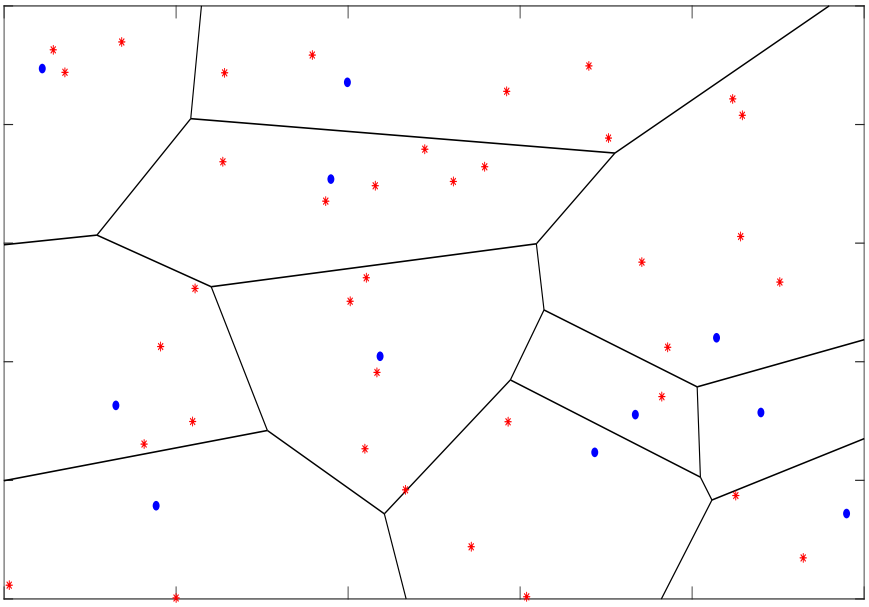

FIGURE 3.1: A two-tier HCN with MBSs and SBSs distributed using independent PPPs. The blue colored dots represent the MBSs while SBSs are denoted by red asterisks.

3.2 System Model

3.2.1 BS Deployment and User Distribution

In this chapter, a two-tier HCN is considered in which both the BS tiers are assumed to be distributed in a service area using independent PPPs as shown in Fig. 3.1. Let ϕ_M, and ϕ_S represent the PPPs for MBSs, and SBSs respectively, while their respective spatial densities (i.e., number of BSs per unit area) are denoted by λ_M, and λ_S. The UEs locations are also considered to be distributed using another independent PPP i.e., ϕ_U with spatial density λ_U. The respective transmit powers of both BS tiers are represented by P_M and P_S, and it is assumed that all MBSs transmit with power P_M, while all the SBSs transmit with P_S and $P_S < P_M$. To account for the disparity in the transmit power of both BS tiers, SBS biasing is considered, i.e., $B_S \geq$0 dB. Let X_M and X_S denote the coordinates

of macro and small BSs in the considered 2-D plane. The analysis is carried out for a typical UE (T-UE) located at the origin, and Silvnyak's Theorem justifies this assumption owing to a special property, i.e., translation invariance or the stationarity of PPPs [39].

3.2.2 Channel Model

Due to the dense deployment of SBSs in the overlaid cellular networks, multiple SBSs can appear in the coverage area of any MBS as $\lambda_S > \lambda_M$. Therefore, disparate link distances are most likely to occur in such deployment scenarios and as a result, DS-PLM has been used to accurately account for the signal attenuations due to the variations in the link distance ranges. Using DS-PLM, the long-term averaged received power at the T-UE from the ith tier BS is given by: $P_{R_{UE_i}}(x_i) = P_i L_0 l(x_i)$, where, $l(x_i) = \begin{cases} {x_i}^{-\alpha_{0i}} & x_i \leq R_{Ci} \\ \eta_i {x_i}^{-\alpha_{1i}} & x_i > R_{Ci}, \end{cases}$ and the constant $\eta_i \stackrel{\triangle}{=} R_{Ci}^{\alpha_{1i}-\alpha_{0i}}$ is introduced to ensure continuity of the DS-PLM. It is important to note that the introduction of η_i conforms with the DS-PLM definitions given in [93] and [153]. Meanwhile, R_{Ci} is the critical distance of the ith tier BS, and α_{0i} and α_{1i} are the far field PLEs for the pre-critical and post-critical distances respectively, while $2 < \alpha_{0i} \leq \alpha_{1i}$. Hence, by employing DS-PLM it has been ensured that both the desired and interfering signals experience a more-realistic distance dependent path loss.

The usage of DS-PLM divides the coverage area of a BS into two regions and these regions are separated by the R_C of that BS. It is well-known in the literature that the size of R_C is mainly dependent on the antenna heights of the communicating stations [37]. For a two-tier HCN, as shown in Fig. 3.2, the overlaying of SBSs on MBSs forms four disjoint regions, as the BSs of both tiers are independently placed. The circle around each BS refers to its R_C and the Fig. 3.2 clearly illustrates that R_{CM} is greater than R_{CS} owing to the disparity in the heights of

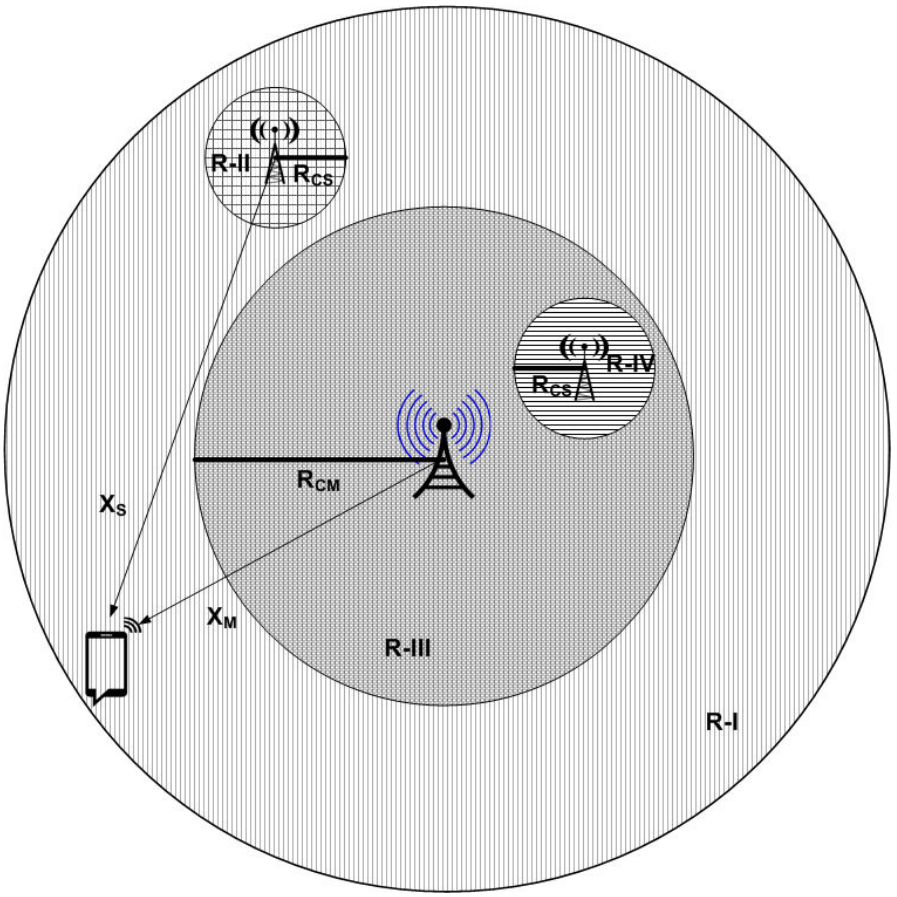

FIGURE 3.2: Critical distance based association regions for T-UE in a two-tier HCN.

TABLE 3.1: Association Regions for T-UE in a two-tier HCN

Regions	**Communication Distance Limits**
R-I	$[X_M > R_{CM} \cap X_S > R_{CS}]$
R-II	$[X_M > R_{CM} \cap X_S < R_{CS}]$
R-III	$[X_M < R_{CM} \cap X_S > R_{CS}]$
R-IV	$[X_M < R_{CM} \cap X_S < R_{CS}]$

MBSs and SBSs. Meanwhile, the figure further illustrates that the UE is located in region R-I as its distance from the nearest MBS and SBS is greater than R_{CM} and R_{CS}, respectively. The description of each association region for the T-UE along with its likelihood which is expressed as a function of R_C and λ is given in Table 3.1.

The UE association strategy (UE-AS) considered in this chapter permits the T-UE to associate with any BS offering the maximum averaged biased received power.

Thus, adopting a flexible UE association to ensure possible extension in the coverage range of SBSs. Dissimilar to the UE-AS employed in [64, 66, 87] which is susceptible to the fading induced ping-pong handover effects, the employed UE association policy successfully evades such issues during UE attachment with any BS. Nonetheless, owing to the densified deployment of SBSs, a simple frequency reuse mechanism is also considered to reduce the excessive aggregate interference experienced by the UEs. The adopted interference management mechanism is implemented by performing the random thinning of the BSs of both tiers using the properties of the PPP. It is assumed that the available frequency band is divided into N equal channels i.e., $F_1, F_2, ..., F_N$ while every BS randomly chooses a channel out of the N available channels. Therefore, the T-UE receives interference from each BS with a likelihood of 1/N which is further equivalent to performing an independent thinning of deployed BSs of both tiers.

$$\Gamma_{X_i}(x_i) = \frac{P_i h_{Xi} \begin{cases} L_0 \left(\frac{d_{0_i}}{x_i}\right)^{\alpha_{0i}} & x_i \leq R_{Ci} \\ L_0 \left(\frac{d_{0_i}}{R_{Ci}}\right)^{\alpha_{0i}} \left(\frac{R_{Ci}}{x_i}\right)^{\alpha_{1i}} & x_i > R_{Ci}, \end{cases}}{\sum\limits_{j \,\epsilon\, \{\phi_{M,n} \,\cup\, \phi_{S,n}\} \setminus i} \left(P_j h_{Xj} \begin{cases} L_0 \left(\frac{d_{0_j}}{x_j}\right)^{\alpha_{0j}} & x_j \leq R_{Cj} \\ L_0 \left(\frac{d_{0_j}}{R_{Cj}}\right)^{\alpha_{0j}} \left(\frac{R_{Cj}}{x_j}\right)^{\alpha_{1j}} & x_j > R_{Cj}, \end{cases} \right) + \sigma^2}, \tag{3.1}$$

The T-UE association with any BS tier is solely based on the highest biased received power in which fading is averaged out; however, for determining the average network coverage probability or the CCDF of SINR, the impact of fading is considered. The expression for received SINR ($\Gamma_{X_i}(x_i)$) at T-UE located at a distance x_i from its associated ith tier BS is given in (3.1), where $\phi_{M,n} \cup \phi_{S,n}$ represents a collection of all MBSs and SBSs that operate at the same frequency channel n, $d_{0_i} = 1$m is the close-in reference distance for both the tiers. The path loss constant at a close-in reference distance d_{0_i} is represented by L_0. The downlink interference fading coefficient denoted as h_{X_i} is modeled as Rayleigh fading whose power is exponentially distributed with unitary mean, i.e., $h_{X_i} \sim \exp(1)$ while a

constant thermal noise power of σ^2 having additive nature is also considered in the system. It is further assumed that none of the deployed BSs of both tiers are unloaded i.e., every BS always has some data for its associated UEs.

3.3 Tier Association Probability (T-AP) and PDF of Distance to the Serving BS

In this section, macro T-AP of T-UE in the presence of a load balancing scheme based on SBS biasing is determined and it is followed by the derivation of necessary distance distributions of T-UE and serving MBSs. The distribution of X_i is given by the 2D null probability of PPP, and the likelihood that there is no BS within the circle of radius x_i,

$$\mathbb{P}\left[X_i > x_i\right] = \exp\left(-\pi\lambda_i x_i^2\right). \tag{3.2}$$

Using (3.2), the PDF of X_i where $x_i \geq 0$ can be expressed as

$$f_{X_i}\left(x_i\right) = 2\pi\lambda_i x_i \exp\left(-\pi\lambda_i x_i^2\right). \tag{3.3}$$

By using 2D null probability, the likelihood that T-UE could be located in any of the four association regions (region specifications in terms of R_{CM} and R_{CS} are described in Table 3.1) is given below:

$$\begin{aligned}
\varpi &= \exp\left(-\pi\lambda_M R_{CM}^2 - \pi\lambda_S R_{CS}^2\right) \\
\varrho &= \exp\left(-\pi\lambda_M R_{CM}^2\right) - \exp\left(-\pi\lambda_M R_{CM}^2 - \pi\lambda_S R_{CS}^2\right) \\
\varsigma &= \exp\left(-\pi\lambda_S R_{CS}^2\right) - \exp\left(-\pi\lambda_M R_{CM}^2 - \pi\lambda_S R_{CS}^2\right) \\
\upsilon &= 1 - \left(\varpi + \varrho + \varsigma\right).
\end{aligned}$$

3.3.1 Tier Association Probability

To account for the disparity in transmit power of BS tiers, biased received power (with $B_M = 0$ dB and $B_S \geq 0$ dB) based UE-AS is employed to ensure a balanced

load between the two tiers of HCN. Thus, the T-UE associates with macro tier only if the received power from the nearest MBS is greater than the power offered by the closest SBS after considering biasing. The complete T-UE association probability with macro tier for all four regions (disjoint) is governed by the total probability law as

$$\mathcal{A}_{\mathcal{M}} = \sum_{k=1}^{4} \mathcal{A}_{\mathcal{M},\mathrm{R_k}}, \tag{3.4}$$

where $\mathcal{A}_{\mathcal{M},\mathrm{R_k}}$ is the joint association probability of T-UE with macro tier while T-UE is located in region k. As discussed earlier, the regions are sensitive to the variation in deployment densities and critical distance sizes of both the tiers.

Lemma 3.3.1*: Using DS-PLM, the association probability of T-UE with macro tier in region R-I is given as*

$$\mathcal{A}_{\mathcal{M},R\text{-}I} = 2\pi\lambda_M \int_{R_{CM}}^{\infty} x_M \begin{cases} \exp\left(-\pi \ \left(\lambda_M x_M^2 + \lambda_S \beta^2\right)\right) \ \mathrm{d}x_M & \beta \geq R_{CS} \\ \exp\left(-\pi \ \left(\lambda_M x_M^2 + \lambda_S R_{CS}^2\right)\right) \ \mathrm{d}x_M & \beta < R_{CS} \end{cases}, \tag{3.5}$$

where $\beta = \left(P_S B_S \eta_S / P_M \eta_M\right)^{1/\alpha_{1S}} x_M^{\alpha_{1M}/\alpha_{1S}}$.

It is obvious from (3.5) that besides λ_i and P_i, the T-UE association probability in R-I is further sensitive to distance dependent PLEs (α_{1M} and α_{1S}), tier biasing factors (B_S and B_M) and critical distance (R_{CM} and R_{CS}).

Proof: The joint association probability of T-UE with macro tier in R-I is given by the following probabilistic event

$$\mathcal{A}_{\mathcal{M},\text{R-I}} = \mathbb{P}\left[{P_r}^M > {P_r}^S, \text{R-I}\right], \tag{3.6}$$

where ${P_r}^M$ and ${P_r}^S$ are the averaged received powers from the nearest macro and small tier BSs respectively. As discussed in section 3.2, the impact of shadowing

and small scale fading is not considered in UE association decisions. Therefore, the averaged received powers using DS-PLM in R-I from both BS tiers are ${P_r}^M = P_M \eta_M L_0 x_M^{-\alpha_{1M}}$ and ${P_r}^S = P_S B_S \eta_S L_0 x_S^{-\alpha_{1S}}$ respectively. Inserting them in (3.6) to get

$$\mathcal{A}_{\mathcal{M},\text{R-I}} = \mathbb{P}\left[P_M \eta_M L_0 x_M^{-\alpha_{1M}} > P_S B_S \eta_S L_0 x_S^{-\alpha_{1S}},\ \text{R-I}\right], \tag{3.7}$$

rearranging the terms in (3.7) gives

$$\mathcal{A}_{\mathcal{M},\text{R-I}} = \mathbb{P}\left[x_S \ > \ \left(\frac{P_S B_S \eta_S}{P_M \eta_M}\right)^{\frac{1}{\alpha_{1S}}} x_M^{\frac{\alpha_{1M}}{\alpha_{1S}}},\ \text{R-I}\right]. \tag{3.8}$$

From Table 3.1, we already know the constraints on X_M and X_S in R-I. Now by conditioning on X_M, (3.8) takes the integral form

$$\mathcal{A}_{\mathcal{M},\text{R-I}} = \int_{R_{CM}}^{\infty} \mathbb{P}\left[(X_S > \beta \ \cap \ X_S > R_{CS}), \text{R-I} | X_M\right] f_{X_M}(x_M)\, \mathrm{d}x_M, \tag{3.9}$$

where $f_{X_M}(x_M)$ is already given in (3.3). The integration limits in (3.9) are from R_{CM} to ∞, as X_M is constrained over the same range as well. Now, simplifying (3.9) by using (3.2) gives the desired expression for association probability of T-UE with macro tier in R-I and completes the proof of (3.5). ■

As per the system model, the association of T-UE for a two tier HCN is a Bernoulli event, i.e., having only two possible outcomes which means the T-UE either associates with macro tier or with the small tier. Therefore, the association probability of T-UE with small tier conditioned on R-I can be expressed as

$$\mathcal{A}_{\mathcal{S}|\text{R-I}} = 1 - \mathcal{A}_{\mathcal{M}|\text{R-I}}, \tag{3.10}$$

where $\mathcal{A}_{\mathcal{M}|\text{R-I}}$ can be easily determined from (3.5) by using conditional probability and the likelihood of T-UE located in R-I (ϖ).

The alternate way to determine the expression of T-UE association with small tier

in R-I is to follow the procedure adopted in the proof of (3.5), and the final result is given as

$$\mathcal{A}_{\mathcal{S},\text{R-I}} = 2\pi\lambda_S \int_{R_{CS}}^{\infty} x_S \begin{cases} \exp\left(-\pi \ \left(\lambda_S x_S^2 + \lambda_M {k_A}^2\right)\right) \ \mathrm{d}x_S & k_A \geq R_{CM} \\ \exp\left(-\pi \ \left(\lambda_S x_S^2 + \lambda_M R_{CM}^2\right)\right) \ \mathrm{d}x_S & k_A < R_{CM} \end{cases}, \quad (3.11)$$

where $k_A = \left(P_M \eta_M / P_S B_S \eta_S\right)^{1/\alpha_{1M}} x_S^{\alpha_{1S}/\alpha_{1M}}$.

Lemma 3.3.2*: The association probability of T-UE with macro tier in region R-II using DS-PLM is given as*

$$\mathcal{A}_{\mathcal{M},R\text{-}II} = 2\pi\lambda_M \int_{R_{CM}}^{\infty} x_M \left[\exp\left(-\pi\lambda_S\gamma^2\right) - \exp\left(-\pi\lambda_S R_{CS}^2\right)\right] \exp\left(-\pi\lambda_M x_M^2\right) \ \mathrm{d}x_M, \quad (3.12)$$

where $\gamma = \left(P_S B_S / P_M \eta_M\right)^{1/\alpha_{0S}} x_M^{\alpha_{1M}} / \alpha_{0S}$.

It is an important result as it justifies the need for SBS densification but preferably in MBS coverage regions where the received power from nearby MBSs is smaller as compared to the power received from SBSs. Based on the UE-AS adopted in this chapter, such regions are MBS cell-boundary regions. Hence, (3.12) brings focus to the introduction of dependency between the location of BSs from both tiers.

Proof: Please refer to Appendix A.1. ■

Similarly, by following the procedure adopted in derivation of (3.12), the expression for association probability of T-UE with small tier in region R-II can be determined and it is given as

$$\mathcal{A}_{\mathcal{S},\text{R-II}} = 2\pi\lambda_S \int_{0}^{R_{CS}} x_S \begin{cases} \exp\left(-\pi \ \left(\lambda_S x_S^2 + \lambda_M {k_B}^2\right)\right) \ \mathrm{d}x_S & k_B \geq R_{CM} \\ \exp\left(-\pi \ \left(\lambda_S x_S^2 + \lambda_M R_{CM}^2\right)\right) \ \mathrm{d}x_S & k_B < R_{CM} \end{cases}, \quad (3.13)$$

where $k_B = (P_M \eta_M / P_S B_S)^{1/\alpha_{1M}} \, x_S^{\alpha_{0S}/\alpha_{1M}}$.

Lemma 3.3.3*: The association probability of T-UE with macro tier in R-III using DS-PLM is given as*

$$\mathcal{A}_{\mathcal{M},R\text{-}III} = 2\pi\lambda_M \int_0^{R_{CM}} x_M \begin{cases} \exp\left(-\pi \ \left(\lambda_M x_M^2 + \lambda_S \kappa^2\right)\right) \ \mathrm{d}x_M & \kappa \geq R_{CS} \\ \exp\left(-\pi \ \left(\lambda_M x_M^2 + \lambda_S R_{CS}^2\right)\right) \ \mathrm{d}x_M & \kappa < R_{CS} \end{cases}, \quad (3.14)$$

where $\kappa = (P_S B_S \eta_S / P_M)^{1/\alpha_{1S}} \, x_M^{\alpha_{0M}/\alpha_{1S}}$.

The expression presented in (3.14) determines the association likelihood of UEs with macro tier when their distance is less than R_{CM}. Naturally, it is most likely that the UEs prefer macro tier association in this region owing to the higher transmit power of MBSs and greater distances from small tier BSs. Intuitively, if the UEs are to be offloaded to smaller tier in this association region then a relatively higher SBS biasing level would be required.

Proof: Please refer to Appendix A.2. ■

The expression for association probability of T-UE with small tier in region R-III can be determined by following the approach used in the derivation of (3.14), and the final result is given as

$$\mathcal{A}_{\mathcal{S},\text{R-III}} = 2\pi\lambda_S \int_{R_{CS}}^{\infty} x_S \left[\exp\left(-\pi\lambda_M {k_C}^2\right) - \exp\left(-\pi\lambda_M R_{CM}^2\right)\right] \exp\left(-\pi\lambda_S x_S^2\right) \ \mathrm{d}x_S, \quad (3.15)$$

where $k_C = (P_M / P_S B_S \eta_S)^{1/\alpha_{0M}} \, x_S^{\alpha_{1S}} / \alpha_{0M}$.

Lemma 3.3.4*: The association probability of T-UE with macro tier in R-IV using DS-PLM is given as*

$$\mathcal{A}_{\mathcal{M},R\text{-}IV} = 2\pi\lambda_M \int_0^{R_{CM}} x_M \left(\exp\left(-\pi \left(\lambda_M x_M^2 + \lambda_S \left(\frac{P_S B_S x_M^{\alpha_{0M}}}{P_M} \right)^{2/\alpha_{0S}} \right) \right) \right.$$

$$- \exp\left(-\pi\left(\lambda_M x_M^2 + \lambda_S R_{CS}^2\right)\right)\Bigg) \mathrm{d}x_M. \quad (3.16)$$

Proof: Please refer to Appendix A.3. ■

Finally, by plugging (3.5), (3.12), (3.14) and (3.16) in (3.4) we get the complete expression for T-UE macro association probability when DS-PLM is used. Moreover, it is clear from the derived expressions of each region that disparity in transmit power of both tiers is the primary reason for creating load imbalance between the BS tiers, and it could be finely tuned by opting subtle values of B_S and R_{CS} as both parameters can assist in proactive offloading of UEs to smaller tier.

Similar to the derivation of (3.16), the association probability of T-UE with small tier in R-IV using DS-PLM is given as

$$\mathcal{A}_{\mathcal{S},\text{R-IV}} = 2\pi\lambda_S \int_0^{R_{CS}} x_S \Bigg(\exp\left(-\pi\left(\lambda_S x_S^2 + \lambda_M \left(\frac{P_M x_S^{\alpha_{0S}}}{P_S B_S}\right)^{2/\alpha_{0M}}\right)\right) - \exp\left(-\pi\left(\lambda_S x_S^2 + \lambda_M R_{CM}^2\right)\right)\Bigg) \mathrm{d}x_S. \quad (3.17)$$

Moreover, the analysis of T-AP using DS-PLM does not add to the complexity as the generalized expression of T-AP in case of SS-PLM is also integral-based [68]. Furthermore, the expression for T-AP is efficiently computed numerically in contrast to the Monté Carlo methods which heavily rely on time consuming and exhaustive experiment repetitions to account for the randomnesses.

Remark 3.3.1*: The derived expression given in (3.4) for macro T-AP using DS-PLM in a two-tier HCN is integral-based, and it is similar to the kth tier association probability expression determined in [68] using SS-PLM. In-fact, (3.4) reduces to the same integral-based expression presented in [68] for SS-PLM based two-tier HCN when* $R_{CM} = R_{CS} = d_{0i} = 1m$ *while* $\alpha_{0_M} = \alpha_{1_M}$ *and* $\alpha_{0_S} = \alpha_{1_S}$ *is considered. Moreover, (3.4) further simplifies to a closed-form solution when it is assumed*

that all path loss exponents are same i.e. $\alpha_{0_M} = \alpha_{0_S} = \alpha_{1_M} = \alpha_{1_S} = \alpha$.

$$\mathcal{A}_{\mathcal{M}} = \frac{\lambda_M}{\left(\lambda_M + (P_S B_S / P_M)^{\frac{2}{\alpha}} \lambda_S\right)} \tag{3.18}$$

From (3.18), it can be easily inferred that the UE association with any tier is more dominantly influenced by its spatial density when compared with either of the transmit powers or biasing factors. This simplified result depicts a different story to the DS-PLM case, which shows a reasonable sensitivity to both critical distance and biasing as they play a vital role in UE offloading to smaller tiers.

3.3.2 Distribution of the Statistical Distance between T-UE and its Serving BS

In order to determine the network coverage, it is important to derive the distance distribution between T-UE and its serving BS. Prior to the derivation of distance PDFs for MBSs is presented, it is vital to understand that the T-UE could be associated with any tier in two ways given the UE association policy is fulfilled i.e., when its distance with the nearest MBS is greater than R_{CM} or lesser to it. Therefore, we derive two PDFs of X_M conditioned on the distance between T-UE and its nearest associated MBS.

Lemma 3.3.5*: The PDF given T-UE is located at distance greater than* R_{CM} *from its associated MBS is given as*

$$f_{X_M|X_M>R_{CM}}(x_M) = \frac{2\pi\lambda_M x_M}{\mathcal{A}_{\mathcal{M},R\text{-}I} + \mathcal{A}_{\mathcal{M},R\text{-}II}} \begin{cases} \exp\left(-\pi\left(\lambda_M x_M^2 + \lambda_S \beta^2\right)\right) & \beta \geq R_{CS} \\ \exp\left(-\pi\left(\lambda_M x_M^2 + \lambda_S \gamma^2\right)\right) & \beta < R_{CS} \end{cases}. \tag{3.19}$$

Proof: For a macro tier associated T-UE which is located at a distance greater than R_{CM} from its nearest MBS, the likelihood of event $X_M > x_M$ is given as

$$\mathbb{P}\left[X_M > x_M\right] = \mathbb{P}\left[X_M > x_M | \left(\mathcal{A}_{\mathcal{M}}, X_M > R_{CM}\right)\right]. \tag{3.20}$$

By converting the right hand side (R.H.S) of (3.20) into joint probability, we get

$$\mathbb{P}\left[X_M > x_M\right] = \frac{\mathbb{P}\left[X_M > x_M, {P_r}^M > {P_r}^S, X_M > R_{CM}\right]}{\mathbb{P}\left[{P_r}^M > {P_r}^S, X_M > R_{CM}\right]}. \tag{3.21}$$

In (3.21), the sub-event $\left[{P_r}^M > {P_r}^S, X_M > R_{CM}\right]$ can be expanded based on the knowledge of association probability regions i.e., R-I and R-II to get

$$\begin{aligned}\left[{P_r}^M > {P_r}^S, X_M > R_{CM}\right] = &\left[{P_r}^M > {P_r}^S, X_M > R_{CM}, X_S > R_{CS}\right] \\ &\cup \left[{P_r}^M > {P_r}^S, X_M > R_{CM}, X_S < R_{CS}\right]. \end{aligned} \tag{3.22}$$

The R.H.S of (3.22) refers to two disjoint events, and by using (3.6) and (A.1), (3.22) can be rewritten as

$$\left[{P_r}^M > {P_r}^S, X_M > R_{CM}\right] = \mathcal{A}_{\mathcal{M},\text{R-I}} + \mathcal{A}_{\mathcal{M},\text{R-II}}. \tag{3.23}$$

Now by inserting (3.23) into (3.21) to get

$$\mathbb{P}\left[X_M > x_M\right] = \frac{\begin{cases}\mathbb{P}\left[X_M > x_M, (X_S > \beta, X_M > R_{CM})\right] & X_S > R_{CS} \\ \mathbb{P}\left[X_M > x_M, (X_S > \gamma, X_M > R_{CM})\right] & X_S < R_{CS}\end{cases}}{\mathcal{A}_{\mathcal{M},\text{R-I}} + \mathcal{A}_{\mathcal{M},\text{R-II}}}. \tag{3.24}$$

The expression in (3.24) is simplified with the help of (3.8) and (3.12), and by using the PDF of X_M, it can be expressed as

$$\mathbb{P}\left[X_M > x_M\right] = \begin{cases} \dfrac{\int_{x_M}^{\infty} \mathbb{P}\left[X_S > \beta \ \cap \ X_S > R_{CS}\right] f_{X_M}(x_M)\, \mathrm{d}x_M}{\mathcal{A}_{\mathcal{M},\text{R-I}} + \mathcal{A}_{\mathcal{M},\text{R-II}}} & \beta \geq \ R_{CS} \\ \dfrac{\int_{x_M}^{\infty} \mathbb{P}\left[X_S > \gamma \ \cap \ X_S < R_{CS}\right] f_{X_M}(x_M)\, \mathrm{d}x_M}{\mathcal{A}_{\mathcal{M},\text{R-I}} + \mathcal{A}_{\mathcal{M},\text{R-II}}} & \beta < \ R_{CS} \end{cases}. \tag{3.25}$$

The CDF of X_M is given by $F_{X_M}(x_M) = 1 - \mathbb{P}[X_M > x_M]$, and the desired PDF of X_M conditioned on distance between T-UE and associated MBS greater than R_{CM} is obtained by taking derivative of its CDF followed by simplification to complete the proof of (3.19). ■

Lemma 3.3.6*: The PDF given T-UE is located at distance smaller than R_{CM} from its associated MBS is given as*

$$f_{X_M|X_M<R_{CM}}(x_M) = \left(\frac{2\pi\lambda_M x_M}{\mathcal{A}_{\mathcal{M},R\text{-}III} + \mathcal{A}_{\mathcal{M},R\text{-}IV}}\right) \begin{cases} \exp\left(-\pi\left(\lambda_M x_M^2 + \lambda_S g_A^2\right)\right) & \kappa \leq \ R_{CS} \\ g_C + \exp\left(-\pi\left(\lambda_M x_M^2 + \lambda_S \kappa^2\right)\right) & \kappa > R_{CS} \end{cases}, \tag{3.26}$$

where

$g_C = \exp(-\pi(\lambda_M x_M^2 + \lambda_S \left(P_S B_S x_M^{\alpha_{0M}}/P_M\right)^{2/\alpha_{0S}})) - \exp\left(-\pi\left(\lambda_M x_M^2 + \lambda_S R_{CS}^2\right)\right)$,
and $g_A = \left(P_S B_S/P_M\right)^{1/\alpha_{0S}} x_M^{\alpha_{0M}/\alpha_{0S}}$.

Proof: Please refer to Appendix A.4. ■

Lemma 3.3.7*: The PDF given T-UE is located at distance greater than R_{CS} from its associated SBS is given as*

$$f_{X_S|X_S>R_{CS}}(x_S) = \frac{2\pi\lambda_S x_S}{\mathcal{A}_{\mathcal{S},R\text{-}I} + \mathcal{A}_{\mathcal{S},R\text{-}III}} \begin{cases} \exp\left(-\pi\left(\lambda_S x_S^2 + \lambda_M {k_A}^2\right)\right) & k_A \geq R_{CM} \\ \exp\left(-\pi\left(\lambda_S x_S^2 + \lambda_M {k_C}^2\right)\right) & k_A < R_{CM} \end{cases}, \tag{3.27}$$

where $\mathcal{A}_{\mathcal{S},\text{R-I}}$ and $\mathcal{A}_{\mathcal{S},\text{R-III}}$ are given in (3.11) and (3.15) respectively.

Proof: For a smaller tier associated T-UE which is located at a distance greater than R_{CS} from its nearest SBS, the likelihood of event $X_S > x_S$ is given as

$$\mathbb{P}\left[X_S > x_S\right] = \mathbb{P}\left[X_S > x_S | \left(\mathcal{A}_{\mathcal{S}}, X_S > R_{CS}\right)\right]. \tag{3.28}$$

By converting the right hand side (R.H.S) of (3.28) into joint probability, we get

$$\mathbb{P}\left[X_S > x_S\right] = \frac{\mathbb{P}\left[X_S > x_S, {P_r}^S > {P_r}^M, X_S > R_{CS}\right]}{\mathbb{P}\left[{P_r}^S > {P_r}^M, X_S > R_{CS}\right]}. \tag{3.29}$$

In (3.29), the sub-event $\mathbb{P}\left[{P_r}^S > {P_r}^M, X_S > R_{CS}\right]$ can be expanded based on the knowledge of association probability regions i.e., R-I and R-III to get

$$\begin{aligned}\mathbb{P}\left[{P_r}^S > {P_r}^M, X_S > R_{CS}\right] = \mathbb{P}\left[{P_r}^S > {P_r}^M, X_S > R_{CS}, X_M > R_{CM}\right] \\ \cup \mathbb{P}\left[{P_r}^S > {P_r}^M, X_S > R_{CS}, X_M < R_{CM}\right].\end{aligned} \tag{3.30}$$

The R.H.S of (3.30) refers to two mutually exclusive events that cannot occur at the same time, and thus can be rewritten as

$$\mathbb{P}\left[{P_r}^S > {P_r}^M, X_S > R_{CS}\right] = \mathcal{A}_{\mathcal{S},\text{R-I}} + \mathcal{A}_{\mathcal{S},\text{R-III}}. \tag{3.31}$$

Now by inserting (3.31) into (3.29) and after simplification, we get

$$\mathbb{P}\left[X_S > x_S\right] = \frac{\begin{cases}\mathbb{P}\left[X_S > x_S, (X_M > k_A \ \cap \ X_S > R_{CS})\right] & X_M \geq R_{CM} \\ \mathbb{P}\left[X_S > x_S, (X_M > k_C \ \cap \ X_S > R_{CS})\right] & X_M < R_{CM}\end{cases}}{\mathcal{A}_{\mathcal{S},\text{R-I}} + \mathcal{A}_{\mathcal{S},\text{R-III}}}, \tag{3.32}$$

By using the PDF of X_S, (3.32) can be expressed as

$$\mathbb{P}\left[X_S > x_S\right] = \begin{cases} \dfrac{\int_{x_S}^{\infty} \mathbb{P}\left[X_M > k_A \ \cap \ X_M > R_{CM}\right] f_{X_S}(x_S)\ \mathrm{d}x_S}{\mathcal{A}_{\mathcal{S},\text{R-I}} + \mathcal{A}_{\mathcal{S},\text{R-III}}} & k_A \geq \ R_{CM} \\ \dfrac{\int_{x_S}^{\infty} \mathbb{P}\left[X_M > k_C \ \cap \ X_M < R_{CM}\right] f_{X_S}(x_S)\ \mathrm{d}x_S}{\mathcal{A}_{\mathcal{S},\text{R-I}} + \mathcal{A}_{\mathcal{S},\text{R-III}}} & k_A < \ R_{CM} \end{cases}. \tag{3.33}$$

The CDF of X_S is given by $F_{X_S}(x_S) = 1 - \mathbb{P}[X_S > x_S]$, and the desired PDF of X_S conditioned on distance between T-UE and associated SBS greater than R_{CS} is obtained by taking derivative of its CDF followed by simplification to complete the proof of (3.27). ■

Lemma 3.3.8*: The PDF given T-UE is located at distance smaller than R_{CS} from its associated SBS is given as*

$$f_{X_S|X_S<R_{CS}}(x_S) = \frac{2\pi\lambda_S x_S \begin{cases} \exp\left(-\pi\left(\lambda_S x_S^2 + \lambda_M q_A^2\right)\right) & k_B \leq \ R_{CM} \\ q_B + \exp\left(-\pi\left(\lambda_S x_S^2 + \lambda_M {k_B}^2\right)\right) & k_B > R_{CM} \end{cases}}{\mathcal{A}_{\mathcal{S},\text{R-II}} + \mathcal{A}_{\mathcal{S},\text{R-IV}}}, \tag{3.34}$$

where
$q_B = \exp(-\pi(\lambda_S x_S^2 + \lambda_M \left(P_M x_S^{\alpha_{0S}} / P_S B_S\right)^{2/\alpha_{0M}})) - \exp\left(-\pi\left(\lambda_S x_S^2 + \lambda_M R_{CM}^2\right)\right)$, and
$q_A = \left(P_M / P_S B_S\right)^{1/\alpha_{0M}} x_S^{\alpha_{0S}/\alpha_{0M}}$.

Proof: Please refer to Appendix A.5. ■

3.4 Coverage Probability

The T-UE is said to be in network coverage if the received instantaneous SINR from its associated BS is above a predefined target τ. As discussed in the previous section, employing DS-PLM divides the coverage area of any BS into two

non-overlapping regions. Hence, the T-UE could be in coverage from tier i by associating with it while lying at a distance smaller or farther than R_{Ci} from nearest BS in that tier i.

Densification of SBSs in the overlaid network is like a double-edged sword, it brings the network resource in close proximity to UEs which helps in achieving the desired data rates but at the cost of excessive interference. To account for the detrimental impact of this increased level of interference, a simple yet effective frequency reuse mechanism has been employed. In accordance with the system model, if the T-UE associates with a BS which operates at frequency channel N, then it would receive interference only from that particular set of BSs that operate at N. Hence, all other BSs operating at different frequency channels will not add to the cumulative interference faced by the T-UE.

For computing the complete network coverage of two-tier HCN, the conditional coverage offered by each of the tiers in both the regions i.e., $X_i > R_{Ci}$ and $X_i < R_{Ci}$, where $i \, \epsilon \, M, S$, is to be determined. Thus, the complete network coverage is governed by the total probability law as

$$\mathbb{C}_{\mathbb{P}} = \sum_{i=1}^{2} \sum_{j=1}^{2} (\mathrm{C}_{\mathrm{P_{i|R_j}}}, \mathcal{A}_{i,R_j}), \tag{3.35}$$

where i refers to the number of BS tiers in HCN, while j indicates the newly formed regions which are dependent on R_{Ci}. The coverage offered by tier i to T-UE located in region j, given the T-UE is associated with tier i is denoted by $\mathrm{C}_{\mathrm{P_{i|R_j}}}$. Moreover, $\mathcal{A}_{i,R_j}$ represents the joint association probability of T-UE with ith tier while it lies in region j. For instance, $\mathcal{A}_{M,R_2}$ refers to macro association of T-UE while the distance between T-UE and its associated MBS is smaller than R_{CM} i.e., $\mathcal{A}_{M,R_2} = \mathcal{A}_{\mathcal{M},\text{R-III}} + \mathcal{A}_{\mathcal{M},\text{R-IV}}$ where $\mathcal{A}_{\mathcal{M},\text{R-III}}$ and $\mathcal{A}_{\mathcal{M},\text{R-IV}}$ have already been determined in section 3.3.1. It is important to note that, the T-UE can only be associated with a single tier at once while being located in one of the two mutually exclusive regions.

The CCDF of SINR ($\Gamma_{X_i}(x_i)$) of T-UE at a distance x_i from its associated ith tier BS can be expressed by using (3.1) as

$$\mathbb{P}[\Gamma_{X_i}(x_i) > \tau] = \mathbb{P}\left[\frac{P_i h_{Xi} l\left(x_i\right)}{I + \sigma^2} > \tau\right], \tag{3.36}$$

where $l(x_i)$ represents the path loss in general, while I denotes the cumulative interference received by T-UE from both co-tier and inter-tier interfering BSs that are operating at a common frequency channel. Solving for h_{Xi} in (3.36) gives

$$\mathbb{P}[\Gamma_{X_i}(x_i) > \tau] = \mathbb{P}\left[h_{Xi} > \frac{\tau\left(I + \sigma^2\right)}{P_i l\left(x_i\right)}\right], \tag{3.37}$$

where h_{Xi} represents the channel gains which are assumed to be Rayleigh distributed, thus the simplified form of (3.37) is given as

$$\mathbb{P}[\Gamma_{X_i}(x_i) > \tau] = \exp\left(\frac{-\tau\sigma^2}{P_i l\left(x_i\right)}\right) \mathcal{L}_{\mathcal{I}_\mathcal{M}}\left(\frac{\tau}{P_i l(x_i)}\right) \mathcal{L}_{\mathcal{I}_\mathcal{S}}\left(\frac{\tau}{P_i l(x_i)}\right), \tag{3.38}$$

where $\mathcal{L}_{\mathcal{I}_\mathcal{M}}$ and $\mathcal{L}_{\mathcal{I}_\mathcal{S}}$ are the Laplace transforms of interference from macro and small tier BSs respectively. It is clear from (3.38) that the UE can associate with any BS tier, but it faces interference from both tier BSs.

3.4.1 Coverage Probability of T-UE Associated with Macro Tier

The coverage probability of T-UE associated with macro tier is defined as the likelihood of receiving instantaneous SINR from the closest MBS at T-UE greater than the predefined threshold τ. As per the system model, the T-UE can associate with macro tier (i.e., receives higher power from the nearest MBS as compared to the nearest SBS) in two regions i.e., when the distance between T-UE and the closest MBS is either greater or smaller than R_{CM}. Therefore, the CCDF of received SINR at T-UE which is located at distance x_i has to be computed for both the regions. Next, we determine the contribution of each region.

Proposition 3.4.1*: The expression for macro tier coverage in the region* $X_M > R_{CM}$ *is given as*

$$\mathrm{C}_{P_M|X_M>R_{CM}}(x_M) = \frac{2\pi\lambda_M}{\mathcal{A}_{\mathcal{M},R\text{-}I} + \mathcal{A}_{\mathcal{M},R\text{-}II}} \int_{R_{CM}}^{\infty} x_M \exp\left(\frac{-\tau\sigma^2}{P_M\eta_M L_0 x_M^{-\alpha_{1M}}}\right) \times \exp\left(\frac{-2\pi\lambda_M\tau {x_M}^2}{N(-2+\alpha_{1M})}\ {}_2F_1\left[1, 1-\frac{2}{\alpha_{1M}}; 2-\frac{2}{\alpha_{1M}}; -\tau\right]\right) \times \begin{cases} \exp\left(-\pi\left(\lambda_M x_M^2 + \lambda_S\beta^2\right)\right) \exp\left(\frac{-2\pi\lambda_S\tau\beta^2}{N(-2+\alpha_{1S})}\right. & \\ \qquad \left. \times\ {}_2F_1\left[1, 1-\frac{2}{\alpha_{1S}}; 2-\frac{2}{\alpha_{1S}}; -\frac{\tau}{B_S}\right]\right) \mathrm{d}x_M & \beta \geq R_{CS} \\ \exp\left(-\pi\left(\lambda_M x_M^2 + \lambda_S\gamma^2\right)\right) \exp\left(\frac{-2\pi\lambda_S\tau g_B x_M^{\alpha_{1M}} {R_{CS}}^{2-\alpha_{1S}}}{N(-2+\alpha_{1S})}\right. & \\ \qquad \left. \times\ {}_2F_1\left[1, 1-\frac{2}{\alpha_{1S}}; 2-\frac{2}{\alpha_{1S}}; -\frac{\tau g_B x_M^{\alpha_{1M}}}{{R_{CS}}^{\alpha_{1S}}}\right]\right) \mathrm{d}x_M & \beta < R_{CS} \end{cases}, \quad (3.39)$$

where $g_B{=}P_S\eta_S/P_M\eta_M$.

Proof: The macro tier coverage in the region $X_M > R_{CM}$ is given by the following integral equation as

$$\mathrm{C}_{P_M|X_M>R_{CM}}(x_M) = \int_{R_{CM}}^{\infty} \mathbb{P}[\Gamma_{X_{M|X_M>R_{CM}}}(x_M) > \tau]\ f_{X_M|X_M>R_{CM}}(x_M)\ \mathrm{d}x_M, \quad (3.40)$$

where $f_{X_M|X_M>R_{CM}}(x_M)$ is already determined in section 3.3.2 and is given in (3.19), while $\mathbb{P}[\Gamma_{X_{M|X_M>R_{CM}}}(x_M) > \tau]$ is yet to be derived. The limits of integration in (3.40) are from R_{CM} to ∞, as the distance between T-UE and the closest MBS (to which the T-UE associates) is greater than R_{CM}.

Using (3.38) and substituting the respective parametric values, the CCDF conditioned on X_M greater than R_{CM} can be expressed as

$$\mathbb{P}[\Gamma_{X_M|X_M>R_{CM}}(x_M) > \tau] = \exp\left(\frac{-\tau\sigma^2 x_M^{\alpha_{1M}}}{P_M\eta_M L_0}\right)\mathcal{L}_{\mathcal{I}_\mathcal{M}}\left(\frac{\tau\ x_M^{\alpha_{1M}}}{P_M\eta_M}\right)\mathcal{L}_{\mathcal{I}_\mathcal{S}}\left(\frac{\tau\ x_M^{\alpha_{1M}}}{P_M\eta_M}\right). \tag{3.41}$$

The computation of (3.41) further requires determining the summation of interference from all co-tier ($\mathcal{L}_{\mathcal{I}_\mathcal{M}}$) and inter-tier ($\mathcal{L}_{\mathcal{I}_\mathcal{S}}$) interfering BSs that are operating at frequency channel N. Using Campbell Mecke theorem and probability generating functional (PGFL) of PPP, the Laplace transform, $\mathcal{L}_{\mathcal{I}_\mathcal{M}}$ is given as

$$\mathcal{L}_{\mathcal{I}_\mathcal{M}}\left(\tau\left(P_M\eta_M\right)^{-1}x_M^{\alpha_{1M}}\right) = \exp\left(\frac{-2\pi\lambda_M}{N}\int_{x_M}^{\infty}\frac{y}{1+\left(x_M^{\alpha_{1M}}\tau\right)^{-1}y^{\alpha_{1M}}}\mathrm{d}y\right), \tag{3.42}$$

where the distance of T-UE from co-tier MBSs which are operating at frequency channel N is greater than R_{CM}. Therefore, the integration limits in computation of $\mathcal{L}_{\mathcal{I}_\mathcal{M}}$ are from x_M to ∞. Simplifying the integrand in (3.42) by substituting $u_M = \left(x_M^{\alpha_{1M}}\tau\right)^{-2/\alpha_{1M}}y^2$ and solving it gives

$$\mathcal{L}_{\mathcal{I}_\mathcal{M}}\left(\tau\left(P_M\eta_M\right)^{-1}x_M^{\alpha_{1M}}\right) = \exp\left(\frac{-2\pi\lambda_M\tau x_M^2}{N(-2+\alpha_{1M})}{}_2F_1\left[1, 1-\frac{2}{\alpha_{1M}}; 2-\frac{2}{\alpha_{1M}}; -\tau\right]\right), \tag{3.43}$$

where ${}_2F_1[\ .\ ]$ is the well-known Gauss Hypergeometric function and (3.43) gives the contribution of macro tier interference in CCDF conditioned on x_M greater than R_{CM}. Similar to (3.42), the $\mathcal{L}_{\mathcal{I}_\mathcal{S}}$ is also expressed as

$$\mathcal{L}_{\mathcal{I}_\mathcal{S}}\left(\tau\left(P_M\eta_M\right)^{-1}x_M^{\alpha_{1M}}\right) = \exp\left(\frac{-2\pi\lambda_S}{N}\begin{cases}\int_\beta^\infty \frac{y}{1+\left(x_M^{\alpha_{1M}}\frac{P_S\eta_S}{P_M\eta_M}\tau\right)^{-1}y^{\alpha_{1S}}}\mathrm{d}y & \beta \le\ R_{CS}\\ \int_\beta^\infty \frac{y}{1+\left(x_M^{\alpha_{1M}}\frac{P_S\eta_S}{P_M\eta_M}\tau\right)^{-1}y^{\alpha_{1S}}}\mathrm{d}y & \beta >\ R_{CS}\end{cases}\right), \tag{3.44}$$

where the integration limits in (3.44) are from β to ∞, as the cross-tier interferers are at least apart by β, given x_M is greater than R_{CM}. Moreover, similar to (3.42), the T-UE faces interference from only those SBSs which are operating at frequency channel N. Simplifying the integrand in (3.44) by substituting $v_M =$

$(x_M^{\alpha_{1M}} P_S \eta_S / P_M \eta_M \tau)^{-2/\alpha_{1S}}\, y^2$ and solving it gives

$$\mathcal{L}_{\mathcal{I}_\mathcal{S}}\left(\tau\left(P_M\eta_M\right)^{-1} x_M^{\alpha_{1M}}\right) = \begin{cases} \exp\left(\frac{-2\pi\lambda_S\tau g_B x_M^{\alpha_{1M}}}{N(-2+\alpha_{1S}){R_{CS}}^{-2+\alpha_{1S}}} \right. \\ \left. \times\ {}_2F_1\left[1, 1-\frac{2}{\alpha_{1S}}; 2-\frac{2}{\alpha_{1S}}; -\frac{\tau g_B x_M^{\alpha_{1M}}}{{R_{CS}}^{\alpha_{1S}}}\right]\right) & \beta \leq\ R_{CS} \\ \exp\left(\frac{-2\pi\lambda_S\tau\beta^2}{N(-2+\alpha_{1S})} \right. \\ \left. \quad \times\ {}_2F_1\left[1, 1-\frac{2}{\alpha_{1S}}; 2-\frac{2}{\alpha_{1S}}; -\frac{\tau}{B_S}\right]\right) & \beta >\ R_{CS} \end{cases}, \tag{3.45}$$

where (3.45) gives the contribution of inter-tier interference in macro CCDF conditioned on x_M greater than R_{CM}. Now by plugging the values of $\mathcal{L}_{\mathcal{I}_\mathcal{M}}$ and $\mathcal{L}_{\mathcal{I}_\mathcal{S}}$ in (3.41), results in

$$\begin{aligned} \mathbb{P}[\Gamma_{X_{M|X_M>R_{CM}}}(x_M) > \tau] = \exp\left(\frac{-\tau\sigma^2}{P_M\eta_M L_0 x_M^{-\alpha_{1M}}}\right) \\ \exp\left(\frac{-2\pi\lambda_M\tau\ x_M^2}{N(-2+\alpha_{1M})}\ {}_2F_1\left[1, 1-\frac{2}{\alpha_{1M}}; 2-\frac{2}{\alpha_{1M}}; -\tau\right]\right) \\ \times \begin{cases} \exp\left(\frac{-2\pi\lambda_S\tau g_B x_M^{\alpha_{1M}}}{N(-2+\alpha_{1S})\left({R_{CS}}^{-2+\alpha_{1S}}\right)} \right. \\ \left. \quad \times\ {}_2F_1\left[1, 1-\frac{2}{\alpha_{1S}}; 2-\frac{2}{\alpha_{1S}}; -\frac{\tau g_B x_M^{\alpha_{1M}}}{{R_{CS}}^{\alpha_{1S}}}\right]\right) & \beta \leq\ R_{CS}\ . \\ \exp\left(\frac{-2\pi\lambda_S\tau\beta^2}{N(-2+\alpha_{1S})}{}_2F_1\left[1, 1-\frac{2}{\alpha_{1S}}; 2-\frac{2}{\alpha_{1S}}; -\frac{\tau}{B_S}\right]\right) & \beta >\ R_{CS} \end{cases} \end{aligned} \tag{3.46}$$

Finally by inserting (3.46) into (3.40), we get the desired expression for macro tier coverage in R_1 to complete the proof of (3.39). ■

Proposition 3.4.2*: The expression for macro tier coverage in the region $X_M < R_{CM}$ is given as*

$$\mathrm{C}_{P_M|X_M<R_{CM}}(x_M) = \frac{2\pi\lambda_M}{\mathcal{A}_{\mathcal{M},\text{R-III}} + \mathcal{A}_{\mathcal{M},\text{R-IV}}} \int_0^{R_{CM}} \left(x_M \exp\left(\frac{-\tau\sigma^2}{P_M L_0 x_M^{-\alpha_{0M}}}\right)\right.$$

$$\times \exp\left[\frac{-2\pi\lambda_S}{N}\left(-\frac{g_A^2}{2}{}_2F_1\left[1,\frac{2}{\alpha_{0S}};1+\frac{2}{\alpha_{0S}};-\frac{B_S}{\tau}\right]\right.\right.$$
$$+\frac{R_{CS}^2}{2}{}_2F_1\left[1,\frac{2}{\alpha_{0S}};1+\frac{2}{\alpha_{0S}};-\frac{P_M R_{CS}^{\alpha_{0S}}}{P_S x_M^{\alpha_{1M}}\tau}\right]$$
$$\left.\left.+\frac{P_S\eta_S\tau x_M^{\alpha_{0M}}R_{CS}^{2-\alpha_{1S}}}{P_M\left(-2+\alpha_{1S}\right)}{}_2F_1\left[1,1-\frac{2}{\alpha_{1S}};2-\frac{2}{\alpha_{1S}};-\frac{P_S\eta_S x_M^{\alpha_{0M}}\tau}{P_M R_{CS}^{\alpha_{1S}}}\right]\right)\right]$$
$$\times \exp\left[-\frac{2\pi\lambda_M}{N}\left(\left(-\frac{x_M^2}{2}\ {}_2F_1\left[1,\frac{2}{\alpha_{0M}};1+\frac{2}{\alpha_{0M}};-\frac{1}{\tau}\right]\right)\right.\right.$$
$$+\frac{R_{CM}^2}{2}\ {}_2F_1\left[1,\frac{2}{\alpha_{0M}};1+\frac{2}{\alpha_{0M}};-\left(\frac{R_{CM}}{x_M}\right)^{\alpha_{0M}}\frac{1}{\tau}\right]$$
$$\left.\left.+\frac{\eta_M\tau x_M^{\alpha_{0M}}R_{CM}^{2-\alpha_{1M}}}{-2+\alpha_{1M}}{}_2F_1\left[1,1-\frac{2}{\alpha_{1M}};2-\frac{2}{\alpha_{1M}};-\frac{\eta_M x_M^{\alpha_{0M}}\tau}{R_{CM}^{\alpha_{1M}}}\right]\right)\right]$$
$$\times\left\{\begin{array}{ll}\exp\left(-\pi\left(\lambda_M x_M^2+\lambda_S g_A^2\right)\right) & \kappa\leq\ R_{CS}\\ g_C+\exp\left(-\pi\left(\lambda_M x_M^2+\lambda_S\kappa^2\right)\right) & \kappa>R_{CS}\end{array}\right)\mathrm{d}x_M. \quad (3.47)$$

Proof: Please refer to Appendix A.6. ■

By evaluating the derived integral-based expressions of conditional coverage in (3.39) and (3.47) for both regions, the conditional coverage of macro tier is obtained.

3.4.2 Coverage Probability of T-UE Associated with Small Tier

The coverage probability of T-UE associated with small tier is defined as the likelihood of receiving instantaneous SINR from the nearest SBS at T-UE greater than the predefined threshold τ. Similar to macro tier association of T-UE, the link distance between T-UE and its associated SBS can be either greater or smaller than the R_{CS}. Hence, the coverage expressions for both regions are required to determine the complete contribution of small tier coverage in the total network coverage offered by the deployed HCN.

Proposition 3.4.3*: The expression for small tier coverage in the region $X_S > R_{CS}$ is given as*

$$\mathrm{C}_{P_S|X_S>R_{CS}}(x_S) = \frac{2\pi\lambda_S}{\mathcal{A}_{\mathcal{S},R\text{-}I} + \mathcal{A}_{\mathcal{S},R\text{-}III}} \int_{R_{CS}}^{\infty} x_S \exp\left(\frac{-\tau\sigma^2}{P_S\eta_S L_0 x_S^{-\alpha_{1S}}}\right) \times \exp\left(\frac{-2\pi\lambda_S\tau\ x_S^2}{N(-2+\alpha_{1S})}\ {}_2F_1\left[1, 1-\frac{2}{\alpha_{1S}}; 2-\frac{2}{\alpha_{1S}}; -\tau\right]\right) \times \begin{cases} \exp\left(-\pi\left(\lambda_S x_S^2 + \lambda_M {k_A}^2\right)\right) \exp\left(\frac{-2\pi\lambda_M\tau B_S k_A^2}{N(-2+\alpha_{1M})} \times {}_2F_1\left[1, 1-\frac{2}{\alpha_{1M}}; 2-\frac{2}{\alpha_{1M}}; -\tau B_S\right]\right) \mathrm{d}x_S & k_A \geq R_{CM} \\ \exp\left(-\pi\left(\lambda_S x_S^2 + \lambda_M {k_C}^2\right)\right) \exp\left(\frac{-2\pi\lambda_M\tau B_S k_D {x_S}^2 {R_{CM}}^{2-\alpha_{1M}}}{N(-2+\alpha_{1M})} \times {}_2F_1\left[1, 1-\frac{2}{\alpha_{1M}}; 2-\frac{2}{\alpha_{1M}}; -\frac{k_D\tau {x_S}^{\alpha_{1S}}}{{R_{CM}}^{\alpha_{1M}}}\right]\right) \mathrm{d}x_S & k_A < R_{CM} \end{cases}, \tag{3.48}$$

where $k_D{=}P_M\eta_M/P_S\eta_S$.

Proof: The small tier coverage in the region $X_S > R_{CS}$ is given by the following integral equation as

$$\mathrm{C}_{P_S|X_S>R_{CS}}(x_S) = \int_{R_{CS}}^{\infty} \mathbb{P}[\Gamma_{X_{S|X_S>R_{CS}}}(x_S) > \tau]\ f_{X_S|X_S>R_{CS}}(x_S)\ \mathrm{d}x_S, \tag{3.49}$$

where $f_{X_S|X_S>R_{CS}}(x_S)$ is given in (3.27), while $\mathbb{P}[\Gamma_{X_{S|X_S>R_{CS}}}(x_S) > \tau]$ is yet to be derived. The limits of integration in (3.49) are from R_{CS} to ∞, as the distance between T-UE and its associated SBS is greater than R_{CS}.

Using (3.38) and substituting the respective parametric values, the CCDF conditioned on X_S greater than R_{CS} can be expressed as

$$\mathbb{P}[\Gamma_{X_{S|X_S>R_{CS}}}(x_S) > \tau] = \exp\left(\frac{-\tau\sigma^2 x_S^{\alpha_{1S}}}{P_S\eta_S L_0}\right) \mathcal{L}_{\mathcal{I}_\mathcal{S}}\left(\frac{\tau\ x_S^{\alpha_{1S}}}{P_S\eta_S}\right) \mathcal{L}_{\mathcal{I}_\mathcal{M}}\left(\frac{\tau\ x_S^{\alpha_{1S}}}{P_S\eta_S}\right). \tag{3.50}$$

The computation of (3.50) further requires determining the summation of interference from all co-tier ($\mathcal{L}_{\mathcal{I}_\mathcal{S}}$) and inter-tier ($\mathcal{L}_{\mathcal{I}_\mathcal{M}}$) interfering BSs that are operating at frequency channel N. The Laplace transform, $\mathcal{L}_{\mathcal{I}_\mathcal{S}}$ is given as

$$\mathcal{L}_{\mathcal{I}_\mathcal{S}}\left(\frac{\tau\ x_S^{\alpha_{1S}}}{P_S\eta_S}\right) = \exp\left(\frac{-2\pi\lambda_S}{N}\int_{x_S}^{\infty}\frac{y}{1+\left(x_S^{\alpha_{1S}}\tau\right)^{-1}y^{\alpha_{1S}}}\mathrm{d}y\right), \tag{3.51}$$

where the distance of T-UE from co-tier SBSs which are operating at frequency channel N is greater than R_{CM}. Therefore, the integration limits in computation of $\mathcal{L}_{\mathcal{I}_\mathcal{S}}$ are from x_S to ∞. Simplifying the integrand in (3.51) by substituting $u_S = \left(x_S^{\alpha_{1S}}\tau\right)^{-2/\alpha_{1S}}y^2$ and solving it gives

$$\mathcal{L}_{\mathcal{I}_\mathcal{S}}\left(\frac{\tau\ x_S^{\alpha_{1S}}}{P_S\eta_S}\right) = \exp\left(\frac{-2\pi\lambda_S\tau x_S^2}{N(-2+\alpha_{1S})}{}_2F_1\left[1,1-\frac{2}{\alpha_{1S}};2-\frac{2}{\alpha_{1S}};-\tau\right]\right), \tag{3.52}$$

where ${}_2F_1[\ .\ ]$ is the well-known Gauss Hypergeometric function and (3.52) gives the contribution of small tier interference in CCDF conditioned on x_S greater than R_{CS}.

Similar to (3.51), the $\mathcal{L}_{\mathcal{I}_\mathcal{M}}$ is also expressed as

$$\mathcal{L}_{\mathcal{I}_\mathcal{M}}\left(\frac{\tau\ x_S^{\alpha_{1S}}}{P_S\eta_S}\right) = \exp\left(\frac{-2\pi\lambda_M}{N}\begin{cases}\int_{k_A}^{\infty}\frac{y}{1+\left(x_S^{\alpha_{1S}}\frac{P_M\eta_M}{P_S\eta_S}\tau\right)^{-1}y^{\alpha_{1M}}}\mathrm{d}y\right) & k_A \leq R_{CM}\\ \int_{k_A}^{\infty}\frac{y}{1+\left(x_S^{\alpha_{1S}}\frac{P_M\eta_M}{P_S\eta_S}\tau\right)^{-1}y^{\alpha_{1M}}}\mathrm{d}y\right) & k_A > R_{CM}\end{cases}, \tag{3.53}$$

where the integration limits in (3.53) are from k_A to ∞, as the cross-tier BS interferers are at least apart by k_A, given x_S is greater than R_{CS}. Moreover, similar to (3.51), the T-UE faces interference from only those MBSs which are operating

at frequency channel N. Simplifying the integrand in (3.53) by substituting $v_S = (x_S^{\alpha_{1S}} P_M \eta_M / P_S \eta_S \tau)^{-2/\alpha_{1M}} y^2$ and solving it gives

$$\mathcal{L}_{\mathcal{I}_\mathcal{M}}\left(\frac{\tau\, x_S^{\alpha_{1S}}}{P_S \eta_S}\right) = \begin{cases} \exp\left(\frac{-2\pi\lambda_M \tau B_S k_A^2}{N(-2+\alpha_{1M})} \right. \\ \quad \left. \times\ {}_2F_1\left[1, 1-\frac{2}{\alpha_{1M}}; 2-\frac{2}{\alpha_{1M}}; -\tau B_S\right]\right) & k_A > R_{CM} \\ \exp\left(\frac{-2\pi\lambda_M \tau B_S k_D {x_S}^2 {R_{CM}}^{2-\alpha_{1M}}}{N(-2+\alpha_{1M})} \right. \\ \left. \times\ {}_2F_1\left[1, 1-\frac{2}{\alpha_{1M}}; 2-\frac{2}{\alpha_{1M}}; -\frac{k_D \tau {x_S}^{\alpha_{1S}}}{{R_{CM}}^{\alpha_{1M}}}\right]\right) & k_A \leq\ R_{CM} \end{cases}, \tag{3.54}$$

where (3.54) gives the contribution of inter-tier interference in small CCDF conditioned on x_S greater than R_{CS}. Now by plugging the values of $\mathcal{L}_{\mathcal{I}_\mathcal{S}}$ and $\mathcal{L}_{\mathcal{I}_\mathcal{M}}$ in (3.50), results in

$$\begin{aligned} \mathbb{P}[\Gamma_{X_{M|X_M>R_{CM}}}(x_M) > \tau] &= \exp\left(\frac{-\tau\sigma^2}{P_M \eta_M L_0 x_M^{-\alpha_{1M}}}\right) \\ &\times \exp\left(\frac{-2\pi\lambda_S \tau \beta^2}{N(-2+\alpha_{1S})} {}_2F_1\left[1, 1-\frac{2}{\alpha_{1S}}; 2-\frac{2}{\alpha_{1S}}; -\frac{\tau}{B_S}\right]\right) \\ &\times \begin{cases} \exp\left(\frac{-2\pi\lambda_M \tau B_S k_A^2}{N(-2+\alpha_{1M})} \right. \\ \quad \left. \times\ {}_2F_1\left[1, 1-\frac{2}{\alpha_{1M}}; 2-\frac{2}{\alpha_{1M}}; -\tau B_S\right]\right) & k_A > R_{CM} \\ \exp\left(\frac{-2\pi\lambda_M \tau B_S k_D {x_S}^2 {R_{CM}}^{2-\alpha_{1M}}}{N(-2+\alpha_{1M})} \right. \\ \left. \times\ {}_2F_1\left[1, 1-\frac{2}{\alpha_{1M}}; 2-\frac{2}{\alpha_{1M}}; -\frac{k_D \tau {x_S}^{\alpha_{1S}}}{{R_{CM}}^{\alpha_{1M}}}\right]\right) & k_A \leq\ R_{CM} \end{cases}. \end{aligned} \tag{3.55}$$

Finally by inserting (3.55) into (3.49), we get the desired expression for small tier coverage in R_1 to complete the proof of (3.48). ■

Proposition 3.4.4*: The expression for small tier coverage in the region $X_S < R_{CS}$ is given as*

$$\begin{aligned}
\mathrm{C}_{P_S|X_S<R_{CS}}(x_S) = \frac{2\pi\lambda_S}{\mathcal{A}_{\mathcal{S},R\text{-}II}+\mathcal{A}_{\mathcal{S},R\text{-}IV}} \int_0^{R_{CS}} \Bigg(x_S \exp\left(\frac{-\tau\sigma^2}{P_S L_0 x_S^{-\alpha_{0S}}}\right) \\
\times \exp\Bigg[\frac{-2\pi\lambda_S}{N}\Bigg(-\frac{x_S^2}{2}{}_2F_1\left[1,\frac{2}{\alpha_{0S}};1+\frac{2}{\alpha_{0S}};-\frac{1}{\tau}\right] \\
+\frac{R_{CS}^2}{2}{}_2F_1\left[1,\frac{2}{\alpha_{0S}};1+\frac{2}{\alpha_{0S}};-\frac{1}{\tau}\left(\frac{R_{CS}}{x_S}\right)^{\alpha_{0S}}\right] \\
+\frac{\eta_S\tau x_S^{\alpha_{0S}}\left(R_{CS}\right)^{2-\alpha_{1S}}}{(-2+\alpha_{1S})}{}_2F_1\left[1,1-\frac{2}{\alpha_{1S}};2-\frac{2}{\alpha_{1S}};-\frac{\tau\eta_S x_S^{\alpha_{0S}}}{R_{CS}^{\alpha_{1S}}}\right]\Bigg)\Bigg] \\
\times \exp\Bigg[-\frac{2\pi\lambda_M}{N}\Bigg(\Bigg(-\frac{\left(x_S^{\alpha_{0S}}P_M\right)^{2/\alpha_{0M}}}{2(P_S B_S)^{2/\alpha_{0M}}}\ {}_2F_1\left[1,\frac{2}{\alpha_{0M}};1+\frac{2}{\alpha_{0M}};-\frac{1}{B_S\tau}\right]\Bigg) \\
+\frac{R_{CM}^2}{2}\ {}_2F_1\left[1,\frac{2}{\alpha_{0M}};1+\frac{2}{\alpha_{0M}};-\left(\frac{P_S R_{CM}^{\alpha_{0M}}}{\tau P_M x_S^{\alpha_{0S}}}\right)\right] \\
+\frac{P_M\eta_M\tau x_S^{\alpha_{0S}}\left(R_{CM}\right)^{2-\alpha_{1M}}}{P_S(-2+\alpha_{1M})}{}_2F_1\left[1,1-\frac{2}{\alpha_{1M}};2-\frac{2}{\alpha_{1M}};-\frac{P_M\tau\eta_M x_S^{\alpha_{0S}}}{P_S R_{CM}^{\alpha_{1M}}}\right]\Bigg)\Bigg] \\
\times \begin{cases} \exp\left(-\pi\left(\lambda_S x_S^2+\lambda_M q_A^2\right)\right) & k_B \le R_{CM} \\ q_B+\exp\left(-\pi\left(\lambda_S x_S^2+\lambda_M {k_B}^2\right)\right) & k_B > R_{CM} \end{cases}\Bigg)\, \mathrm{d}x_S. \quad (3.56)
\end{aligned}$$

Proof: The expression for $\mathrm{C}_{P_S|X_S<R_{CS}}(x_S)$ can be similarly derived by following the procedure adopted in the derivation of (3.48). ■

Finally, the complete network coverage expression is determined from (3.35) when conditional coverage expressions of both tiers i.e., (3.39), (3.47), (3.48), and (3.56) are multiplied with their respective regional T-UE association probabilities.

3.4.3 Computational Complexity Comparison

In this subsection, we present the simulation algorithms for determining the coverage/outage in a two-tier HCN using DS-PLM and SS-PLM respectively. These algorithms are then used to estimate the computational complexity of the network performance evaluation using both PLMs [154].

Algorithm 1 Algorithm for determining coverage/outage in a two-tier HCN using SS-PLM

$S \leftarrow \lambda_S A$ i.e., The SBSs deployed in the network for each simulation run
$M \leftarrow \lambda_M A$ i.e., The MBSs deployed in the network for each simulation run
$x_U \leftarrow (0, 0)$ i.e., T-UE is fixed at the origin
for $m = 1$ to M **do**
    $x_M \leftarrow$ (Distance of T-UE from mth MBS)
    $P_{UM}(m) \leftarrow P_M h_{XM} L_0 \left(\frac{d_{0_M}}{x_M(m)}\right)^{\alpha_{0M}}$
end for
$x_{M_{MIN}} \leftarrow \ min(x_M)$ i.e., Identifying the nearest MBS from T-UE
$P_{UM_{MAX}} \leftarrow \ max(P_{UM})$
for $s = 1$ to S **do**
    $x_S \leftarrow$ (Distance of T-UE from sth SBS)
    $P_{US}(s) \leftarrow P_S B_S h_{XS} L_0 \left(\frac{d_{0_S}}{x_S(s)}\right)^{\alpha_{0S}}$
end for
$x_{S_{MIN}} \leftarrow \ min(x_S)$ i.e., Identifying the nearest SBS from T-UE
$P_{US_{MAX}} \leftarrow \ max(P_{US})$
if $(P_{UM_{MAX}} > P_{US_{MAX}})$ **then**
    if $(\Gamma(x_{M_{MIN}}) > \tau)$ **then**
        Macro Coverage
        else
            Outage
    end if
    else
    if $(\Gamma(x_{S_{MIN}}) > \tau)$ **then**
        Small Coverage
        else
            Outage
    end if
end if
$\mathbb{C} \leftarrow$ [Macro Coverage, Small Coverage, Outage]
return $\mathbb{C}$

In Algorithm 1, firstly the received power from all the BSs of both BS tiers is determined at the T-UE. Secondly, in accordance with the UE-AS adopted in this chapter, the averaged received powers from the nearest MBS and SBS are then compared and the T-UE association decision is made. Once the tier association of T-UE is determined, the received SINR from the associated BS is then compared with the target SINR threshold. Finally, this last comparison decides whether the T-UE is under coverage from the associated BS or not. Similar to algorithm 1, the T-UE association with any BS tier in DS-PLM (i.e., Algorithm 2) is also

Algorithm 2 Algorithm for determining coverage/outage in a two-tier HCN using DS-PLM

$S \leftarrow \lambda_S A$
$M \leftarrow \lambda_M A$
$x_U \leftarrow (0,0)$
for $m = 1$ to M **do**
  $x_M \leftarrow$ (Distance of T-UE from mth MBS)
  if $x_M(m) \leq R_{CM}$ **then**
    $P_{UM}(m) \leftarrow P_M h_{XM} L_0 \left(\frac{d_{0_M}}{x_M(m)}\right)^{\alpha_{0M}}$
    else
    $P_{UM}(m) \leftarrow P_M h_{XM} L_0 \left(\frac{d_{0_M}}{R_{CM}}\right)^{\alpha_{0M}} \left(\frac{R_{CM}}{x_M(m)}\right)^{\alpha_{1M}}$
  end if
end for
$x_{M_{MIN}} \leftarrow min(x_M)$
$P_{UM_{MAX}} \leftarrow max(P_{UM})$

for $s = 1$ to S **do**
  $x_S \leftarrow$ (Distance of T-UE from sth SBS)
  if $x_S(s) \leq R_{CS}$ **then**
    $P_{US}(s) \leftarrow P_S B_S h_{XS} L_0 \left(\frac{d_{0_S}}{x_S(s)}\right)^{\alpha_{0S}}$
    else
    $P_{US}(s) \leftarrow P_S B_S h_{XS} L_0 \left(\frac{d_{0_S}}{R_{CS}}\right)^{\alpha_{0S}} \left(\frac{R_{CS}}{x_S(s)}\right)^{\alpha_{1S}}$
  end if
end for
$x_{S_{MIN}} \leftarrow min(x_S)$
$P_{US_{MAX}} \leftarrow max(P_{US})$

if $(P_{UM_{MAX}} > P_{US_{MAX}})$ **then**
  if $(\Gamma(x_{M_{MIN}}) > \tau)$ **then**
    Macro Coverage
    else
      Outage
  end if
  else
  if $(\Gamma(x_{S_{MIN}}) > \tau)$ **then**
    Small Coverage
    else
      Outage
  end if
end if
$\mathbb{C} \leftarrow$ [Macro Coverage, Small Coverage, Outage]
return $\mathbb{C}$

determined firstly but the received power in this case is additionally dependent on the respective BS tier critical distances of both tiers.

Remark 3.4.1*: It is worth mentioning here that the network coverage estimation using SS-PLM and DS-PLM algorithms follow a linearly growing complexity order i.e., $O(\lambda_M+\lambda_S)$, where λ_M and λ_S refer to the spatial densities of MBSs and SBSs respectively in a given network with coverage area A. It is clearly observable from both the algorithms that the number of computations never exceeds the linear trend. For example, the number of computations in case of loop are function of either S or M. It is also clear from each of the algorithms that there are no nested loops involved. Hence, as described above, the complexity of the simulation algorithm in each of the cases stays linear. Nonetheless, given the excessive deployment of SBSs in meeting the capacity demands, $O(\lambda_M+\lambda_S)$ can be safely approximated by $O(\lambda_S)$.*

3.5 Numerical and Simulation Results

In order to validate the accuracy of derived mathematical expressions of both performance metrics using DS-PLM, the resultant expressions of (3.4) and (3.35) are evaluated numerically and compared with Monté Carlo simulations. In our simulation setup, without loss of generality, a T-UE is placed at the origin for each network realization while BSs of both tiers are deployed for numerous times. Hence, the reported results of both metrics for any simulation scenario are based on average values. Moreover, following parametric values have been considered for generating all the results for DS-PLM: $\lambda_M = 1/(\pi 500^2)$BSs /m^2, $P_M = 53$ dBm, $P_S = 33$ dBm, thermal noise $(\sigma^2) = -104$ dBm, $\alpha_{0_M} = \alpha_{0_S} = 2.7$, $\alpha_{1_M} = \alpha_{1_S} = 3.9$, $L_0 = 5.1286e-04$, $R_{CM} = 300$m, and $R_{CS} = 55$m unless specified explicitly. Similarly, the T-AP and network coverage results for the SS-PLM are generated for $\alpha_M = \alpha_S = 3.9$ while other relevant parameters of both tiers remain the same as considered for DS-PLM.

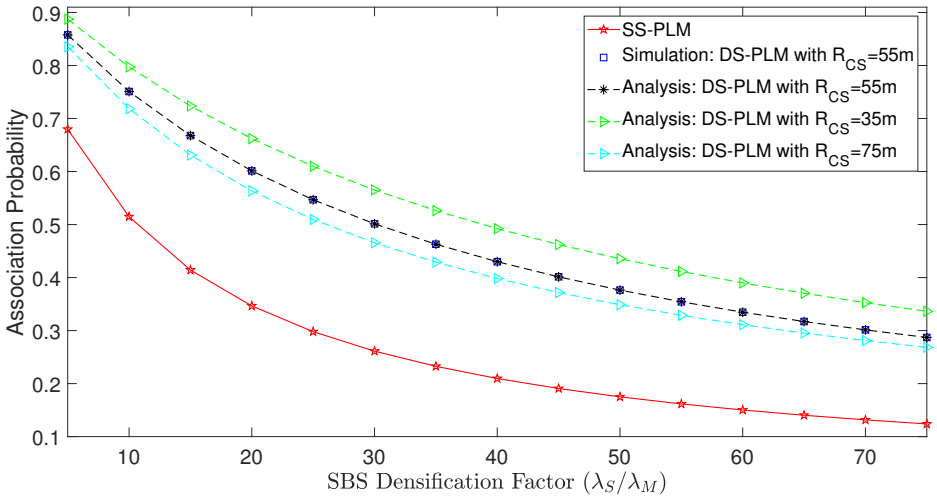

FIGURE 3.3: Comparison of macro T-AP for varying λ_S using SS-PLM and DS-PLM.

3.5.1 Tier Association Probability

In order to validate the accuracy of derived expression for macro T-AP using DS-PLM in a two-tier HCN, both the analytical and simulation results are plotted in Fig. 3.3 for varying small tier density (λ_S) . It is clear from the figure that for an unbiased UE-AS, both the curves (i.e., analytical and simulation) are in complete agreement of each other, and hence it corroborates the accuracy of T-AP analysis presented in this chapter.

3.5.1.1 Comparison of T-AP using SS-PLM and DS-PLM

Fig. 3.3 further illustrates that when the path loss is estimated through *one size fits all approach* i.e., SS-PLM, the densification of SBSs results in significant offloading of UEs to small tier. This is because the distance between UEs and SBSs decrease with the increasing λ_S, and thus it improves the received signal strength at UEs from their nearby SBSs. On the contrary, densifying SBSs in case of DS-PLM fails to swiftly reduce the UE load from macro tier owing to the reduction in BS association area due to DS-PLM consideration. Hence, the association of cell-edge UEs is steered towards their nearby BSs. In other words, UEs receive better power levels from both tier BSs owing to a smaller path loss for shorter link

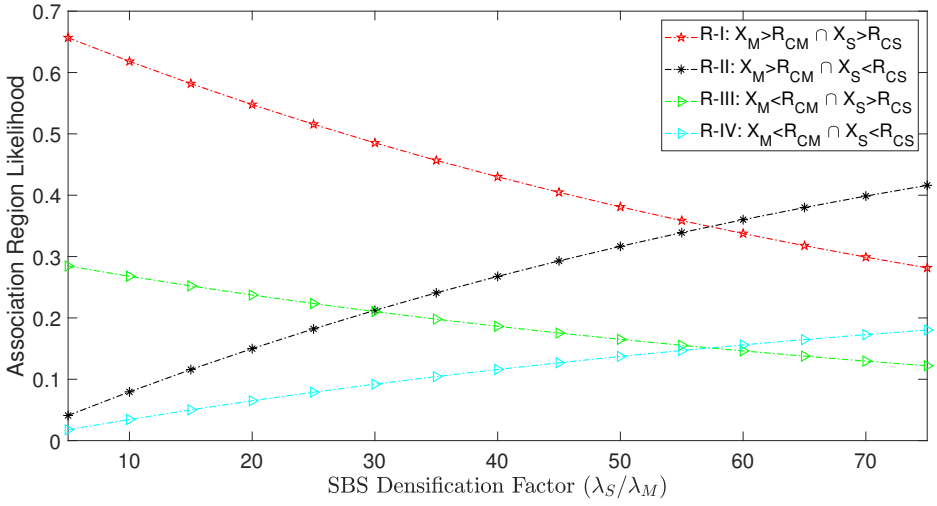

(a)

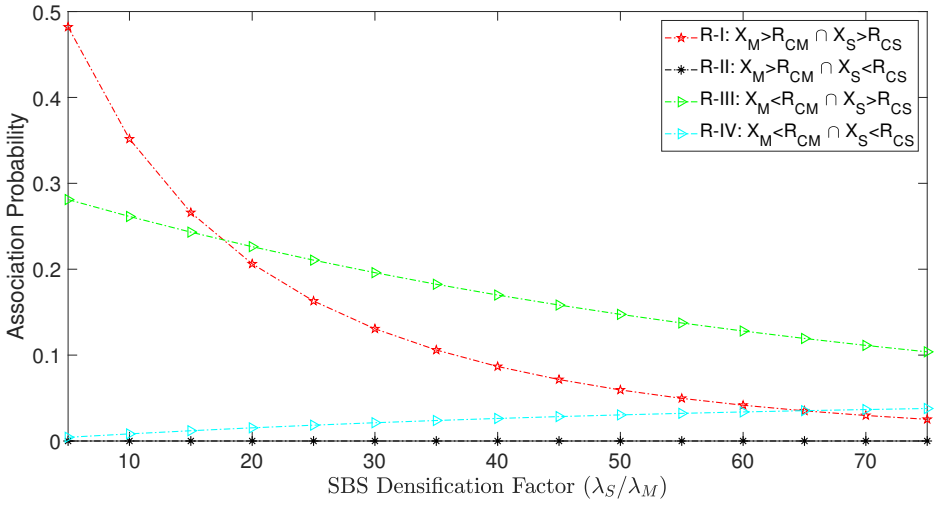

(b)

FIGURE 3.4: Association region-based macro T-AP using DS-PLM against varying small tier density.

distance only which restricts a rapid reduction in macro tier load. For instance, at $\lambda_S = 10\lambda_M$, the SS-PLM estimates that 48% of the UEs associate with the smaller tier while the DS-PLM predicts it to be 25% with smaller tier R_{CS}=55m. Thus, the SS-PLM clearly underestimates UE access load on macro tier which is equivalent to overestimating the UE offloading benefit of SBS densification.

It is also evident from Fig. 3.3 that the increase in R_{CS} size along with the SBS densification further reduces the UE association load on macro tier. For instance, at $\lambda_S = 10\lambda_M$ and $R_{CS} = 35m$, approximately 20% of the UEs associate

with smaller tier while by increasing R_{CS} size to 55m, the UE association with smaller tier increases up to 25%. Similarly, by further increasing the R_{CS} size to 75m for the same level of SBS densificatoin, the UE association with smaller BS tier increases to 28% approximately. This is because, the increase in R_{CS} size increases the likelihood of UEs residing within the R_{CS} distance from their respective nearest SBSs. Hence, the nearby UEs receive signal with a smaller decay rate from SBSs which increases the association of UEs with smaller BS tier. Fig. 3.3 further illustrates that increasing R_{CS} beyond an optimal value can lead to reduced offloading of UEs to smaller BS tier, owing to the increased distance from SBSs. For instance, it is clear from Fig. 3.3 that the vertical offset in macro T-AP curves have reduced when R_{CS} is increased from 35m to 75m. Meanwhile, it is pertinent to mention here that R_{CS} is a design parameter and its value depends mainly on the heights of the transmitter and UE antennas. However, the recent literature advocates that the heights of the SBS antennas must to be lowered to avoid excessive interference to the macro associated users. Therefore, improvement in the UE offloading at the cost of increased interference is not a feasible solution.

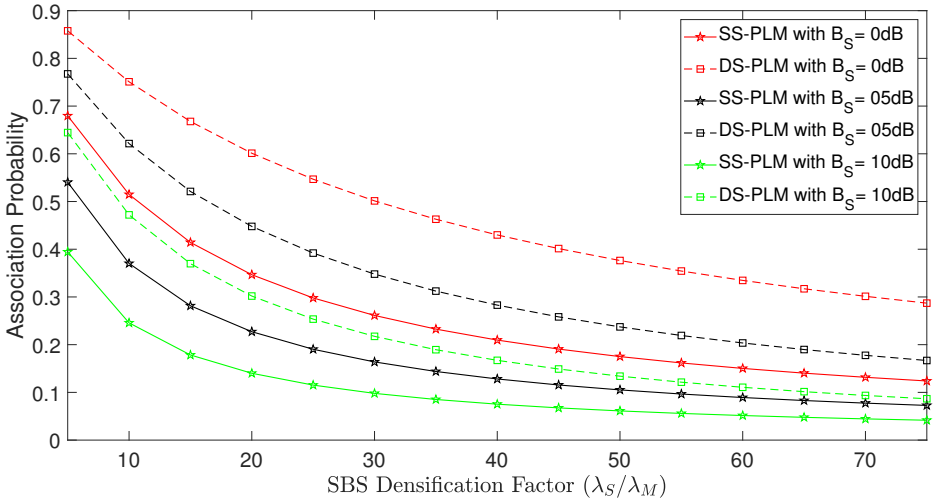

FIGURE 3.5: Comparison on the impact of SBS biasing on macro T-AP against varying λ_S using both DS-PLM and SS-PLM.

For a thorough insight of UEs association with macro tier using DS-PLM, Fig. 3.4 is plotted against varying λ_S. It is worth noting here that when DS-PLM is used instead of SS-PLM to estimate the path loss, then the coverage area of an HCN gets divided in four disjoint regions which are written as R-I, R-II, R-III and R-IV

in Fig. 3.4. In Fig. 3.4(a), the y-axis denotes the likelihood of each region, i.e., for any given SBS densification factor, the probability that the T-UE falls in each of the regions is plotted. Meanwhile, in Fig. 3.4(b), the y-axis represents the macro tier association probability of the T-UE in each of the above described regions.

It can be readily observed from the figure that the T-AP is significantly impacted by SBS densification, as the distance between UEs and SBSs is directly related to it. Moreover, it is evident from Fig. 3.4(b) that at lower levels of SBS densification, the UEs prefer associating with macro tier as reflected by higher macro T-AP in regions R-I and R-III respectively. This is because, the power received by UEs from their respective nearest MBSs is typically higher than the power offered by the closest SBSs. Furthermore, at lower SBS densification, the distance between UEs and their respective nearest SBSs in mostly greater than R_{CS} and given the transmit power disparity between both tiers, the UEs prefer macro tier association which leads to a lightly loaded small tier.

Contrarily, higher SBS densification does lead to a considerable offloading of UEs to small tier as the distance between UEs and their closest SBSs significantly decrease. Interestingly, when the distance between UEs and their nearest SBSs is smaller than R_{CS}, some of the UEs may also lie at distances smaller than R_{CM} as well (R-IV), given a much bigger size of R_{CM} as compared to R_{CS}. Therefore, the disparity in transmit powers of both tiers impels some of the UEs to associate with their nearest MBSs.

Consequently, the DS-PLM consideration has highlighted two important observations in T-AP: 1) using SS-PLM overestimates the UE offloading to smaller BS tier in dense network deployments, as SS-PLM is not well-suited for estimating the received power levels in disparate link distances and 2) the need for employing an effective load balancing strategy to ensure fairness in UEs load distribution amongst BS tiers.

3.5.1.2 Impact of SBS Biasing on T-AP

The disparity in transmit power of BS tiers emphasizes the need for adopting load balancing strategies, and static SBS biasing helps in artificially increasing the association regions of SBSs which leads to more intense UE offloading from macro tier. It is evident from Fig. 3.5 that adopting SBS biasing at smaller λ_S has a pronounced effect on UE steering than at higher values of λ_S. This is because, the UEs are distantly located from SBSs at lower λ_S but when biasing is applied it steers significant number of UEs to smaller tier as cell ranges of SBSs are increased. While on the other hand, considering biased UE-AS in highly dense scenarios is relatively less effective in steering UEs as most of the UEs already receive higher signal strength from SBSs owing to the decrease in distance from SBSs. Given the overestimation of UEs offloading to small tier in dense HCNs using SS-PLM, employing SBS biasing to further reduce the load on macro tier only adds to the inaccuracy in estimating the tier loads. While on the contrary, using DS-PLM and given its high accuracy as compared to SS-PLM in estimating the path loss in dense networks, the UE offloading benefit is relatively better estimated by DS-PLM.

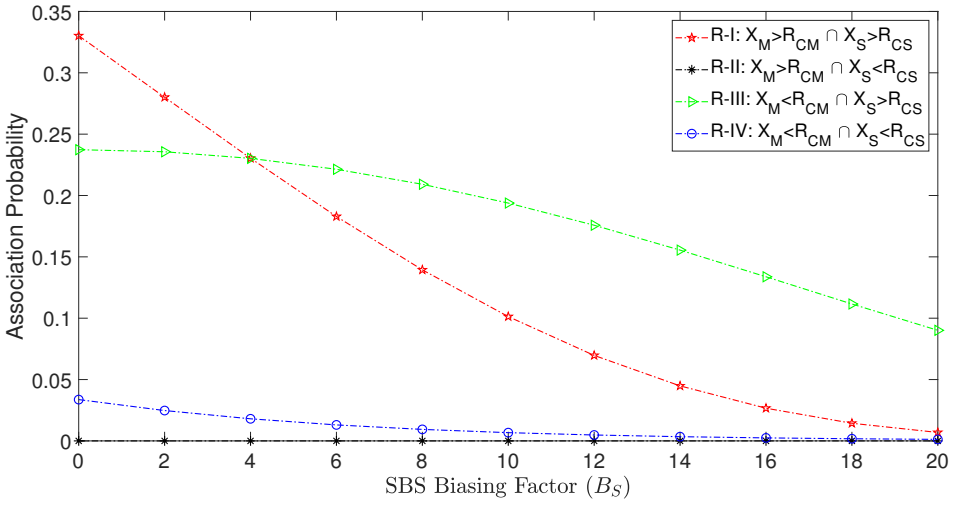

FIGURE 3.6: Association region-based macro T-AP for varying SBS biasing using DS-PLM.

It is worth mentioning here that the association region of any SBS is directly related to its distance from the neighboring MBSs, and hence the usefulness of SBS biasing is also sensitive to this distance. For a better understanding of the

effectiveness of SBS biasing in HCNs, a region-wise macro T-AP is shown against varying SBS biasing factor (B_S). In Fig. 3.6 for a fixed λ_S =20λ_M, macro T-AP for varying SBS biasing is plotted for each of the association regions. It is clear from the figure that by increasing B_S for a fixed λ_S, the macro T-AP decreases in all the regions.

The SBS biasing is found to be most effective in R-I, because in this UE association region the distance between UEs and their nearest MBSs is already greater than R_{CM}. In R-II, the UEs dominantly associate with smaller tier as they are mostly lying within the R_{CS} of their proximate SBSs. It can be seen from the figure that in R-III, a relatively higher level of B_S is required to offload UEs to smaller tier and this is because the UEs are lying within the R_{CM} of their nearest MBSs and receive strong signals from them. Finally, in R-IV, since the UEs are located within the critical distance of both tier BSs, hence a moderate B_S would improve the UEs offloading to smaller tier BSs.

3.5.2 Coverage Probability

In this subsection, network coverage (SINR distribution) results are presented for varying τ and λ_S from different aspects including unbiased and biased association scenarios, incorporation of frequency reuse and integration of both biasing and frequency reuse mechanisms. Firstly, the validation of network coverage analysis estimated using DS-PLM is presented for varying SINR threshold τ, at $\lambda_S = 50\lambda_M$ and SBS densification factor, λ_S/λ_M for τ =0 dB in Fig. 3.7 (a) and Fig. 3.7 (b) respectively. It is clear from both these figures that the simulation and analytical results perfectly match with each other which corroborates the accuracy of DS-PLM analysis for network coverage presented in this chapter. Furthermore, it also means that the derived analytical expression for SINR distribution can thus be used not only to predict the performance trends but also in obtaining critical system design insights.

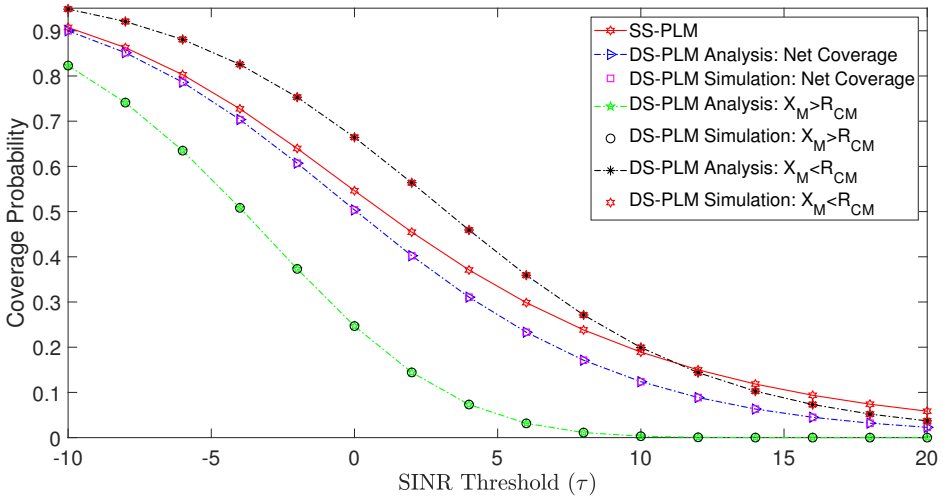

(a)

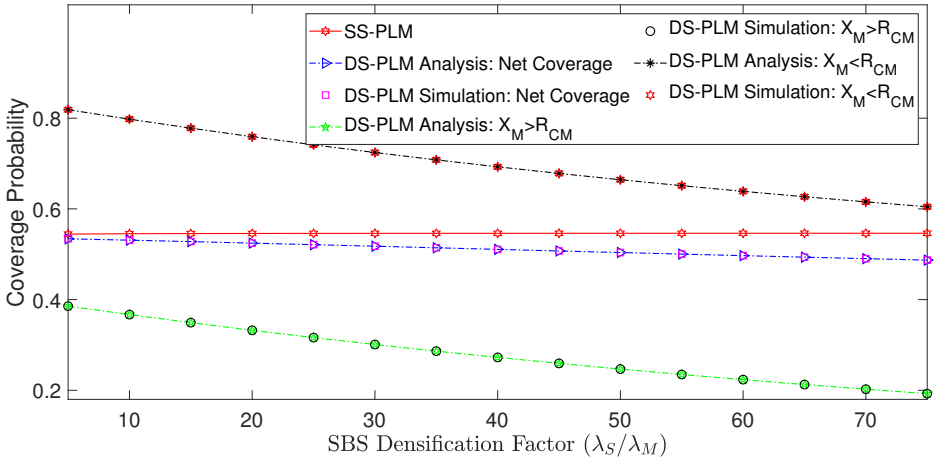

(b)

FIGURE 3.7: Validation and comparison of network coverage performance analysis against varying (a) SINR threshold and (b) Small tier density using both SS-PLM and DS-PLM.

3.5.2.1 Comparison of Network Coverage using SS-PLM and DS-PLM

It is clear from Fig. 3.7(a) that the network coverage estimated using both SS-PLM and DS-PLM is a monotonically decreasing function of τ, owing primarily to the increased strictness in network coverage criteria. Moreover, it is also evident from the figure that the simplistic approach of estimating the path loss using SS-PLM leads to the overestimation of network coverage in the dense network scenario as compared to DS-PLM. This is because, SS-PLM fails to accurately

estimate the received/interfering signal strengths in dense network deployments where disparate link distances are extensively present. While on the contrary, DS-PLM accounts for the varying communicating and interfering links by assuming distance dependent path loss for each of them. Besides this, DS-PLM usage also reduces the coverage area of each BS which not only ensures UEs association with their nearby BSs, but it also avoids the underestimation of interference received from the neighboring/interfering BSs.

For gaining better insight of the coverage estimation using DS-PLM, region-wise macro tier coverage curves for both regions ($X_M > R_{CM}$ and $X_M < R_{CM}$) are also plotted in Fig. 3.7(a). It can be easily observed from the figure that UEs residing within R_{CM} of their associated MBSs can stay in network coverage for higher values of τ as well due to better received signal strength. While the UEs residing at distances greater than R_{CM} of their associated MBSs generally receive inadequate signal strengths to sustain stricter network coverage criteria, and hence face network outage at higher value of τ. Thus, it can be readily seen from the figure that the difference between estimated network coverages by both PLMs increase with the increasing τ. For instance at τ=0 dB, the SS-PLM overestimates the network coverage by 8% while at τ= 10dB the difference substantially increases to nearly 50%.

In Fig. 3.7(b), a comparison of the estimated network coverage for both PLMs against varying SBS densification is presented. It can be readily observed from the figure that the estimated network coverage using SS-PLM is independent of variation in λ_S. This independence of SINR distribution inferences that the cellular operators may freely densify their infrastructures, as the increase in interference is counterbalanced by the improved received power at the UEs owing to the decrease in the size of link distances. Contrarily, the network coverage is found to be a decreasing function of λ_S when DS-PLM is used to estimate the path loss instead of SS-PLM. A region-wise macro tier coverage shown in figure also verifies that the increase in SBS density causes a decrease in the overall network coverage, as UEs receive excessive from nearby interfering SBSs. The SINR invariance observed in case of SS-PLM is largely due to the inability of SS-PLM in accurately estimating

the strengths of desired and interfering signals in dense network deployments. It is for the same reason that the difference in estimated coverages using both PLMs increase with increase in SBS density. For instance at a lower SBS densification level i.e., (λ_S= 10λ_M), the coverage estimated by both PLMs is nearly the same, since the deployed network is sparse and disparate link distances are hardly present. While on the contrary, at a higher SBS densification level i.e., (λ_S= 50λ_M), the percentage difference in estimated coverage values using both PLMs increases to nearly 8%.

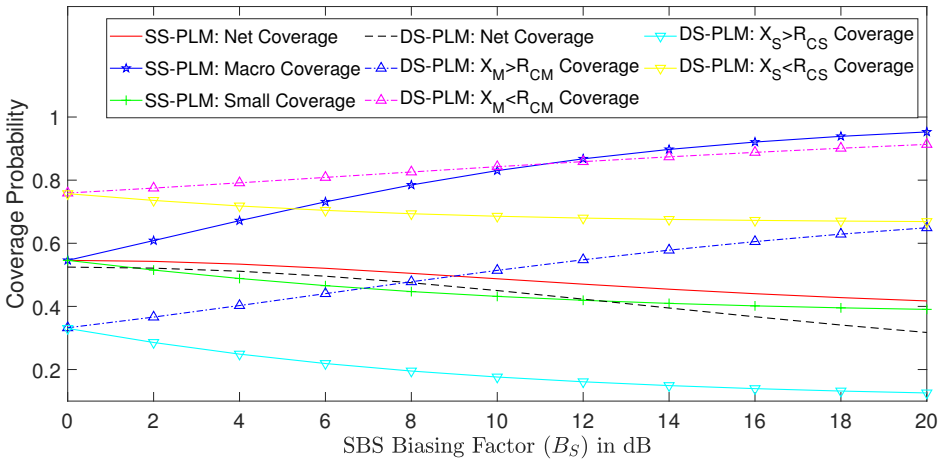

FIGURE 3.8: Network coverage for varying SBS biasing factor (B_S)

3.5.2.2 Impact of SBS Biasing on Network Coverage

For a fixed λ_S and τ, the impact of B_S variation on the network coverage estimated using both SS-PLM and DS-PLM is presented in Fig. 3.8. It is clear from the figure that SBS biasing results in performance degradation of the network i.e., coverage probability reduces for both PLMs with the increase in B_S. Although SBS biasing helps in offloading the UEs from heavily loaded macro tier to smaller tier, but it does so at the cost of increased network outage as the received interference at offloaded UEs increase significantly. The pushing of UEs to smaller tier from macro tier improves the coverage offered by macro tier, as most of its boundary residing UEs are pushed to associate with nearby BSs of smaller tier. While on

the other hand, these pushed UEs receive excessive interference from their nearby MBSs which increases the outage probability in smaller tier.

At a relatively lower SBS densification level (like λ_S=20λ_M), the difference between estimated coverage using both PLMs is 4% (unbiased UE-AS), as at such a lower densification (sparsely deployed SBS), there are very few disparate link distances. Contrarily, this difference increases with the increase in B_S factor, owing to the incorrect estimation of region enhancement due to SBS biasing. For instance, by considering a biased UE-AS with B_S= 10 dB, and τ= 0 dB, the coverage estimated using SS-PLM reduces by approximately 12% while in case of DS-PLM, the estimated network coverage decreases by 16.5 %. It is clear from these statistics that similar to the overestimation of UEs offloading to smaller tier in case of T-AP, the SS-PLM usage underestimates the coverage degradation caused due to the consideration of SBS biasing.

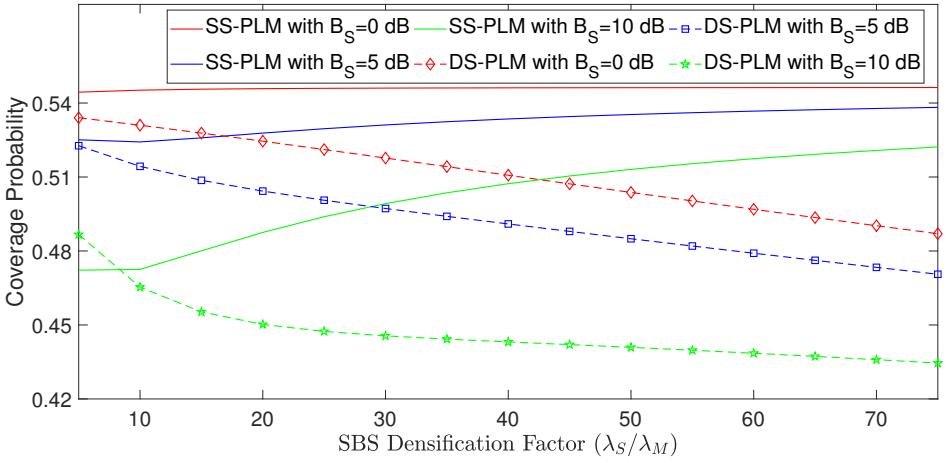

FIGURE 3.9: Impact of SBS biasing on network coverage for varying SBS densification

In order to better understand the impact of SBS biasing on network coverage for varying SBS densification using both SS-PLM and DS-PLM, Fig. 3.9 is plotted. The figure illustrates that when the network coverage is estimated using any of these PLMs, the consideration of SBS biasing has a significant impact at lower λ_S as compared to the higher values of λ_S. This is because, the UEs association with smaller tier is minimal at lower values of λ_S due to greater distances from

nearby SBSs and transmit power disparity between BS tiers. By offloading UEs at lower λ_S using biased UE-AS results in an excessive interference at the offloaded UEs from nearby MBSs, and hence it leads to considerable degradation in the overall network coverage. This negative impact of SBS biasing reduces with the increase in λ_S, as the distance between UEs and SBSs reduce, and owing to this, the UEs prefer small tier association. Moreover, at higher SBS densification, the equilibrating effect of increased signal strength and interference ensures the network coverage remains constant for higher values of λ_S in case of SS-PLM. Contrarily, in case of DS-PLM, the SINR distribution is a decreasing function of SBS densification. Therefore, considering biased UE-AS further degrades the network coverage, and hence it highlights an additional limitation of using SS-PLM in analyzing the performance of dense networks.

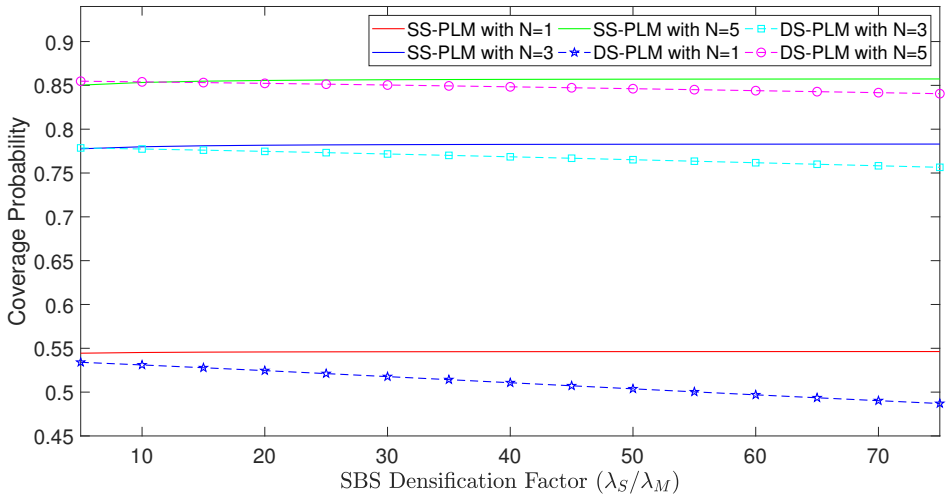

FIGURE 3.10: Impact of frequency reuse factor (N) on network coverage for varying SBS densification

3.5.2.3 Impact of Incorporating Frequency Reuse on Network Coverage

Given the need for densified SBSs in meeting the rapidly increasing capacity demands of emerging networks, the decreasing distance between deployed infrastructures requires utilization of efficient interference management mechanisms to avoid performance degradation of the networks. Fig. 3.10 depicts the effect of employing

frequency reuse mechanism in dense deployment of SBSs in a two-tier dense HCN using both SS-PLM and DS-PLM. The figure demonstrates that at any fixed λ_S and target SINR τ, increasing the reuse factor N improves the overall network coverage for both PLMs as the number of interfering BSs reduces and interference received from both BS tiers diminishes as well. Moreover, it is important to note that the biggest jump in network coverage is achieved for both PLMs when N is increased from 1 to 2. This is because, the number of interfering BSs from both tiers have reduced to half on average. Similarly, the increase in network coverage for any further increase in N reduces from the earlier value as the number of interferer BSs have already reduced, and fewer interfering BSs contribute to the interference faced by UEs.

It is imperative to mention here that the difference between estimated network coverages using both PLMs reduces with the increase in N. This is because, the density of interfering BSs from both tiers decrease with the increase in N, and this reduced density is equivalent of a network scenario where interfering BSs are sparsely located. Moreover, it is already well-known in the literature that the accuracy of SS-PLM in estimating path loss of sparse networks is comparable to that of DS-PLM as disparate link distances are minimal. Hence, Fig. 3.10 illustrates similar observations. For instance, when universal frequency reuse is considered i.e., N=1, the difference between estimated coverages at a relatively higher SBS densification of λ_S=50λ_M is 8%, which reduces to 2.3% at N=3 and further decreases to 1.2% at N=5.

3.5.2.4 Impact of Integrated SBS Biasing and Frequency Reuse Incorporation on Network Coverage

In Fig. 3.11 for a fixed λ_S and τ, the impact of varying SBS biasing B_S on network coverage estimated using both PLMs for different values of reuse factor N is depicted. The figure illustrates that for a fixed value of B_S, increasing N improves the network coverage as the number of interfering BSs from both BS tiers are reduced, and the UEs experience lesser interference from interfering BSs

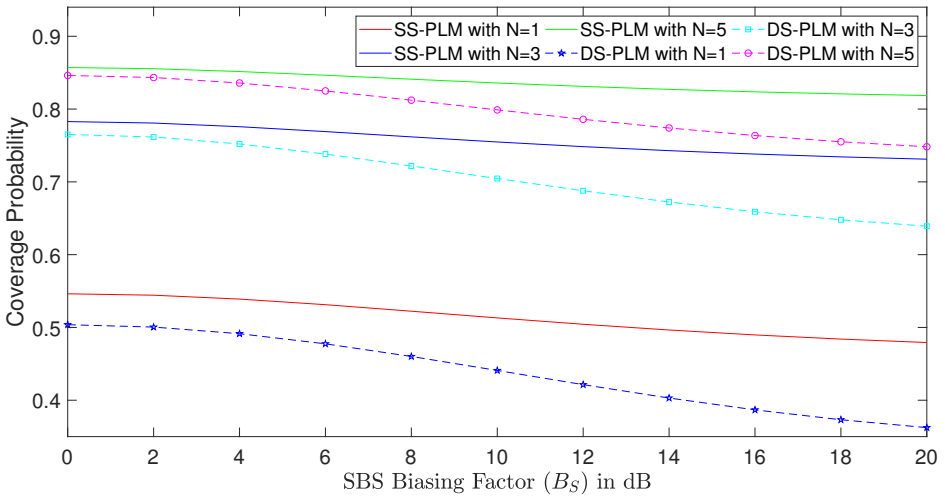

FIGURE 3.11: Impact of SBS biasing (B_S) on network coverage over varying frequency reuse factor (N)

of both the tiers. Contrarily, by increasing B_S while ensuring a fixed N degrades the network coverage owing to the excessive interference faced by UEs due to high offloading of UEs to small tier. Moreover, it is also evident from the figure that at lower levels of B_S, the difference between estimated coverage using both PLMs is relatively small but it increases considerably at higher values of B_S. This is because, the offloaded UEs receive strong interference from their proximate MBSs. For instance at λ_S=50λ_M, τ= 0 dB,N= 3 and B_S= 2 dB, the difference estimated network coverages using both PLMs is 2.5% which swiftly increases to 14.4% when B_S is increased to 20 dB.

The joint impact of incorporating both SBS biasing and frequency reuse on network coverage estimated using both PLMs in the presence of SBS densification is shown in Fig. 3.12. The figure clearly illustrates that the joint incorporation of both mechanisms is highly conducive in dense deployments of SBSs as it not only ensures a balanced tier load but it is equally effective in avoiding excessive interference occurring mostly due to SBS densification and UEs offloading from macro tier to small tier. Given better accuracy of estimating the path loss in dense networks, the usage of DS-PLM clearly highlights the shortcomings of using SS-PLM in analyzing the performance of dense networks. Moreover, employing DS-PLM further demonstrates the realistic advantage associated with joint consideration of

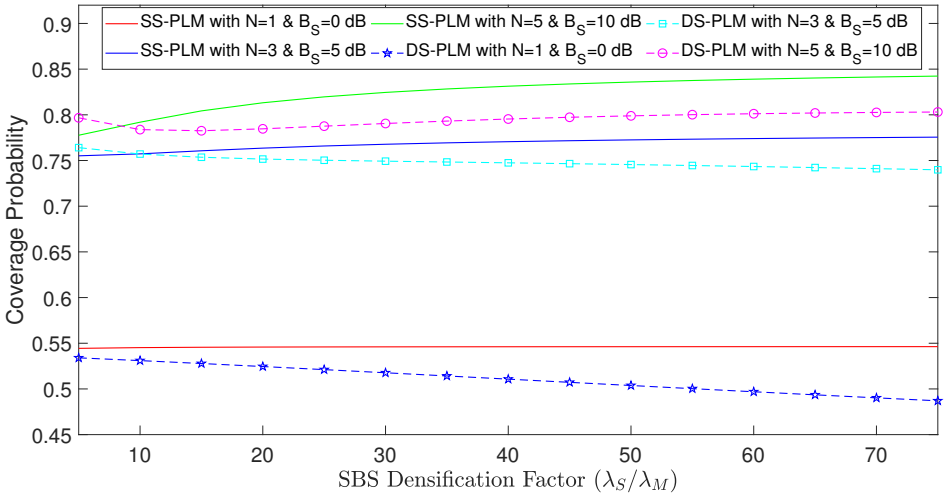

FIGURE 3.12: Joint impact of reuse factor (N) and SBS biasing B_S on network coverage for varying SBS densification.

SBS biasing and frequency reuse mechanisms. Thus, giving critical design insights for finding optimal parametric values in cellular planning.

3.6 Conclusion

In this chapter, the downlink performance of a two-tier uniform HCN has been analyzed by using the DS-PLM. Intuitive mathematical expressions for the TAP and network coverage have been derived which lead to useful insights in cellular planning. Meanwhile, to account for the disparity in transmit power of BS tiers and to overcome the excessive interference faced by the UEs, load balancing and interference abating mechanisms have been jointly considered as well. A thorough comparison of the estimated network performance using both SS-PLM and DS-PLM clearly highlighted the limitation of SS-PLM consideration in dense network scenarios.

Chapter 4

Coverage Analysis of Dense Coverage-Centric HCNs using DS-PLM

This chapter extends the work presented in Chapter 3. It was highlighted in the last chapter that the usage of DS-PLM is well-suited for analyzing the performance of dense HCNs owing to its better accuracy in estimating the strength of desired and interference signals in disparate link distances. It was also observed that the cellular network coverage not only depends on the SBS densification, but the random placement of SBSs in the overlaid network also results in the performance degradation due to excessive interference. Nonetheless, it was also noticed that the UEs mostly prefer associating with macro tier, whenever the distance between UE and its nearest MBS is smaller than R_{CM}. Consequently, a correlation needs to be introduced between the positioning of MBSs and SBSs to better avail the potential of dense deployments of SBSs. Hence, a coverage-centric SBS deployment strategy i.e., muting the SBSs that exist at distances smaller than R_{CM} from each MBS, is adopted in this chapter, and the coverage performance of NuHCNs is analyzed using DS-PLM.

Remaining parts of the chapter are organized in the following manner: Section 4.1 provides a brief introduction to the problem. System model is presented in

section 4.2, which is followed by section 4.3 that presents the analysis for macro T-AP and statistical distance distributions for communicating distances greater and smaller than R_{CM}. In Section 4.4, the derivation of network coverage expression is presented for the two-tier NuHCNs. Numerical results are discussed in section 4.5, while the chapter is concluded in section 4.6.

4.1 Introduction

Cellular networks are developing from voice-oriented to always available and uninterrupted mobile-broadband data networks. Deploying densified SBSs in support of MBSs has been one of the primary driving forces in meeting the ever increasing capacity demands of emerging wireless networks [40]. The addition of these SBSs in the overlaid network is like a *double-edged sword*, it brings the network resource in close proximity of UEs but the excessive interference also has a detrimental impact on the performance of dense HCNs [155, 156]. Besides this, the disparity in transmit power of BS tiers is the root cause for load imbalance between the BS tiers as UEs. Thus, it is of paramount importance to address the excessive interference experienced by UEs and the disparity of UEs association with different BS tiers to avail maximum potential of multi-tier cellular networks [157].

It is a common assumption in the literature that the locations of BSs and UEs are distributed using independent PPPs, but these spatially un-correlated deployments of BSs and UEs do not help in improving the downlink performance of HCNs [102]. Given random deployment of SBSs and transmit power disparity between BS tiers, the SBSs located in near proximity of MBSs cause excessive interference to macro associated UEs while the offloaded UEs to small tier also face excessive interference from MBSs [91]. Moreover, it is also a common assumption to consider a fully-loaded system i.e., all BSs are assumed to be always transmitting and serving their respective UEs [66, 68]. The MBSs are generally known to have large coverage areas and hence, this assumption is valid for them. However, it is not

true for the SBSs and as result, it leads to a pessimistic network coverage estimation. Therefore, it is important to consider the impact of BS loading especially given the density of BSs is quickly approaching the density of user devices. It has been shown in numerous research works [72, 158–161] that the network coverage improves if the activity factor of low-powered BS tiers is assumed to be lesser than 1 i.e., all the SBSs are not active at all the times.

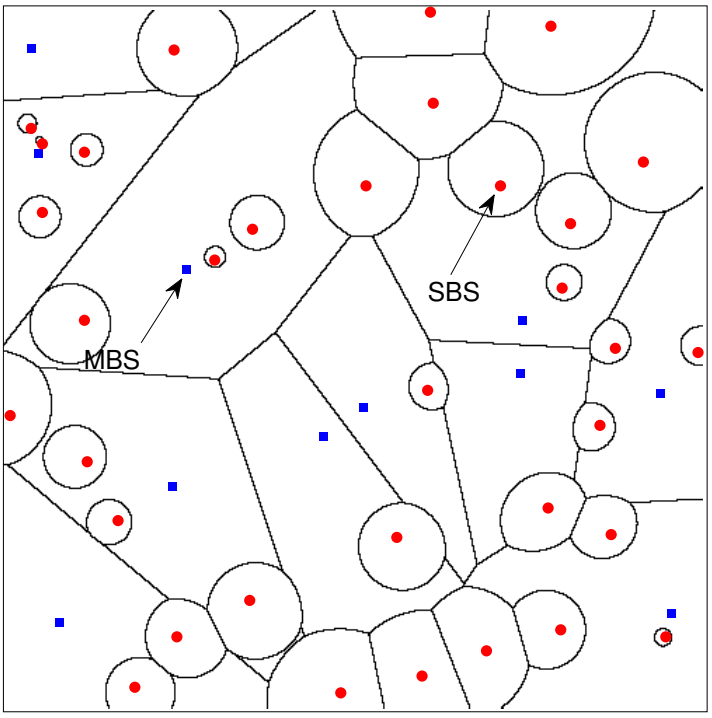

FIGURE 4.1: A two-tier HCN depicting the coverage regions of BSs from both BS tiers

A two-tier HCN is shown in Fig. 4.1 which clearly shows that the coverage region of any SBS is sensitive to its distance from the neighboring MBSs. The SBSs which are located in near-vicinity of MBSs have very small coverage areas, while those located at the far distances from MBSs have reasonable coverage areas. Besides this, it is also evident that a moderate level of SBS biasing would not be helpful in increasing the coverage areas of those SBSs which are in close proximity of MBSs. These observations clearly suggest that densifying SBSs without taking into consideration the distance from neighboring MBSs would not lead to improvement

in the network coverage, and hence it highlights the need for exploring selective or non-uniform densification of SBSs [162]. It is important to mention here that the emerging networks are bound to be dense, especially given their astounding success in meeting the high capacity demands over the past few years. Therefore, to accurately estimate the path losses in such disparate link distance based scenarios, it is important to employ more accurate and realistic PLMs that can efficiently estimate the propagation environment.

By using DS-PLM, the coverage area of a BS is divided into two non-overlapping regions separated by a critical distance and this special distance is well-known to be dependent upon the antenna heights of the communicating stations [37]. For a two-tier HCN in which BSs of both tiers are randomly deployed using two independent PPPs, the SBSs that exist at distances smaller than the critical distance of each MBS are deactivated to form an NuHCN. This selective SBS deactivation ensures that most of the SBSs are deployed at locations where MBSs have weaker coverage. Moreover, the UEs that are located within the critical distance of any MBS are bound to associate with that MBS, as the UEs mostly receive a stronger signal from MBS as compared to the nearest SBS within that distance range [163].

4.2 System Model

4.2.1 BS Deployment and User Distribution

This chapter considers a two-tier BS system comprising of macro and small BSs which are distributed in a service area using distinct PPPs, represented as ϕ_M and ϕ_S respectively. The deployed BSs have distinct spatial densities (λ_M and λ_S) and transmit powers (P_M and P_S) as well, while it is further assumed that $\lambda_S \geq \lambda_M$ and $P_S < P_M$. Besides this, the UEs are also assumed to be distributed through an independent PPP represented as ϕ_{UE} having density λ_U. The analysis is carried out for a T-UE which is assumed to be located at the origin and Silvnyak's Theorem justifies this assumption owing to a special property of PPPs [39].

4.2.2 Channel Model

Using DS-PLM, the power received (S_{DL_i}) by the T-UE at a distance X_i from an ith tier BS is given as,

$$S_{DL_i}(x_i) = \begin{cases} P_i h_{X_i} L_0 \left(\frac{x_{0i}}{x_i}\right)^{\alpha_{0i}} & x_i \leq R_{Ci} \\ P_i h_{X_i} L_0 \left(\frac{x_{0i}}{R_{Ci}}\right)^{\alpha_{0i}} \left(\frac{R_{Ci}}{x_i}\right)^{\alpha_{1i}} & x_i > R_{Ci}, \end{cases} \tag{4.1}$$

where the fading coefficient denoted as h_{X_i} is considered to be Rayleigh distributed and its power is exponentially distributed with unity mean, i.e., $h_{X_i} \sim \exp(1)$. Besides this, the close-in reference distance for both BS tiers is represented by $x_{0_i} = 1\text{m}$, while the path loss observed at x_{0_i} is denoted by L_0. Moreover, as can be seen from (4.1), the received power expression ignores shadowing effect and this assumption is considered to improve the tractability of our analysis. In contrast to the SS-PLM where signals decay with increasing distance but at a single rate, employing DS-PLM ensures the desired and interfering signals both experience a more realistic distance dependent path loss using dual decay rates. This effectively means that there is a disparity in signal decay rate beyond the BS critical distance R_{Ci}. The far field signal decay rate or the PLE for distances smaller than R_{Ci} is represented by α_{0i}, while α_{1i} denotes the PLE for distances farther than R_{Ci}.

Given dense deployment of SBSs, multiple SBSs can appear in the coverage area of any MBS and thus can badly effect the services offered by MBS to its UEs depending upon their location w.r.t the serving MBS. Therefore, to safeguard the services' quality offered by MBSs to their UEs specially in their near-vicinity, an NuHCN is considered in which the SBSs located within the R_{CM} of any MBS are assumed to be muted (as shown in Fig. 4.2). With the available state-of-art technology, it is expected that the cellular operators are well-aware of the SBSs locations. Hence, by using subtle provisioning processes, the deployment of SBSs in certain regions can be easily avoided. This occurs today with the operators assigning FBSs to the selected sites based on the system constraints, where the proposed non-uniform SBS deployment scheme can be applicable [107, 115]. The UE association policy adopted in this chapter is based on maximum average biased

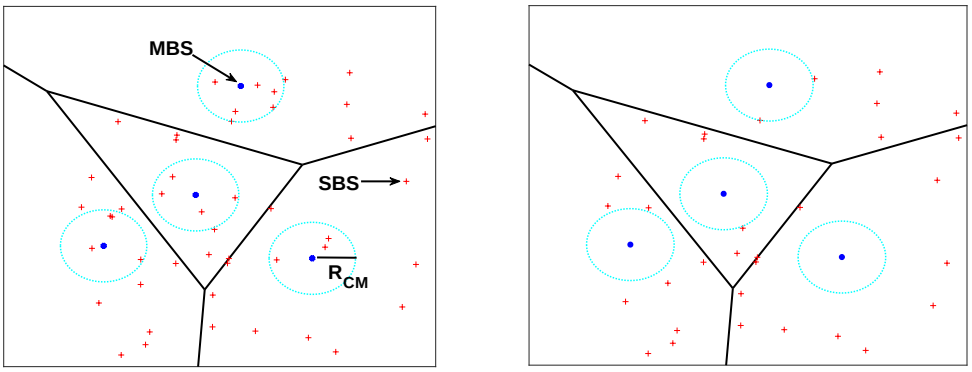

(a) (b)

FIGURE 4.2: Transformation of a uniformly distributed HCN to an NuHCN by muting SBSs lying within the critical region of MBSs.

received power. Moreover, to account for the disparity in transmit powers of both tiers in NuHCNs, static SBS biasing is also employed to offload UEs from macro to small tier.

It is further assumed that none of the deployed BSs in the NuHCN are unloaded i.e., every BS has some data for its associated UEs. It is important to note that by removing the SBSs from the near-vicinities of MBSs, the SBSs are mostly located outside of macro cell-center region. Hence, it is a valid assumption that none of the deployed BSs in the NuHCN are unloaded. Moreover, to ensure that the aggregate interference received by the UEs is reduced substantially, a simple frequency reuse mechanism is incorporated which helps in countering the decrease in received SINRs at UEs due to their offloading from macro tier and excessive SBS densification. The adopted frequency reuse mechanism divides the available bandwidth resource into N equal channels i.e., $F_1, F_2, ..., F_N$ while each BS randomly chooses 1 out of N channels. Since, independently thinning out a PPP results into another PPP; hence, the tractability associated with PPP is retained.

The instantaneous received SINR (Γ_i) at T-UE which is associated with ith tier BS is given as

$$\Gamma_i = \frac{S_{DL_i}}{\sum\limits_{j \,\epsilon\, \{\phi_{M,N} \,\cup\, \phi_{S,N}\}\backslash i} S_{DL_j} + \sigma^2}, \tag{4.2}$$

TABLE 4.1: Association Regions for T-UE in a two-tier NuHCN

Regions	**Communicating Distance Ranges**
R-I	$[X_M < R_{CM}]$
R-II	$[X_M > R_{CM} \cap X_S > R_{CS}]$
R-III	$[X_M > R_{CM} \cap X_S < R_{CS}]$

where $\phi_{M,N} \cup \phi_{S,N}$ represents a collection of MBSs and SBSs operating at frequency channel (i.e., N) over which the serving BS of T-UE also operates.

4.3 Tier Association Probability (T-AP) and Probability Density Function (PDF) of Distance to the Serving BS

In this section, the derivations of macro T-AP expression and distance distributions for each of the association regions i.e., ($X_M > R_{CM}$ and $X_M < R_{CM}$) to the serving MBS are presented. The critical distance based T-UE association regions are shown in Fig. 4.3, where a UE is located in region R-II as its distance from the nearest MBS and SBS is greater than R_{CM} and R_{CS}, respectively.

In a two-dimensional homogeneous PPP, the probability of having no BS in a circle of radius x_i which is also the distance to the nearest i-th tier BS is given using [164] as,

$$\mathbb{P}\left[X_i > x_i\right] = \exp\left(-\pi\lambda_i x_i^2\right). \tag{4.3}$$

Using (4.3), the likelihood that the T-UE can be located in any of the association regions (see Table 4.1 for region details) of a two-tier NuHCN can be expressed as,

$$\begin{aligned}
\varsigma &= 1 - \exp\left(-\pi\lambda_M R_{CM}^2\right). \\
\varpi &= \exp\left(-\pi\left(\lambda_M R_{CM}^2 + \lambda_S R_{CS}^2\right)\right). \\
\varrho &= \exp\left(-\pi\lambda_M R_{CM}^2\right) - \exp\left(-\pi\left(\lambda_M R_{CM}^2 + \lambda_S R_{CS}^2\right)\right).
\end{aligned}$$

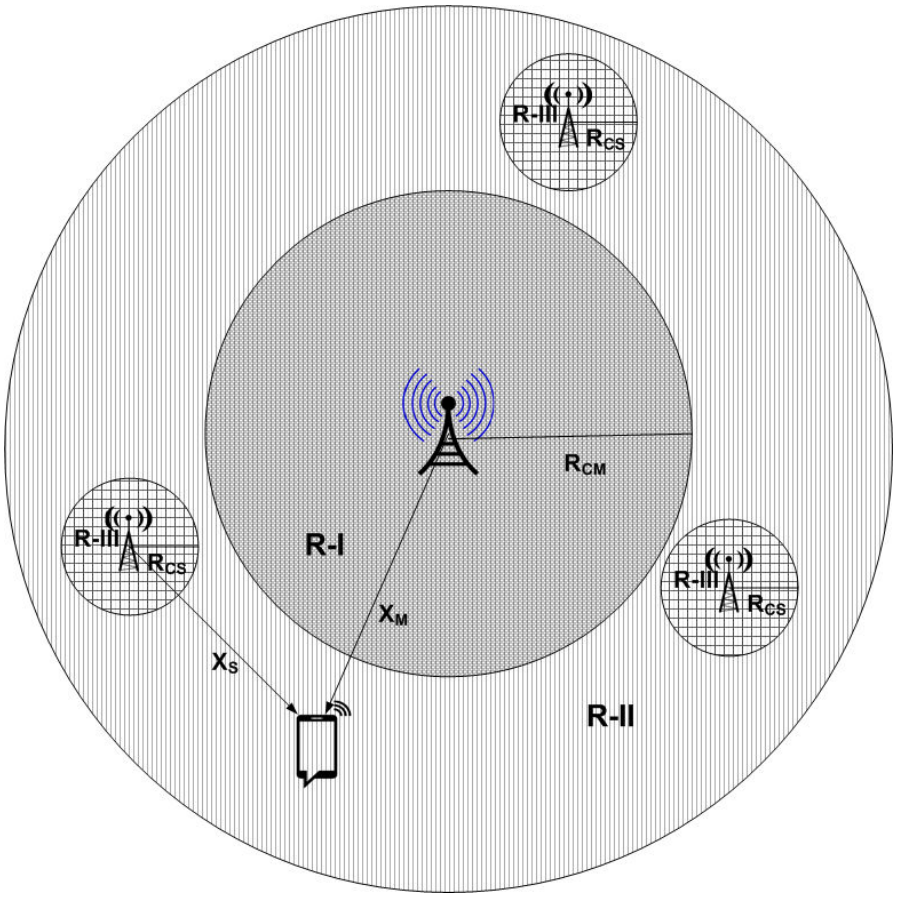

FIGURE 4.3: Critical distance based association regions for T-UE in a two-tier NuHCN.

It is clear from these expressions that the location of T-UE in any of the association regions is dependent on both the tier densities and critical distances. The PDF of X_i where $x_i \geq 0$ can also be expressed using (4.3) as,

$$f_{X_i}(x_i) = 2\pi\lambda_i x_i \exp\left(-\pi\lambda_i x_i^2\right). \tag{4.4}$$

4.3.1 Tier Association Probability

The association of T-UE with any BS tier is chiefly dependent on BS density, transmit power and distance from the nearest BS of that tier. Using DS-PLM, the importance of distance between the deployed BSs and UEs considerably increase owing to the disparity in estimated path loss (due to different power decay rates) for smaller and larger communicating distances. In accordance with the system

model, if the T-UE lies within the R_{CM} of its nearest MBS, then it is forced to associate with it (i.e., the nearest MBS) as all SBSs within the R_{CM} of each MBS are muted. Meanwhile, the T-UE association with any BS for the remaining coverage areas of the NuHCN is solely based on the highest averaged biased received power.

The likelihood that T-UE associates with macro tier in a two-tier NuHCN, when the path loss is estimated using DS-PLM is given as,

$$\mathcal{A}_{\mathcal{M}} = \mathcal{A}_{\mathcal{M},R_{\text{OUT}}} + \mathcal{A}_{\mathcal{M},R_{\text{IN}}}, \tag{4.5}$$

where $\mathcal{A}_{\mathcal{M},R_{\text{OUT}}}$ refers to the T-UE association with macro tier when the nearest MBS is at least apart by R_{CM}, while $\mathcal{A}_{\mathcal{M},R_{\text{IN}}}$ denotes the T-UE association with macro tier when the distance between T-UE and its closest MBS is less than R_{CM}.

Lemma 4.3.1*: When the T-UE is located within the R_{CM} of its nearest neighbor, it is only permitted to associate with it and its likelihood is given using the 2D null probability as:*

$$\mathcal{A}_{\mathcal{M},X_M<R_{CM}} = 1 - \exp\left(-\pi \ \left(\lambda_M R_{CM}^2\right)\right) \tag{4.6}$$

It is clear from (4.6) that the T-UE association probability in R-I is independent of λ_S and R_{CS} as the SBSs within R_{CM} are muted. Moreover, it is interesting to note here that the T-UE association within R_{CM} is not affected by the BS transmit powers and PLEs (pre-critical and post-critical) of both tiers either, as the only dominant factor dictating this likelihood is the R_{CM} which is also the size of exclusion region. As described earlier, when the T-UE is located within the R_{CM} of its nearest MBS, it receives network services from macro tier only. Therefore, the T-UE association with small tier within R-I, i.e., $\mathcal{A}_{\mathcal{S},X_S<R_{CS}} = 0$.

When the distance between T-UE and its nearest MBS is greater than R_{CM}, and the T-UE receives higher power from it as compared to the closest SBS even after considering extended cell range of small BS tier, then this resultant association probability of T-UE with macro tier falls in two regions i.e., R-II and R-III as given in Table 4.1.

Lemma 4.3.2*: The association probability of T-UE with macro tier in R-II is given as,*

$$\mathcal{A}_{\mathcal{M},R\text{-}II} = 2\pi\lambda_M \int_{R_{CM}}^{\infty} x_M \begin{cases} \exp\left(-\pi \ \left(\lambda_M x_M^2 + \lambda_S (g_1(x_M))^2\right)\right) \ \mathrm{d}x_M & g_1(x_M) \geq R_{CS} \\ \exp\left(-\pi \ \left(\lambda_M x_M^2 + \lambda_S R_{CS}^2\right)\right) \ \mathrm{d}x_M & g_1(x_M) < R_{CS} \end{cases}, \tag{4.7}$$

where $g_1(x_M) = \left(P_S B_S \eta_S / P_M \eta_M\right)^{1/\alpha_{1S}} x_M^{\alpha_{1M}/\alpha_{1S}}$ and $\eta_i = R_{Ci}^{\alpha_{1i}-\alpha_{0i}}$.

It is obvious from (4.7) that besides λ_i and P_i, the T-UE association probability in R-II is dependent upon α_{1i}, B_S and R_{Ci} as well.

Proof: The joint association probability of T-UE with macro tier in R-II is given by the following probabilistic event

$$\mathcal{A}_{\mathcal{M},\text{R-II}} = \mathbb{P}\left[{P_r}^M > {P_r}^S, \text{R-II}\right], \tag{4.8}$$

where ${P_r}^M$ and ${P_r}^S$ are received powers from the nearest macro and small tier BSs respectively. By using DS-PLM, the averaged received powers from the respective nearest BSs of both tiers in R-II are ${P_r}^M = P_M \eta_M L_0 x_M^{-\alpha_{1M}}$ and ${P_r}^S = P_S B_S \eta_S L_0 x_S^{-\alpha_{1S}}$ respectively. Inserting them in (4.8) to get

$$\mathcal{A}_{\mathcal{M},\text{R-II}} = \mathbb{P}\left[P_M \eta_M L_0 x_M^{-\alpha_{1M}} > P_S B_S \eta_S L_0 x_S^{-\alpha_{1S}}, \ \text{R-II}\right], \tag{4.9}$$

rearranging the terms in (4.9) gives

$$\mathcal{A}_{\mathcal{M},\text{R-II}} = \mathbb{P}\left[x_S \ > \ \left(\frac{P_S B_S \eta_S}{P_M \eta_M}\right)^{\frac{1}{\alpha_{1S}}} x_M^{\frac{\alpha_{1M}}{\alpha_{1S}}}, \ \text{R-II}\right]. \tag{4.10}$$

From Table 4.1, we already know the constraints on X_M and X_S in R-II, and based on those (4.10) takes the integral form as

$$\mathcal{A}_{\mathcal{M},\text{R-II}} = \int_{R_{CM}}^{\infty} \mathbb{P}\left[(x_S > g_1(x_M) \ \cap \ x_S > R_{CS}), \text{R-II}\right] \ f_{X_M}(x_M) \ \mathrm{d}x_M, \tag{4.11}$$

where $f_{X_M}(x_M)$ is already given in (4.4). The integration limits in (4.11) are from R_{CM} to ∞, as X_M is constrained over the same range as well. Now, simplifying (4.11) by using (4.3) gives the desired expression for association probability of T-UE with macro tier in R-II and completes the proof of (4.7). ■

Similarly, by following the procedure adopted in the derivation of (4.7), the association probability of T-UE with small tier in R-II using DS-PLM is given as:

$$\mathcal{A}_{\mathcal{S},\text{R-II}} = 2\pi\lambda_S \int_{R_{CS}}^{\infty} x_S \begin{cases} \exp\left(-\pi \ \left(\lambda_S x_S^2 + \lambda_M {k_A}^2\right)\right) \ \mathrm{d}x_S & k_A \geq R_{CM} \\ \exp\left(-\pi \ \left(\lambda_S x_S^2 + \lambda_M R_{CM}^2\right)\right) \ \mathrm{d}x_S & k_A < R_{CM} \end{cases}, \quad (4.12)$$

where $k_A = \left(P_M \eta_M / P_S B_S \eta_S\right)^{1/\alpha_{1M}} x_S^{\alpha_{1S}/\alpha_{1M}}$.

Lemma 4.3.3*: The association probability of T-UE with macro tier in R-III using DS-PLM is given as:*

$$\mathcal{A}_{\mathcal{M},\text{R-III}} = 2\pi\lambda_M \int_{R_{CM}}^{\infty} x_M \exp\left(-\pi\lambda_M x_M^2\right) \left(\exp\left(-\pi\lambda_S \gamma^2\right) - \exp\left(-\pi\lambda_S R_{CS}^2\right) \right) \mathrm{d}x_M. \quad (4.13)$$

where $\gamma = \left(P_S B_S / P_M \eta_M\right)^{1/\alpha_{0S}} x_S^{\alpha_{0S}/\alpha_{1M}}$. The expression given in (4.13) clearly highlights the parameters that affect the T-UE association with macro tier in this specific region.

Proof: Please refer to Appendix B.1. ■

Similarly, by following the procedure adopted in the derivation of (4.13), the association probability of T-UE with small tier in R-III using DS-PLM is given as:

$$\mathcal{A}_{\mathcal{S},\text{R-III}} = 2\pi\lambda_S \int_{0}^{R_{CS}} x_S \begin{cases} \exp\left(-\pi \ \left(\lambda_S x_S^2 + \lambda_M {k_B}^2\right)\right) \ \mathrm{d}x_S & k_B \geq R_{CM} \\ \exp\left(-\pi \ \left(\lambda_S x_S^2 + \lambda_M R_{CM}^2\right)\right) \ \mathrm{d}x_S & k_B < R_{CM} \end{cases}, \quad (4.14)$$

where $k_B = \left(P_M \eta_M / P_S B_S\right)^{1/\alpha_{1M}} x_S^{\alpha_{0S}/\alpha_{1M}}$.

Finally, by plugging (4.6), (4.7), (4.13) in (4.5) we get the complete expression for T-UE macro association probability when DS-PLM is used to estimate the path

loss in a two-tier NuHCN.

Remark 4.3.1*: It is clear from the derived expressions of each region that disparity in transmit power of both tiers is the primary reason which creates load imbalance between the BS tiers, and it could be finely tuned by opting subtle values of* B_S *and* R_{CS} *as both parameters can assist in proactive offloading of UEs to the smaller BS tier.*

4.3.2 Distribution of the Statistical Distances Between T-UE and its Serving BS for the two-tier NuHCN

In this subsection, we present the PDFs for T-UE association distances with macro tier w.r.t R_{CM} i.e., for link distances greater and smaller than R_{CM}.

Lemma 4.3.4*: The PDF given T-UE is macro tier associated and located at distances greater than* R_{CM} *from its nearest MBS is given as*

$$f_{X_M|X_M>R_{CM}}(x_M) = \frac{2\pi\lambda_M x_M \begin{cases} \exp\left(-\pi\left(\lambda_M x_M^2 + \lambda_S (g_1(x_M))^2\right)\right) & g_1(x_M) \geq R_{CS} \\ \exp\left(-\pi\left(\lambda_M x_M^2 + \lambda_S \gamma^2\right)\right) & g_1(x_M) < R_{CS} \end{cases}}{\mathcal{A}_{\mathcal{M},\text{R-II}} + \mathcal{A}_{\mathcal{M},\text{R-III}}}. \quad (4.15)$$

Proof:

For a macro tier associated T-UE which is located at a distance greater than R_{CM} from its nearest MBS, the likelihood of event $X_M > x_M$ is given as

$$\mathbb{P}\left[X_M > x_M\right] = \mathbb{P}\left[X_M > x_M \middle| \left(\mathcal{A}_{\mathcal{M}}, X_M > R_{CM}\right)\right]. \quad (4.16)$$

Using conditional probability, the right hand side (R.H.S) of (4.16) can be expressed in terms of a joint probability event as,

$$\mathbb{P}\left[X_M > x_M\right] = \frac{\mathbb{P}\left[X_M > x_M, {P_r}^M > {P_r}^S, X_M > R_{CM}\right]}{\mathbb{P}\left[{P_r}^M > {P_r}^S, X_M > R_{CM}\right]}, \quad (4.17)$$

where the denominator in (4.17) is given by

$$\left[{P_r}^M > {P_r}^S, X_M > R_{CM}\right] = \mathcal{A}_{\mathcal{M},\text{R-II}} + \mathcal{A}_{\mathcal{M},\text{R-III}}. \tag{4.18}$$

The integral form of (4.17) can be expressed as

$$\mathbb{P}\left[X_M > x_M\right] = \frac{\int_{x_M}^{\infty} \mathbb{P}\Big[(X_S > g_1(x_M) \cap X_S > R_{CS}) \cup (X_S > \gamma \cap X_S \leq R_{CS})\Big]}{\mathcal{A}_{\mathcal{M},\text{R-II}} + \mathcal{A}_{\mathcal{M},\text{R-III}}} \times f_{X_M}(x_M)\, \mathrm{d}x_M. \tag{4.19}$$

The proof of PDF of X_M conditioned on link distance between T-UE and associated MBS greater than R_{CM} completes after taking derivative and some simplifications. ■

Lemma 4.3.5*: The PDF given T-UE is macro tier associated and located at distances smaller than R_{CM} from its nearest MBS, is given as*

$$f_{X_M|X_M<R_{CM}}(x_M) = \frac{2\pi\lambda_M x_M \exp\left(-\pi\lambda_M x_M^2\right)}{1-\exp\left(-\pi\lambda_M R_{CM}^2\right)}. \tag{4.20}$$

Proof: The PDF expression given in (4.20) can be easily derived using 2-D null probability. ■

Lemma 4.3.6*: The PDF given T-UE is small tier associated and located at distances greater than R_{CS} from its nearest SBS is given as*

$$f_{X_S|X_S>R_{CS}}(x_S) = \frac{2\pi\lambda_S x_S}{\mathcal{A}_{\mathcal{S},\text{R-II}}} \begin{cases} \exp\left(-\pi\left(\lambda_S x_S^2 + \lambda_M {k_A}^2\right)\right) & k_A \geq R_{CM} \\ \exp\left(-\pi\left(\lambda_S x_S^2 + \lambda_M {R_{CM}}^2\right)\right) & k_A < R_{CM} \end{cases}, \tag{4.21}$$

where $\mathcal{A}_{\mathcal{S},\text{R-II}}$ is already given in (4.12).

Proof: The PDF expression given in (4.21) can be derived by following the derivation steps of (4.15). ■

Lemma 4.3.7*: The PDF given T-UE is small tier associated and located at distances smaller than R_{CS} from its nearest SBS is given as*

$$f_{X_S|X_S<R_{CS}}(x_S) = \frac{2\pi\lambda_S x_S}{\mathcal{A}_{\mathcal{S},R\text{-}III}} \begin{cases} \exp\left(-\pi\left(\lambda_S x_S^2 + \lambda_M R_{CM}^2\right)\right) & k_B \leq R_{CM} \\ q_B + \exp\left(-\pi\left(\lambda_S x_S^2 + \lambda_M {k_B}^2\right)\right) & k_B > R_{CM} \end{cases}. \tag{4.22}$$

Proof: The PDF expression given in (4.22) can be derived by following the derivation steps of (4.15). ■

4.4 Coverage Probability

The T-UE is said to be in network coverage if the received instantaneous SINR from its associated BS is above a predefined threshold τ. The overall network coverage in a two-tier cellular network is the sum of coverages offered by both BS tiers, i.e., $\mathrm{C_{P_i}}$ and is expressed as

$$\mathbb{C}_{\mathbb{P}} = \sum_{i=1}^{2} \mathrm{C_{P_i}}. \tag{4.23}$$

Therefore, for computing the overall network coverage, individual contributions of both macro and small tiers for both regions i.e., $X_i > R_{Ci}$ and $X_i < R_{Ci}$ are to be determined. The coverage probability of tier i can be expressed as

$$\mathrm{C_{P_i}} = \mathrm{C_{P_i|X_i>R_{Ci}}}\mathcal{A}_{i,X_i>R_{Ci}} + \mathrm{C_{P_i|X_i<R_{Ci}}}\mathcal{A}_{i,X_i<R_{Ci}}, \tag{4.24}$$

where $\mathrm{C_{P_i|X_i>R_{Ci}}}$ and $\mathrm{C_{P_i|X_i<R_{Ci}}}$ denote the conditional coverage offered by tier i in both regions respectively, while $\mathcal{A}_{i,X_i>R_{Ci}}$ and $\mathcal{A}_{i,X_i<R_{Ci}}$ represent the joint association probabilities in both regions respectively.

Now by using [68], the probability that T-UE is in coverage, which is equivalent to the CCDF of SINR ($\Gamma_{X_i}(x_i)$) at a distance x_i from its associated ith tier BS

can be expressed as

$$\mathbb{P}[\Gamma_{X_i}(x_i) > \tau] = \exp\left(\frac{-\tau\sigma^2}{P_i l\left(x_i\right)}\right) \prod_{i \,\epsilon\, \{\phi_{M,N} \,\cup\, \phi_{S,N}\}} \mathcal{L}_{\mathcal{I}_\rangle}\left(\frac{\tau}{P_i l(x_i)}\right), \tag{4.25}$$

where $l(x_i)$ refers to the generic path loss function, while $\mathcal{L}_{\mathcal{I}_\rangle}$ denotes the Laplace transform of cumulative interference received at T-UE due to both the inter-tier and co-tier BSs that are operating at frequency channel N.

4.4.1 Coverage Probability of T-UE Associated with Macro Tier

For a two-tier NuHCN, the T-UE can associate with macro tier when its distance is either greater or smaller than the R_{CM}. However, it is important to note that when the distance between T-UE and nearest MBS is smaller than R_{CM} then in that scenario the T-UE is forced to associate with that MBS. Meanwhile, if the distance between T-UE and nearest MBS is greater than R_{CM}, then in that case the T-UE association decision wil be made on the highest average received power. Therefore, conditional macro tier coverage for each of the association regions is to be determined and is presented next.

Proposition 4.4.1*: The macro tier coverage for link distance (X_M) greater than R_{CM} corresponds to the cumulative likelihood in association regions R-II and R-III, respectively. The resultant expression for the region $X_M > R_{CM}$ is given as*

$$\mathrm{C}_{P_M|X_M>R_{CM}}(x_M) = \int_{R_{CM}}^{\infty} \frac{2\pi\lambda_M x_M}{\mathcal{A}_{\mathcal{M},\text{R-II}} + \mathcal{A}_{\mathcal{M},\text{R-III}}} \left(\exp\left(\frac{-\tau\sigma^2}{P_M \eta_M L_0 x_M^{-\alpha_{1M}}}\right) \times \exp\left(\frac{-2\pi\lambda_M \tau\, x_M^2}{N(-2+\alpha_{1M})} {}_2F_1\left[1, 1-\frac{2}{\alpha_{1M}}; 2-\frac{2}{\alpha_{1M}}; -\tau\right]\right)\right)$$

$$\times \begin{cases} \exp\left(\frac{-2\pi\lambda_S\tau(g_1(x_M))^2}{N(-2+\alpha_{1S})}\ {}_2F_1\left[1,1-\frac{2}{\alpha_{1S}};2-\frac{2}{\alpha_{1S}};-\frac{\tau}{B_S}\right]\right) \\ \qquad \times\ \exp\left(-\pi\left(\lambda_M x_M^2+\lambda_S g_1(x_M)^2\right)\right)\ \mathrm{d}x_M & g_1(x_M)\geq R_{CS} \\ \exp\left(\frac{-2\pi\lambda_S}{N}\left(\frac{(g_0(x_M))^2}{2}\ {}_2F_1\left[1,\frac{2}{\alpha_{0S}};1+\frac{2}{\alpha_{0S}};-\frac{B_S}{\tau}\right]\right.\right. \\ \quad +\frac{R_{CS}^2}{2}\ {}_2F_1\left[1,\frac{2}{\alpha_{0S}};1+\frac{2}{\alpha_{0S}};-\frac{P_M\eta_M(R_{CS})^{\alpha_{0S}}}{P_S\tau(x_M)^{\alpha_{1M}}}\right]+\frac{P_SB_S\tau\ x_M^{\alpha_{1M}}}{P_M\eta_M(-2+\alpha_{0S})} \\ \quad \left.\left.\times\ \left(R_{CS}^{2-\alpha_{0S}}\right){}_2F_1\left[1,1-\frac{2}{\alpha_{0S}};2-\frac{2}{\alpha_{0S}};-\frac{P_SB_S\tau(x_M)^{\alpha_{1M}}}{P_M\eta_M(R_{CS})^{\alpha_{0S}}}\right]\right)\right) \\ \times\ \exp\left(-\pi\left(\lambda_M x_M^2+\lambda_S R_{CS}^2+\lambda_S\left(\frac{P_SB_S}{P_M\eta_M}\right)^{\frac{2}{\alpha_{0S}}}x_S^{\frac{2\alpha_{0S}}{\alpha_{1M}}}\right)\right)\ \mathrm{d}x_M & g_1(x_M)<R_{CS} \end{cases} \tag{4.26}$$

where $g_0(x_M)=(P_SB_S/P_M\eta_M)^{1/\alpha_{0S}}x_M^{\alpha_{1M}/\alpha_{0S}}$ and
$g_1(x_M)=(P_SB_S\eta_S/P_M\eta_M)^{1/\alpha_{1S}}\ x_M^{\alpha_{1M}/\alpha_{1S}}$.

Proof: The macro tier coverage for link distance X_M greater than R_{CM} is given by the following integral equation as

$$\mathrm{C}_{P_M|X_M>R_{CM}}(x_M)=\int_{R_{CM}}^{\infty}\mathbb{P}[\Gamma_{X_{M|X_M>R_{CM}}}(x_M)>\tau]\ f_{X_M|X_M>R_{CM}}(x_M)\ \mathrm{d}x_M, \tag{4.27}$$

where $f_{X_M|X_M>R_{CM}}(x_M)$ is already determined in section 4.3.2 and is given in (4.15), while $\mathbb{P}[\Gamma_{X_{M|X_M>R_{CM}}}(x_M)>\tau]$ is yet to be derived. The limits of integration in (4.27) are from R_{CM} to ∞, as the distance between T-UE and closest MBS (to which the T-UE associates) is greater than R_{CM}.

Using (4.25) and by substituting the respective parametric values, the CCDF conditioned on X_M greater than R_{CM} can be expressed as

$$\mathbb{P}[\Gamma_{X_M|X_M>R_{CM}}(x_M)>\tau]=\exp\left(\frac{-\tau\sigma^2x_M^{\alpha_{1M}}}{P_M\eta_ML_0}\right)\mathcal{L}_{\mathcal{I}_\mathcal{M}}\left(\frac{\tau\ x_M^{\alpha_{1M}}}{P_M\eta_M}\right)\mathcal{L}_{\mathcal{I}_\mathcal{S}}\left(\frac{\tau\ x_M^{\alpha_{1M}}}{P_M\eta_M}\right). \tag{4.28}$$

In (4.28), the cumulative effect of co-tier and inter-tier interference is to be determined and Laplace transform is used to determine their contributions. Meanwhile, it is important to note that only those BSs from both tiers interfere with the reference link that are operating at frequency channel i.e., N. Using Campbell Mecke

theorem and PGFL property of the PPP, the Laplace transform of co-tier interference $\mathcal{L}_{\mathcal{I}_\mathcal{M}}$ is given as

$$\mathcal{L}_{\mathcal{I}_\mathcal{M}}\left(\frac{\tau\ x_M^{\alpha_{1M}}}{P_M\eta_M}\right) = \exp\left(\frac{-2\pi\lambda_M}{N}\int_{x_M}^{\infty}\frac{y}{1+\left(x_M^{\alpha_{1M}}\tau\right)^{-1}y^{\alpha_{1M}}}\mathrm{d}y\right). \tag{4.29}$$

The integration limits in computation of $\mathcal{L}_{\mathcal{I}_\mathcal{M}}$ in (4.29) are from x_M to ∞, as the nearest co-tier interferer must be at least farther than x_M. Simplifying the integrand in (4.29) by substituting $u_M = \left(x_M^{\alpha_{1M}}\tau\right)^{-2/\alpha_{1M}}y^2$ and solving it gives

$$\mathcal{L}_{\mathcal{I}_\mathcal{M}}\left(\frac{\tau\ x_M^{\alpha_{1M}}}{P_M\eta_M}\right) = \exp\left(\frac{-2\pi\lambda_M\tau x_M^2}{N(-2+\alpha_{1M})}{}_2F_1\left[1,1-\frac{2}{\alpha_{1M}};2-\frac{2}{\alpha_{1M}};-\tau\right]\right), \tag{4.30}$$

where ${}_2F_1[\ .\ ]$ is the well-known Gauss Hypergeometric function and (4.30) gives the contribution of macro tier interference in CCDF conditioned on x_M greater than R_{CM}.

Similar to (4.29), the $\mathcal{L}_{\mathcal{I}_\mathcal{S}}$ is also expressed as

$$\mathcal{L}_{\mathcal{I}_\mathcal{S}}\left(\frac{\tau\ x_M^{\alpha_{1M}}}{P_M\eta_M}\right) = e^{\left[\frac{-2\pi\lambda_S}{N}\begin{cases}\int_{g_0(x_M)}^{\infty}\frac{y}{1+\left(x_M^{\alpha_{1M}}\frac{P_S}{P_M\eta_M}\tau\right)^{-1}y^{\alpha_{0S}}}\mathrm{d}y & g_1(x_M)\le R_{CS}\\ \int_{g_1(x_M)}^{\infty}\frac{y}{1+\left(x_M^{\alpha_{1M}}\frac{P_S\eta_S}{P_M\eta_M}\tau\right)^{-1}y^{\alpha_{1S}}}\mathrm{d}y & g_1(x_M)> R_{CS}\end{cases}\right]}. \tag{4.31}$$

It is clear from (4.31), that computing the received interference from neighboring SBSs requires solving two integrals. This is because, the T-UE may associate with macro tier both within and outside R_{CS} while its distance from the nearest MBS is greater than R_{CM}. The received interference from within R_{CS} is determined

with integration limits $g_0(x_M)$ to ∞ while the limits for the second integral are from $g_1(x_M)$ to ∞. Meanwhile, similar to (4.29), the T-UE receives interference from only those SBSs which are operating at the frequency of its associated MBS.

Now, simplifying the integrands in (4.31) by using suitable substitutions gives

$$\mathcal{L}_{\mathcal{I}_S}\left(\frac{\tau\ x_M^{\alpha_{1M}}}{P_M\eta_M}\right) = \begin{cases} \exp\left(\frac{-2\pi\lambda_S\tau(g_1(x_M))^2}{N(-2+\alpha_{1S})}\right. \\ \left.\times\ {}_2F_1\left[1, 1-\frac{2}{\alpha_{1S}}; 2-\frac{2}{\alpha_{1S}}; -\frac{\tau}{B_S}\right]\right) \\ \qquad\qquad\qquad\qquad\qquad\qquad\qquad\qquad g_1(x_M) \geq R_{CS} \\ \exp\left(\frac{-2\pi\lambda_S}{N}\left(\frac{(g_0(x_M))^2}{2}\right.\right. \\ \times\ {}_2F_1\left[1, \frac{2}{\alpha_{0S}}; 1+\frac{2}{\alpha_{0S}}; -\frac{B_S}{\tau}\right] + \frac{R_{CS}^2}{2} \\ \times\ {}_2F_1\left[1, \frac{2}{\alpha_{0S}}; 1+\frac{2}{\alpha_{0S}}; -c_2(x_M)\right] \\ +\frac{P_S\eta_S\tau\ x_M^{\alpha_{1M}}}{P_M\eta_M(-2+\alpha_{1S})}\left(R_{CS}^{2-\alpha_{1S}}\right) \\ \left.\left.\times\ {}_2F_1\left[1, 1-\frac{2}{\alpha_{1S}}; 2-\frac{2}{\alpha_{1S}}; -c_3(x_M)\right]\right)\right) \\ \qquad\qquad\qquad\qquad\qquad\qquad\qquad\qquad g_1(x_M) < R_{CS} \end{cases}, \tag{4.32}$$

where,

$c_2(x_M) = (P_M\eta_M(R_{CS})^{\alpha_{0S}})/(P_S\tau(x_M)^{\alpha_{1M}})$ and $c_3(x_M) = (P_S\eta_S\tau(x_M)^{\alpha_{1M}})/(P_M\eta_M(R_{CS})^{\alpha_{1S}})$.

Now by plugging the respective values of $\mathcal{L}_{\mathcal{I}_\mathcal{M}}$ and $\mathcal{L}_{\mathcal{I}_\mathcal{S}}$ in (4.27), completes the proof of (4.26). ■

Proposition 4.4.2*: The macro tier coverage for link distance smaller than R_{CM} corresponds to the coverage likelihood in R-I. The resultant expression for the network coverage in region $X_M < R_{CM}$ is given as*

$$\mathrm{C}_{P_M|X_M<R_{CM}}(x_M) = \frac{2\pi\lambda_M}{(1-\exp\left(-\pi\lambda_M R_{CM}^2\right))} \times \int_0^{R_{CM}} \frac{x_M \exp\left(-\left(2\pi\lambda_S + \pi\lambda_M x_M^2 + \tau\sigma^2\right)\right)}{\exp\left(P_M L_0 x_M^{-\alpha_{0M}} + N(-2+\alpha_{1S})\right)}$$

$$\times \begin{cases} \left(-\frac{P_S \tau \eta_S x_M^{\alpha_{0M}} (R_{CM}-x_M)^{-2+\alpha_{1S}}}{P_M} \right. \\ \left. \times \ {}_2F_1\left[1, 1-\frac{2}{\alpha_{1S}}; 2-\frac{2}{\alpha_{1S}}; -\frac{P_S \eta_S x_M^{\alpha_{0M}} \tau}{P_M (R_{CM}-x_M)^{\alpha_{1S}}}\right] \right) & x_M \leq R_{CM} - R_{CS} \\ \left(-\frac{P_S \tau \eta_S x_M^{\alpha_{0M}} (R_{CM}+R_{CS}-x_M)^{-2+\alpha_{1S}}}{P_M} \right. \\ \left. \times \ {}_2F_1\left[1, 1-\frac{2}{\alpha_{1S}}; 2-\frac{2}{\alpha_{1S}}; -\frac{P_S \eta_S x_M^{\alpha_{0M}} \tau}{P_M (R_{CM}+R_{CS}-x_M)^{\alpha_{1S}}}\right] \right) & x_M > R_{CM} - R_{CS} \end{cases}$$

$$\times \exp\left[\frac{-2\pi\lambda_M}{N} \left(\left(-\frac{x_M^2}{2} \ {}_2F_1\left[1, \frac{2}{\alpha_{0M}}; 1+\frac{2}{\alpha_{0M}}; -\frac{1}{\tau}\right] \right) + \frac{R_{CM}^2}{2} \right. \right.$$

$$\times \ {}_2F_1\left[1, \frac{2}{\alpha_{0M}}; 1+\frac{2}{\alpha_{0M}}; -\left(\frac{R_{CM}}{x_M}\right)^{\alpha_{0M}} \frac{1}{\tau}\right] + \frac{\eta_M \tau x_M^{\alpha_{0M}} (R_{CM})^{2-\alpha_{1M}}}{-2+\alpha_{1M}}$$

$$\left. \left. \times \ {}_2F_1\left[1, 1-\frac{2}{\alpha_{1M}}; 2-\frac{2}{\alpha_{1M}}; -\frac{\eta_M \tau (x_M)^{\alpha_{0M}}}{(R_{CM})^{\alpha_{1M}}}\right] \right) \right] \mathrm{d}x_M. \quad (4.33)$$

Proof: Please refer to Appendix B.2. ■

4.4.2 Coverage Probability of T-UE Associated with Small Tier

For a two-tier NuHCN, the T-UE can associate with small tier when its distance is either greater or smaller than the R_{CS}. Therefore, the expressions for the conditional coverage of small tier in each of the association regions needs to be determined.

Proposition 4.4.3*: The small tier coverage for link distance (X_S) greater than R_{CS} corresponds to the cumulative likelihood in association region R-II and can be expressed as*

$$\mathrm{C}_{P_S|X_S>R_{CS}}(x_S) = \frac{2\pi\lambda_S}{\mathcal{A}_{\mathcal{S},R\text{-}II}} \int_{R_{CS}}^{\infty} x_S \exp\left(\frac{-\tau\sigma^2}{P_S \eta_S L_0 x_S^{-\alpha_{1S}}} \right)$$

$$\times \exp\left(\frac{-2\pi\lambda_S \tau \ x_S^2}{N(-2+\alpha_{1S})} \ {}_2F_1\left[1, 1-\frac{2}{\alpha_{1S}}; 2-\frac{2}{\alpha_{1S}}; -\tau\right] \right)$$

$$\times \begin{cases} \exp\left(-\pi\left(\lambda_S x_S^2 + \lambda_M {k_A}^2\right)\right) \exp\left(\frac{-2\pi\lambda_M \tau B_S k_A^2}{N(-2+\alpha_{1M})}\right. \\ \qquad \left.\times\ {}_2F_1\left[1, 1-\frac{2}{\alpha_{1M}}; 2-\frac{2}{\alpha_{1M}}; -\tau B_S\right]\right) \mathrm{d}x_S & k_A \geq R_{CM} \\ \exp\left(-\pi\left(\lambda_S x_S^2 + \lambda_M {R_{CM}}^2\right)\right) \exp\left(\frac{-2\pi\lambda_M \tau B_S k_D {x_S}^2 {R_{CM}}^{2-\alpha_{1M}}}{N(-2+\alpha_{1M})}\right. \\ \qquad \left.\times\ {}_2F_1\left[1, 1-\frac{2}{\alpha_{1M}}; 2-\frac{2}{\alpha_{1M}}; -\frac{k_D \tau {x_S}^{\alpha_{1S}}}{{R_{CM}}^{\alpha_{1M}}}\right]\right) \mathrm{d}x_S & k_A < R_{CM} \end{cases}, \tag{4.34}$$

where $k_D{=}P_M\eta_M/P_S\eta_S$.

Proof: The expression given in (4.34) can be derived by following the derivation steps of 4.26. ■

Proposition 4.4.4*: The small tier coverage for link distance (X_S) smaller than R_{CS} corresponds to the cumulative likelihood in association region R-III. The resultant expression for $X_S < R_{CS}$ is given as*

$$\begin{aligned} \mathrm{C}_{P_S|X_S<R_{CS}}(x_S) = \frac{2\pi\lambda_S}{\mathcal{A}_{\mathcal{S},\text{R-II}} + \mathcal{A}_{\mathcal{S},\text{R-IV}}} \int_0^{R_{CS}} \Bigg(& x_S \exp\left(\frac{-\tau\sigma^2}{P_S L_0 x_S^{-\alpha_{0S}}}\right) \\ & \times \exp\Bigg[\frac{-2\pi\lambda_S}{N}\Bigg(-\frac{x_S^2}{2}{}_2F_1\left[1, \frac{2}{\alpha_{0S}}; 1+\frac{2}{\alpha_{0S}}; -\frac{1}{\tau}\right] \\ & + \frac{R_{CS}^2}{2}{}_2F_1\left[1, \frac{2}{\alpha_{0S}}; 1+\frac{2}{\alpha_{0S}}; -\frac{1}{\tau}\left(\frac{R_{CS}}{x_S}\right)^{\alpha_{0S}}\right] \\ & + \frac{\eta_S \tau x_S^{\alpha_{0S}} \left(R_{CS}\right)^{2-\alpha_{1S}}}{(-2+\alpha_{1S})}{}_2F_1\left[1, 1-\frac{2}{\alpha_{1S}}; 2-\frac{2}{\alpha_{1S}}; -\frac{\tau\eta_S x_S^{\alpha_{0S}}}{R_{CS}^{\alpha_{1S}}}\right]\Bigg)\Bigg] \Bigg) \end{aligned}$$

$$\times \begin{cases} \exp\left(-\pi\left(\lambda_S x_S^2 + \lambda_M {R_{CM}}^2\right)\right) \\ \qquad \times \exp\left[-\frac{2\pi\lambda_M}{N}\left(\frac{P_M\eta_M\tau x_S^{\alpha_{0S}} (R_{CM})^{2-\alpha_{1M}}}{P_S(-2+\alpha_{1M})}\right)\right. \\ \quad \left.\times {}_2F_1\left[1, 1-\frac{2}{\alpha_{1M}}; 2-\frac{2}{\alpha_{1M}}; -\frac{P_M\tau\eta_M x_S^{\alpha_{0S}}}{P_S R_{CM}^{\alpha_{1M}}}\right]\right] \mathrm{d}x_S & k_B < R_{CM}. \\ \exp\left[-\frac{2\pi\lambda_M B_S \tau {k_B}^2}{N(-2+\alpha_{1M})}\ {}_2F_1\left[1, 1-\frac{2}{\alpha_{1M}}; 2-\frac{2}{\alpha_{1M}}; -B_S\tau\right]\right] \\ \qquad \times \left(q_B + \exp\left(-\pi\left(\lambda_S x_S^2 + \lambda_M {k_B}^2\right)\right)\right)\ \mathrm{d}x_S & k_B > R_{CM} \end{cases} \tag{4.35}$$

Proof: The expression for the conditional coverage of small tier in R-III given in (4.35) can be similarly derived by adopting the derivation procedure of regional macro tier coverage expressions.

Finally, the complete network coverage expression is determined from (4.23) when the respective conditional coverage expressions of both tiers given in (4.26), (4.33), (4.34) and (4.35) are multiplied with their respective regional association probabilities.

Remark 4.4.1*: It is important to note that the network coverage analysis using DS-PLM does not introduce any additional complexity in computation, as the number of integrals in the final expressions of the analysis carried out for both PLMs are the same. Therefore, the DS-PLM based analysis is more useful as compared to the SS-PLM, owing to the valuable design insights that its usage leads to without adding significant computational complexities.*

4.5 Numerical and Simulation Results

The analytical expressions for the tier association and coverage probabilities have been derived in sections 4.3 and 4.4 respectively. In this section, the accuracy of derived expressions for both performance metrics is validated thorough Monté Carlo simulations. The simulation setup involves placing the T-UE at origin, while the MBS and SBS locations are generated 10^6 times using independent PPPs to ensure all possible BS location possibilities. Furthermore, for ensuring coverage-centric SBS deployments, the SBSs are placed only in those regions where MBSs have either poor or limited coverage. This selective SBS positioning is achieved by assuming that the SBSs lying within the R_{CM} of any MBS are removed or deactivated. Hence, a thinned density of SBSs is considered for the coverage analysis, while original density is assumed for T-AP as all SBSs were available for UEs association. Moreover, for generating the numerical results in this chapter, all necessary parametric values considered are as follows: P_M= 53 dBm, P_S= 33

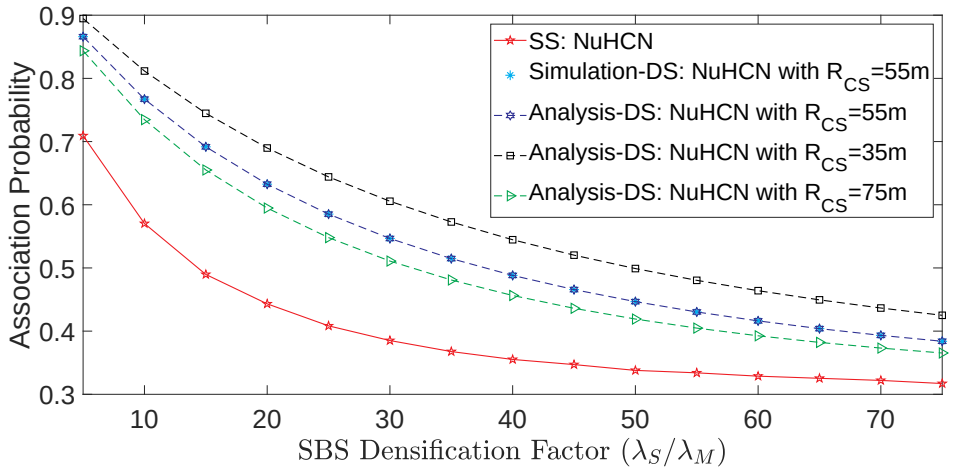

(a)

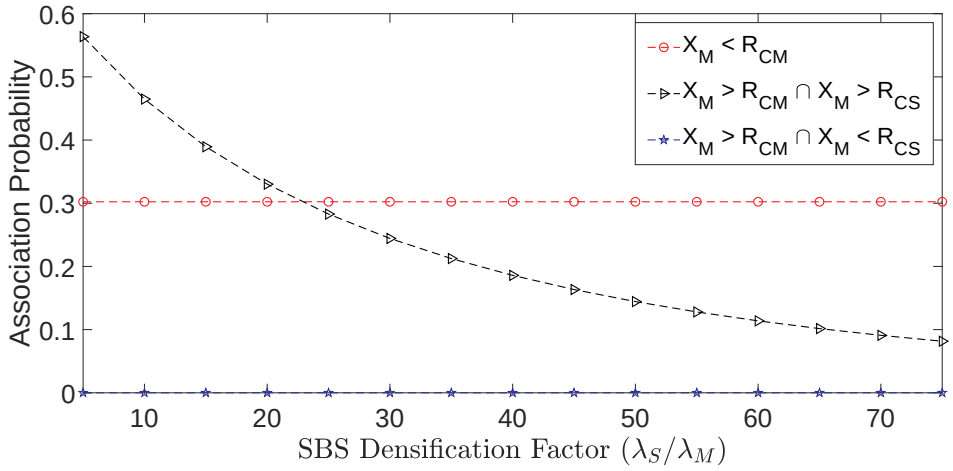

(b)

FIGURE 4.4: Comparison of macro T-AP against varying small tier density

dBm, R_{CM}= 300m,R_{CS}= 55m, B_M= 0 dB, $\alpha_{0M} = \alpha_{0S}$= 2.7, $\alpha_{1M} = \alpha_{1S}$= 3.9, L_0= -32.9 dB and σ^2= -104 dBm.

In order to investigate the performance of DS-PLM based two-tier NuHCN, and for an extensive comparison, we compare the results for both performance metrics with DS-PLM based uniform HCNs and SS-PLM based NuHCNs as well.

4.5.1 Tier Association Probability

In this subsection, the validation of macro T-AP analysis for the two-tier NuHCN using DS-PLM is presented initially, while the estimated macro T-AP results are

further compared with the SS-PLM based NuHCNs. Moreover, a similar comparison is presented for a CRE-based UE association policy as well.

4.5.1.1 Validation of Macro T-AP Analysis and Comparison with Other System Scenarios

For a two-tier NuHCN, a comparison of macro T-AP estimated using SS-PLM and DS-PLM for varying the SBS densification factor (λ_S/λ_M) is depicted in Fig. 4.4(a). It can be readily observed from the figure that the analytical and simulation results for the DS-PLM are in complete agreement with each other and thus, it validates the correctness of T-AP analysis.

Besides this, it is also evident from the figure that the UEs association with macro tier decreases with the increase in λ_S owing to the decrease in distance between UEs and their nearby SBSs. Though, this decrease in distance certainly ensures improved signal strength from SBSs but the SS-PLM clearly overestimates the UEs association with small tier due to the simplistic approach of assuming a fixed signal degradation rate for all distance ranges. Contrarily, the DS-PLM adopts a relatively more realistic strategy based on disparate path loss, to account for the inhomogeneous signal attenuations over varying communicating distances. Consequently, it estimates the UEs association with any BS tier more precisely when compared with the SS-PLM. For instance, it can be seen from the figure that at $\lambda_S = 50\lambda_M$, around 34% of the UEs associate with macro tier as estimated by SS-PLM while the DS-PLM predicts it to be 45% approximately. Thus, the SS-PLM clearly underestimates the UE access load on macro tier. Moreover, it is also evident from the figure that the UEs association with macro tier is dependent on R_{CS} size as well.

For a detailed insight of UEs association with macro tier using DS-PLM, region-wise UEs association is plotted in Fig.4.4(b) against the varying SBS densification factor. It can be seen from the figure that when UEs lie within the R_{CM} of any MBS, they associate with macro tier only without taking into consideration the received power level from their respective nearest SBSs. While it can also be

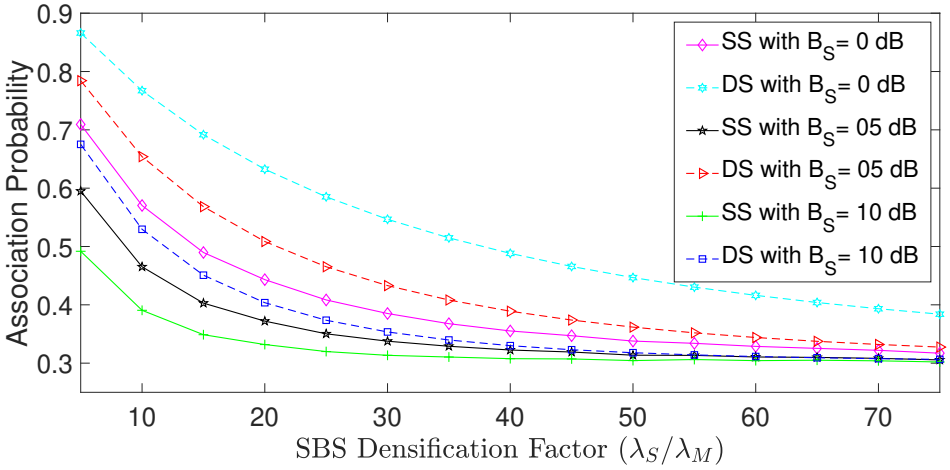

FIGURE 4.5: Comparison of macro T-AP in NuHCNs for both unbiased and biased UE associations.

observed from the figure that UEs prefer associating with small tier whenever the distance from the respective nearest SBS is smaller than R_{CS} owing to the higher received power level from them. Moreover, the UEs mostly receive higher signal strength from their proximate MBSs at small λ_S values due to two major reasons i.e., 1) difference in transmit powers of both BS tiers, 2) the distance between UEs and their respective closest SBSs is usually greater than R_{CS}. Consequently, the need for effective UE steering strategies is highlighted to reduce the UE access burden off macro tier.

4.5.1.2 Impact of SBS Biasing on T-AP in NuHCNs

The disparity in transmit power of BS tiers is the principal cause of load imbalance between BS tiers in uniform HCNs, and it is no different in case of NuHCNs as well. Thus, to account for this difference, static SBS biasing is employed to offload UEs to small BS tier. It is clear from Fig. 4.5 that the SBS biasing helps in offloading UEs to smaller tier which reduces the UE access load on macro tier. It is also evident from the figure that SBS biasing is more effective at relatively lower SBS densification factor. This is because at smaller values of λ_S/λ_M, the UEs mostly lie at distances greater than R_{CS} from their nearest SBSs. Moreover, the transmit power disparity between both BS tiers also paves the way for macro

tier association of UEs. Contrarily, with the consideration of SBS biasing, the association region of SBSs remarkably enhances (as MBSs are far from SBSs) which helps in steering of UEs towards smaller BS tier.

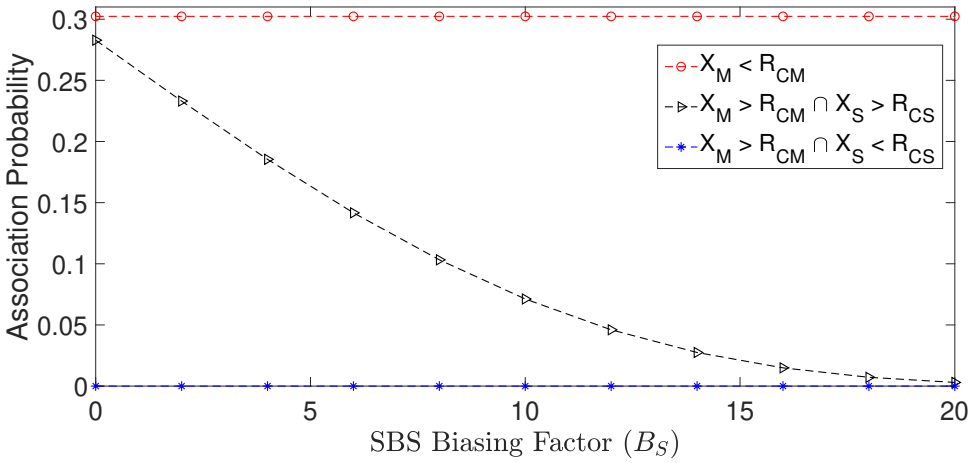

FIGURE 4.6: Impact of SBS biasing on region-based macro T-AP in DS-PLM based NuHCNs.

The SS-PLM usage leads to inaccurate estimation of the load served by any BS tier especially in dense deployment scenarios. Therefore, employing SBS biasing in conjunction with SS-PLM only adds to the error in estimation of the UE access load served by various BS tiers. While DS-PLM is relatively more accurate in estimating the tier load as compared to SS-PLM, hence, it lends same accuracy in the case of biased UE-AS as well. For instance at $\lambda_S = 25\lambda_M$ with B_S=10 dB, the macro T-AP of UEs estimated by SS-PLM decreases by 33%, while in case of DS-PLM, the macro T-AP decreases by 56%. Moreover, for determining the impact of SBS biasing in all UE association regions of the two-tier NuHCN, Fig. 4.6 is plotted. It is clear from the figure that whenever T-UE falls within the R_{CM} of its nearest MBS, increasing B_S has no impact on the macro T-AP in that region. This is because, the macro T-AP within the R_{CM} (i.e., the inhibition region for SBSs) is independent of the received power from nearby SBSs. Contrarily, increasing the biasing factor when the distance between T-UE and the nearest MBS is greater than R_{CM}, the macro T-AP swiftly decreases owing to the increase in size of SBS association regions. These observations categorically suggest that the utility of employing biased UE-AS was underestimated by using SS-PLM.

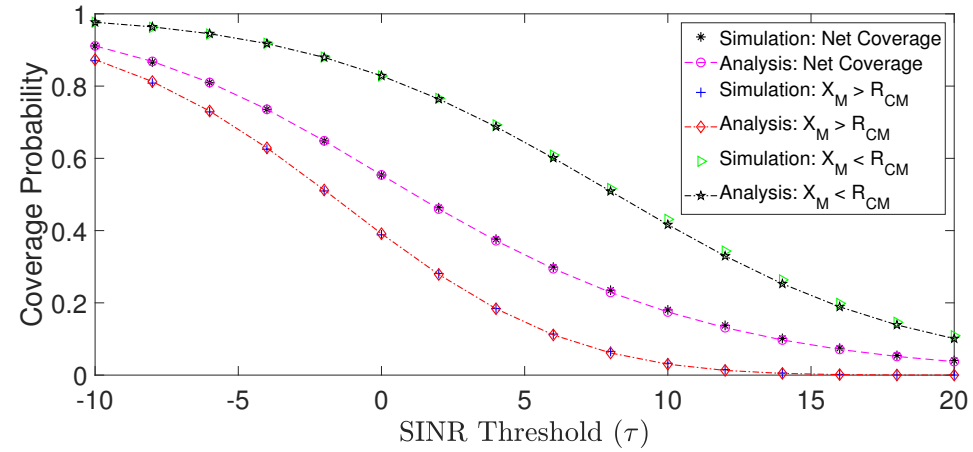

(a)

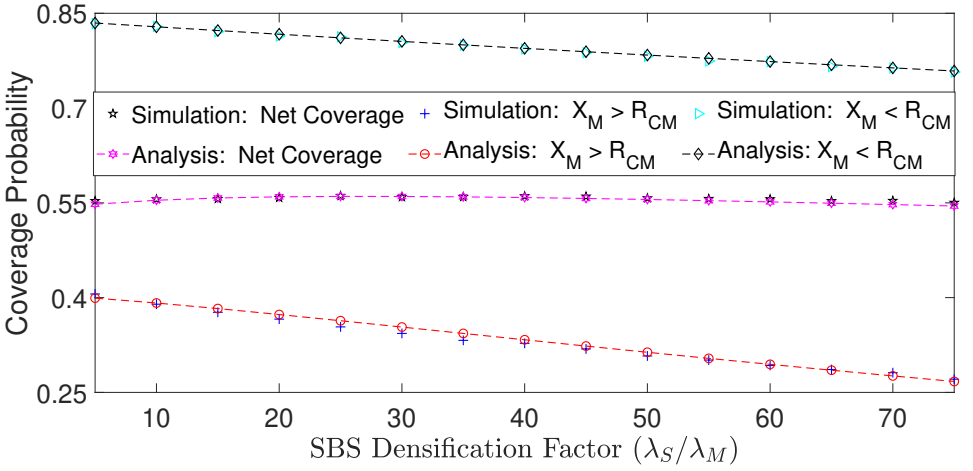

(b)

FIGURE 4.7: Validation of network coverage analysis against varying (a) SINR threshold and (b) Small tier density

4.5.2 Coverage Probability

In this subsection, the validation of network coverage analysis is presented firstly and it is followed by various comparisons of the results achieved for coverage probability through DS-PLM based NuHCNs with multiple system scenarios including SS-PLM based uniform and NuHCNs and DS-PLM based uniform HCNs. Moreover, the individual and joint impact of incorporating SBS biasing and traditional frequency reuse mechanisms in DS-PLM based NuHCNs is also investigated, and it is further compared with other system scenarios as discussed above.

4.5.2.1 Validation of Coverage Analysis

In order to validate the coverage analysis, the estimated results are plotted against varying SINR threshold, τ and SBS densification factor, λ_S/λ_M in Fig. 4.7(a) and Fig. 4.7(b) respectively. It is evident from both the figures that the analytical results are reasonably consistent with the simulation results. Hence, the derived analytical expression for coverage probability can be used to predict the performance trends and in obtaining critical system design insights as well.

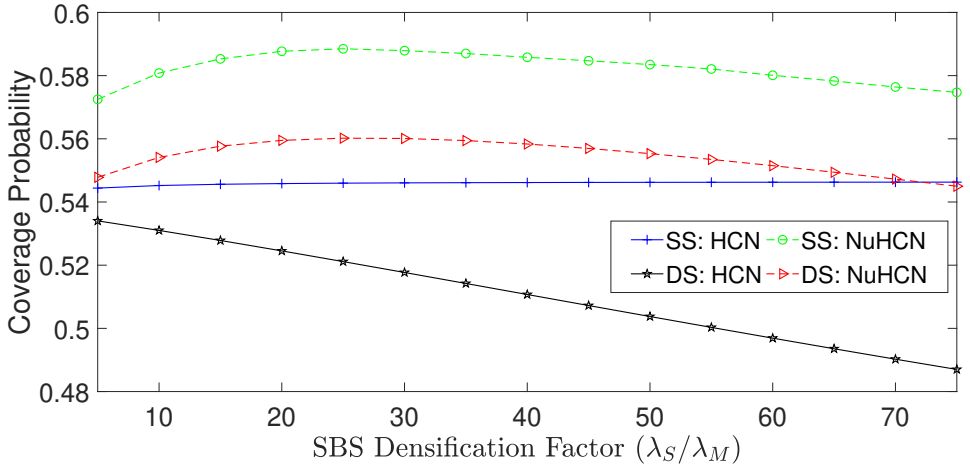

FIGURE 4.8: Network coverage against varying SBS densification factor (λ_S/λ_M)

4.5.2.2 Performance comparison of network coverage with other system scenarios

The impact of varying SBS densification factor (λ_S/λ_M) on the network coverage estimated through different system scenarios based on SS-PLM and DS-PLM is depicted in Fig. 4.8. It can be observed from the figure that the network coverage in case of SS-PLM based uniform HCNs is independent of variation in λ_S. This is because, the increase in received signal strength due to the increasing SBS density is counter balanced by the rise in interfering signal strength. Contrarily, given better accuracy of DS-PLM in estimating the path loss especially in dense networks, the SINR distribution in DS-PLM based uniform HCNs is found to be

a monotonically decreasing function of λ_S. However, with the consideration of SBS thinning (i.e., dependent), the strongest interferers in the vicinity of MBSs are muted and as a result, the overall network coverage improves in both SS-PLM and DS-LM scenarios. For instance at $\lambda_S = 50\lambda_M$ and τ =0 dB, thinning out the selective SBSs improves the coverage by 6% in SS-PLM scenario while by 9% in DS-PLM. Hence, using SS-PLM underestimates the benefit associated with non-uniform deployment of SBSs in HCNs.

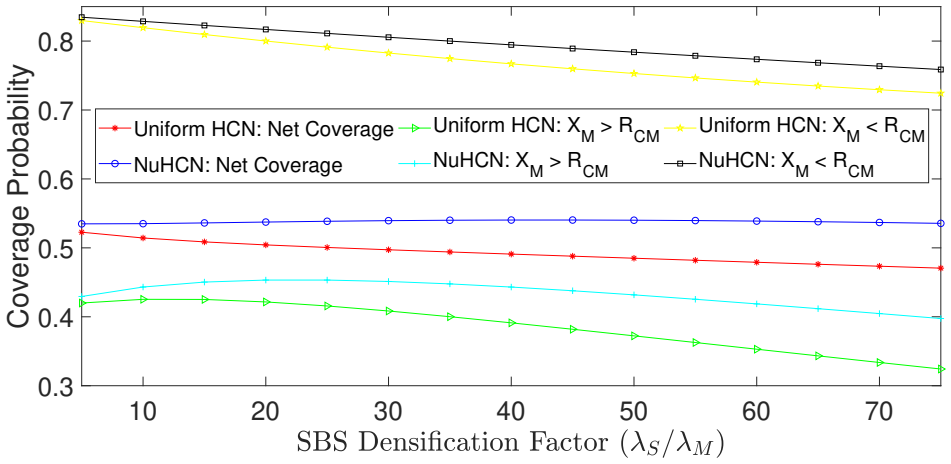

FIGURE 4.9: Coverage comparison for SBS-biasing in uniform HCNs and NuHCNs

4.5.2.3 Impact of SBS biasing and Frequency Reuse on Network Coverage

Given better accuracy of DS-PLM in estimating the path loss in dense HCNs, and for a fair assessment of determining the impact of utilizing SBS biasing and interference management on network coverage, Fig. 4.9 and Fig. 4.10 depict a region-wise macro-tier coverage estimated using DS-PLM for both uniform HCNs and NuHCNs.

It can be observed from Fig. 4.9 that adopting biased UE-AS is advantageous in NuHCNs, as the overall network coverage increases. Contrarily, the coverage reduces with the consideration of biased UE-AS in uniform HCNs as the offloaded UEs receive strong interference from their nearby MBSs. For instance at λ_S=50λ_M,

τ =0 dB, and B_S= 5 dB, the macro-tier cell-edge region coverage increases by around 14% while the overall network coverage in NuHCNs improves by 10%. The non-uniform deployment of SBSs achieved through muting the SBSs within the R_{CM} of each MBS has ensured that only those UEs are offloaded to small-tier BSs which are located far away from their nearest MBS and as a result, receive weak interference from their nearby MBSs.

To account for the excessive interference received at UEs either due to the densification of SBSs or UE offloading, traditional frequency reuse mechanism has been considered. Fig. 4.10 illustrates that with the usage of frequency reuse mechanism, the number of potential interferers is decreased and as a result, the overall coverage in both uniform HCNs and NuHCNs increases. However, using the frequency reuse mechanism in NuHCNs yields more gain when compared with the uniform HCNs. For instance at λ_S= 50λ_M, τ= 0 dB and N= 3, the network coverage estimated using DS-PLM in NuHCNs is 3% higher than the uniform HCNs. Moreover, it can also be observed that the consideration of frequency reuse has approximately same impact on both the cell-center and cell-edge regions of macro tier.

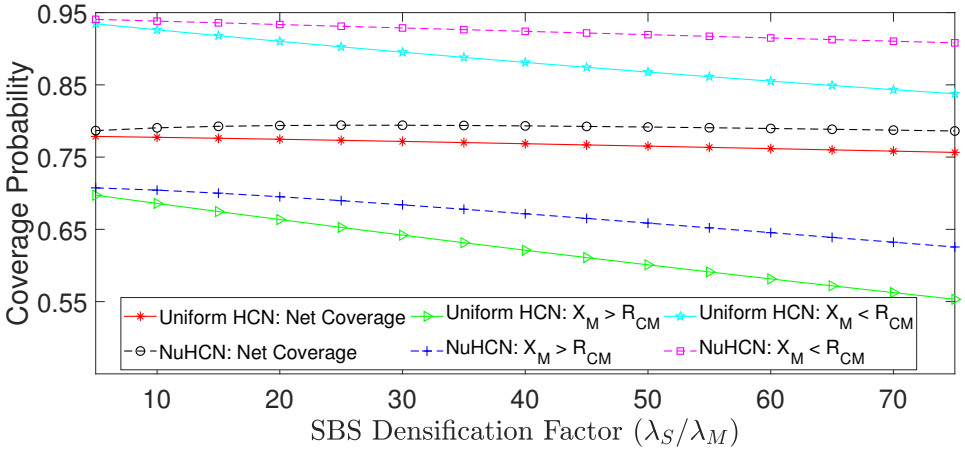

FIGURE 4.10: Comparison of the evaluated network coverage with frequency reuse consideration in uniform HCNs and NuHCNs

To highlight the impact of jointly considering the incorporation of both SBS biasing and frequency reuse mechanisms on the region-wise macro-tier coverage estimated using DS-PLM for both uniform HCNs and NuHCNs, Fig. 4.11 is presented. It can be seen from the figure that the joint incorporation of both mechanisms

in conjunction with non-uniform deployment of SBSs results in a 4% increase in the overall network coverage. Moreover, it is also evident from the figure that the joint incorporation of both mechanisms have a little impact on macro-tier coverage for cell-center region, while in case of cell-edge region, the coverage improves by around 5%.

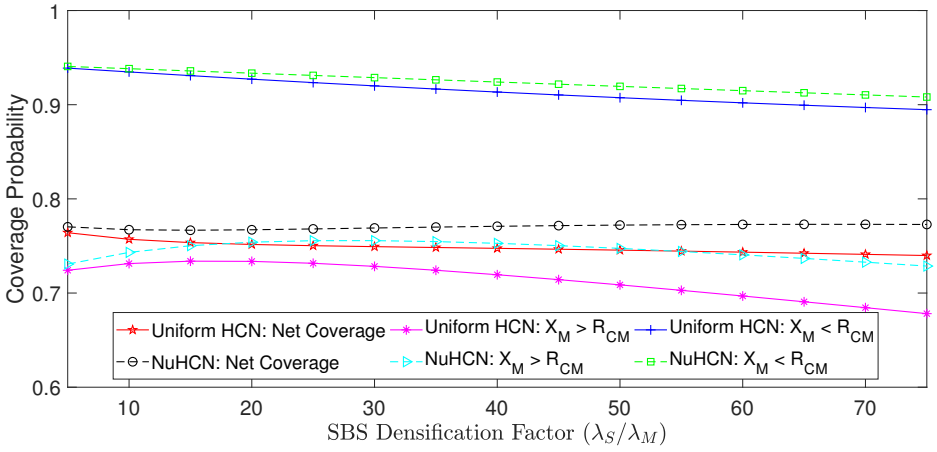

FIGURE 4.11: Comparison of the estimated network coverage with integration of SBS biasing and frequency reuse in uniform HCNs and NuHCNs

4.6 Conclusion

In this chapter, the downlink performance of a two-tier NuHCN has been analyzed using a more realistic PLM based on the dual-slope to effectively account for the disparate link distances between the communicating stations. The SBSs located within the R_{CM} of any MBS have been assumed to be muted, and this correlation between the locations of MBSs and SBSs lead to improvement in the coverage performance of dense HCNs. Meanwhile, the presented model of NuHCNs has been further studied with the consideration of SBS offloading and interference mitigation mechanisms. The obtained results of the proposed scheme have been compared with the uniform and non-uniform HCNs whose performance have been evaluated using SS-PLM and DS-PLM respectively. It has been observed that the usage of SS-PLM leads to inaccurate estimation of the benefits associated with UE offloading and interference mitigation mechanisms in NuHCNs.

Chapter 5

Conclusion and Future Research Directives

In this chapter, the general conclusions drawn from this dissertation are summarized and some potential extensions to this work are briefly discussed as well.

5.1 Conclusion

In this thesis, we have investigated the coverage performance of densely deployed HCNs that additionally consider the load balancing and interference management mechanisms as well. It has been found that the densification of SBSs causes a decrease in the network coverage due to the excessive interference received by the UEs. Consequently, it is essential to utilize interference management schemes that effectively account for the excessive interference received by the UEs in the densely deployed cellular networks. Meanwhile, it is pertinent to mention that the randomness associated with the BS positions substantially increases with the dense deployment of SBSs, and as a result, this increased randomness necessitates adopting more tractable network modeling strategies that can evade the limitations of existing approaches. Additionally, the existence of disparate link distances is also

a common phenomenon in the densely deployed cellular networks; hence, employing SS-PLM to evaluate the performance of dense networks leads to significant inaccuracies. Therefore, in this dissertation, the downlink performance analysis of dense HCNs has been carried out using the tools from stochastic geometry while DS-PLM has been used to estimate the path loss. The following passages provide a chapter-wise conclusion of the research work presented in chapters 3 and 4 respectively.

In chapter 3, DS-PLM has been employed to study and analyze the downlink performance of a two-tier dense HCN with uniformly distributed BS tiers having disparities in transmit power and infrastructure density. The adopted HCN model permits flexible UE association based on the range extension of SBSs to avoid overburdening of the macro tier while the traditional frequency reuse mechanism has been considered to reduce the excessive interference received by the UEs. Analytical expressions for the tier association and coverage probability have been derived for a randomly chosen user using the tools from stochastic geometry and validated through simulations. With the help of numerical results, a thorough comparison of the evaluated network performance using both SS-PLM and DS-PLM has been carried out for each performance metric and the observed results have clearly reinforced the limited suitability of the usage of SS-PLM in the densely deployed cellular networks. For instance, the usage of SS-PLM overestimated the benefits associated with the densification of SBSs and the range extension of SBSs in the tier association probability. Meanwhile, the estimated network coverage using SS-PLM demonstrated a scale-invariant behavior from any change in the SBS density, i.e., the densification of SBSs had no effect on the coverage probability. However, when the network coverage was estimated using DS-PLM, it was found to be a monotonically decreasing function of SBS density; hence highlighting the need for employing efficient interference management mechanisms. Finally, it has been concluded that the joint consideration of SBS biasing and the traditional frequency reuse mechanisms significantly improve the coverage performance of dense HCNs while the benefits associated with their joint consideration can be accurately estimated using the DS-PLM.

In chapter 4, the usage of DS-PLM has been extended to the case of non-uniformly distributed BS tiers in dense HCNs. It was observed in chapter 3 that a more realistic assessment of the network performance of the densely deployed cellular networks can be obtained by employing DS-PLM, owing to its ability to accurately estimate the path loss in the disparate desired/interfering link distance scenarios. Keeping in view the transmit power disparity between MBSs and SBSs, the SBSs that fall within the critical distance of any MBS have been proposed to be muted, as their likelihood of being active BSs is negligible. By introducing this partial spatial correlation between the locations of MBSs and SBSs, the interference received by macro associated users residing within the MBS cell-center region reduces significantly which leads to a substantial improvement in the network coverage. This coverage-centric based HCN model has been further studied with the joint consideration of range extension of SBSs and interference mitigation mechanisms. Mathematical expressions for the tier association and coverage probability have been derived for a randomly chosen user using the tools from stochastic geometry and validated through simulations. A rigorous comparison of the evaluated network performance using both SS-PLM and DS-PLM has been carried out for each performance metric and the observed results exhibit that the usage of SS-PLM leads to underestimation of the benefits associated with UEs offloading to lightly loaded BS tier and interference abating mechanisms in the densely deployed non-uniform HCNs.

5.2 Future Work

There are several possible extensions of the presented research work in this thesis, some of which are briefly discussed below:

Analyzing the network performance of finite cellular networks: A possible extension of the presented work involves estimating the network performance of a finite-sized cellular network, as practically the BSs are deployed in a finite region. Keeping in view the analytical tractability, we had assumed the location

of BSs to be modeled as distinct homogeneous PPPs in an infinite region. Owing the translation-invariant and isotropic properties of the homogeneous PPPs, the estimated network performance is location-independent. Consequently, the statistical characteristics derived at the typical user device are same for all the other user devices. However, the network performance in finite networks is sensitive to the location of user devices and their distance from the deployed network infrastructures. Hence, the users located in the near vicinity of BS cell-center region experience different network characteristics to those residing in the cell-boundary regions. Therefore, for precisely capturing the estimated network performance in a finite region, it is important to derive the expressions for metrics of interest by removing the assumption of PPP based abstraction of the BS locations.

Performance analysis cellular networks with decoupled access enabled Traditionally, the user devices have been forced to associate with a single BS for their uplink and downlink services. However, the exponential upsurge in mobile data usage and recent trends in network densification suggest employing more flexible user association strategies, e.g., the decoupled access. With the evolution of heterogeneity in the wireless cellular networks, a user device can access the deployed network infrastructure through multiple BSs and thus may choose to associate with different BSs for its downlink and uplink, respectively. This amenity of choosing amongst multiple BSs for downlink and uplink is termed as the Decoupled UL/DL (DUDe) access. It has been reported in numerous recent studies that the network performance improves with the consideration of decoupled access. The work presented in this thesis considers a coupled access for the user devices, i.e., a UE is forced to associate with a single BS for both its uplink and the downlink. Hence, the presented work can be extended by enabling the decoupled association of the UEs.

Impact of the anisotropic path loss on the coverage performance of dense cellular networks In conventional cellular networks, it was generally assumed that the BS locations were relatively regular while the locations of user devices were random. However, with the widespread success of network densification in meeting the capacity demands of the emerging cellular networks, the

randomness associated with locations of BSs has drastically increased. Meanwhile, various studies have shown that the BS locations in both single-tier and multi-tier cellular networks can be accurately modeled by the usage of various point process models. It is interesting to note that the coverage area of the deployed cellular networks using these models is generally obtained through the usage of Poisson-Voronoi tessellation (PVT) method. However, it is pertinent to mention that the impact of environment on the signal propagation is not considered in the PVT based model, and hence smooth cellular coverage boundaries are obtained through it. Contrarily, in practical cellular networks, signals experience the anisotropic nature of the path loss fading and as a result, the cellular coverage boundaries are extremely irregular shaped. Moreover, the network performance is greatly impact by the network geometry. Therefore, it would be an interesting extension of the presented work to consider the impact of environment on wireless signal propagation and estimate the network performance while using the DS-PLM.

The studies presented in this thesis can be extended by jointly considering more practical load-aware UE association strategies and spectrally efficient interference management schemes. Similarly, the proposed work can also be extended by employing dependent/repulsive point processes to better characterize the locations of BSs in a multi-tier cellular network scenario. Another possible extension of the presented work involves evaluating the network performance when user devices are located in clusters in any specific area e.g., in shopping malls or stadiums.

Bibliography

[1] "Ericsson mobility report, June 2019." [Online]. Available: https://www.ericsson.com/en/mobility-report/reports/june-2019

[2] M. Patzold, "5G is going live in country after country [Mobile Radio]," *IEEE Veh. Tech. Mag.*, vol. 14, no. 4, pp. 4–10, 2019.

[3] J. G. Andrews, S. Buzzi, W. Choi, S. V. Hanly, A. Lozano, A. C. Soong, and J. C. Zhang, "What will 5G be?" *IEEE J. on Sel. Areas Commun.*, vol. 32, no. 6, pp. 1065–1082, 2014.

[4] Q. C. Li, H. Niu, A. T. Papathanassiou, and G. Wu, "5G network capacity: Key elements and technologies," *IEEE Veh. Technol. Mag.*, vol. 9, no. 1, pp. 71–78, 2014.

[5] A. Damnjanovic, J. Montojo, Y. Wei, T. Ji, T. Luo, M. Vajapeyam, T. Yoo, O. Song, and D. Malladi, "A survey on 3GPP heterogeneous networks," *IEEE Wireless Commun.*, vol. 18, no. 3, pp. 10–21, 2011.

[6] W. Webb, *Wireless Communications: The Future*. John Wiley & Sons, Jan 2007.

[7] M. Dohler, R. W. Heath, A. Lozano, C. B. Papadias, and R. A. Valenzuela, "Is the PHY layer dead?" *IEEE Commun. Mag.*, vol. 4, no. 49, pp. 159–165, 2011.

[8] V. Chandrasekhar, J. G. Andrews, and A. Gatherer, "Femtocell networks: A survey," *IEEE Commun. Mag.*, vol. 46, no. 9, pp. 59–67, 2008.

[9] Q. Li, G. Li, W. Lee, M.-i. Lee, D. Mazzarese, B. Clerckx, and Z. Li, "MIMO techniques in WiMAX and LTE: a feature overview," *IEEE Commun. Mag.*, vol. 48, no. 5, pp. 86–92, 2010.

[10] T. L. Marzetta, "Noncooperative cellular wireless with unlimited numbers of base station antennas," *IEEE Trans. on Wireless Commun.*, vol. 9, no. 11, pp. 3590–3600, 2010.

[11] E. Björnson, E. G. Larsson, and M. Debbah, "Massive MIMO for maximal spectral efficiency: How many users and pilots should be allocated?" *IEEE Trans. on Wireless Commun.*, vol. 15, no. 2, pp. 1293–1308, 2015.

[12] T. L. Marzetta, "Massive MIMO: An introduction," *Bell Labs Technical J.*, vol. 20, pp. 11–22, 2015.

[13] E. Björnson, E. G. Larsson, and T. L. Marzetta, "Massive MIMO: Ten myths and one critical question," *IEEE Commun. Mag.*, vol. 54, no. 2, pp. 114–123, 2016.

[14] A. L. Swindlehurst, E. Ayanoglu, P. Heydari, and F. Capolino, "Millimeter-wave massive MIMO: The next wireless revolution?" *IEEE Commun. Mag.*, vol. 52, no. 9, pp. 56–62, 2014.

[15] A. Ghosh, T. A. Thomas, M. C. Cudak, R. Ratasuk, P. Moorut, F. W. Vook, T. S. Rappaport, G. R. MacCartney, S. Sun, and S. Nie, "Millimeter-wave enhanced local area systems: A high-data-rate approach for future wireless networks," *IEEE J. on Sel. Areas in Commun.*, vol. 32, no. 6, pp. 1152–1163, 2014.

[16] A. Ghosh, "The 5G mmwave radio revolution." *Microwave Journal*, vol. 59, no. 9, 2016.

[17] Z. Pi, J. Choi, and R. Heath, "Millimeter-wave gigabit broadband evolution toward 5G: Fixed access and backhaul," *IEEE Commun. Mag.*, vol. 54, no. 4, pp. 138–144, 2016.

[18] P. Cramton, "Spectrum auction design," *Review of Industrial Organization*, vol. 42, no. 2, pp. 161–190, 2013.

[19] F. Boccardi, R. W. Heath, A. Lozano, T. L. Marzetta, and P. Popovski, "Five disruptive technology directions for 5G," *IEEE Commun. Mag.*, vol. 52, no. 2, pp. 74–80, 2014.

[20] T. S. Rappaport, G. R. MacCartney, M. K. Samimi, and S. Sun, "Wideband millimeter-wave propagation measurements and channel models for future wireless communication system design," *IEEE Trans. on Commun.*, vol. 63, no. 9, pp. 3029–3056, 2015.

[21] M. Shafi, A. F. Molisch, P. J. Smith, T. Haustein, P. Zhu, P. De Silva, F. Tufvesson, A. Benjebbour, and G. Wunder, "5G: A tutorial overview of standards, trials, challenges, deployment, and practice," *IEEE J. on Sel. Areas in Commun.*, vol. 35, no. 6, pp. 1201–1221, 2017.

[22] I. A. Hemadeh, K. Satyanarayana, M. El-Hajjar, and L. Hanzo, "Millimeter-wave communications: Physical channel models, design considerations, antenna constructions, and link-budget," *IEEE Commun. Surveys & Tutorials*, vol. 20, no. 2, pp. 870–913, 2017.

[23] J. A. Azevedo and F. E. Santos, "A model to estimate the path loss in areas with foliage of trees," *AEU-International J. of Electronics and Commun.*, vol. 71, pp. 157–161, 2017.

[24] C. H. Doan, S. Emami, D. A. Sobel, A. M. Niknejad, and R. W. Brodersen, "Design considerations for 60 GHz CMOS radios," *IEEE Commun. Mag.*, vol. 42, no. 12, pp. 132–140, 2004.

[25] R. C. Daniels and R. W. Heath, "60 GHz wireless communications: Emerging requirements and design recommendations," *IEEE Veh. Tech. Mag.*, vol. 2, no. 3, pp. 41–50, 2007.

[26] A. Bleicher, "The 5G phone future: Samsung's millimeter-wave transceiver technology could enable ultrafast mobile broadband by 2020," *IEEE Spectrum*, vol. 50, no. 7, pp. 15–16, 2013.

[27] O. El Ayach, S. Rajagopal, S. Abu-Surra, Z. Pi, and R. W. Heath, "Spatially sparse precoding in millimeter wave MIMO systems," *IEEE Trans. on Wireless Commun.*, vol. 13, no. 3, pp. 1499–1513, 2014.

[28] X. Ge, S. Tu, G. Mao, C.-X. Wang, and T. Han, "5G ultra-dense cellular networks," *IEEE Wireless Commun.*, vol. 23, no. 1, pp. 72–79, 2016.

[29] P. Lin, J. Zhang, Y. Chen, and Q. Zhang, "Macro-Femto heterogeneous network deployment and management: from business models to technical solutions," *IEEE Wireless Commun.*, vol. 18, no. 3, pp. 64–70, 2011.

[30] T. Nakamura, S. Nagata, A. Benjebbour, Y. Kishiyama, T. Hai, S. Xiaodong, Y. Ning, and L. Nan, "Trends in small cell enhancements in LTE advanced," *IEEE Commun. Mag.*, vol. 51, no. 2, pp. 98–105, 2013.

[31] Y. Kishiyama, A. Benjebbour, T. Nakamura, and H. Ishii, "Future steps of LTE-A: evolution toward integration of local area and wide area systems," *IEEE Wireless Commun.*, vol. 20, no. 1, pp. 12–18, 2013.

[32] J. G. Andrews, "Seven ways that HetNets are a cellular paradigm shift," *IEEE Commun. Mag.*, vol. 51, no. 3, pp. 136–144, 2013.

[33] X. Chu, D. Lopez-Perez, Y. Yang, and F. Gunnarsson, *Heterogeneous Cellular Networks: Theory, Simulation and Deployment.* Cambridge University Press, 2013.

[34] H. Tataria, K. Haneda, A. F. Molisch, M. Shafi, and F. Tufvesson, "Standardization of propagation models for terrestrial cellular systems: A historical perspective," *International J. of Wireless Inf. Networks*, vol. 28, no. 1, pp. 20–44, 2020.

[35] A. Goldsmith, *Wireless Communications.* Cambridge university press, 2005.

[36] T. S. Rappaport *et al.*, *Wireless Communications: Principles and Practice*, 2nd ed. Prentice Hall PTR, New Jersey,USA, 1996.

[37] M. J. Feuerstein, K. L. Blackard, T. S. Rappaport, S. Y. Seidel, and H. H. Xia, "Path loss, delay spread, and outage models as functions of antenna height for microcellular system design," *IEEE Trans. on Veh. Tech.*, vol. 43, no. 3, pp. 487–498, 1994.

[38] R. Bendlin, V. Chandrasekhar, R. Chen, A. Ekpenyong, and E. Onggosanusi, "From homogeneous to heterogeneous networks: A 3GPP long term evolution rel. 8/9 case study," in *Proc. IEEE 45th Annual Conference on Information Sciences and Systems*, March 2011, pp. 1–5.

[39] S. N. Chiu, D. Stoyan, W. S. Kendall, and J. Mecke, *Stochastic Geometry and its Applications*. John Wiley & Sons, 2013.

[40] D. López-Pérez, M. Ding, H. Claussen, and A. H. Jafari, "Towards 1 Gbp-s/UE in cellular systems: Understanding ultra-dense small cell deployments," *IEEE Commun. Surveys & Tutorials*, vol. 17, no. 4, pp. 2078–2101, 2015.

[41] H. Claussen, D. Lopez-Perez, L. Ho, R. Razavi, and S. Kucera, *Small Cell Networks: Deployment, Management, and Optimization*. John Wiley & Sons, 2017.

[42] R. Q. Hu and Y. Qian, "An energy efficient and spectrum efficient wireless heterogeneous network framework for 5G systems," *IEEE Commun. Mag.*, vol. 52, no. 5, pp. 94–101, 2014.

[43] J. Zander, "Beyond the ultra-dense barrier: Paradigm shifts on the road beyond 1000x wireless capacity," *IEEE Wireless Commun.*, vol. 24, no. 3, pp. 96–102, 2017.

[44] T. Wang, P. Li, X. Wang, Y. Wang, T. Guo, and Y. Cao, "A comprehensive survey on mobile data offloading in heterogeneous network," *Wireless Networks*, vol. 25, no. 2, pp. 573–584, 2019.

[45] M. Kountouris and V. Minh Nguyen, "Fundamental limits of ultra-dense networks," *Ultra-dense Networks for 5G and Beyond: Modelling, Analysis, and Applications*, 2019.

[46] H. Inaltekin, M. Chiang, H. V. Poor, and S. B. Wicker, "On unbounded path-loss models: Effects of singularity on wireless network performance," *IEEE J. on Sel. Areas Commun.*, vol. 27, no. 7, 2009.

[47] H. Inaltekin, "Gaussian approximation for the wireless multi-access interference distribution," *IEEE Trans. on Signal Processing*, vol. 60, no. 11, pp. 6114–6120, 2012.

[48] V. H. Mac Donald, "Advanced mobile phone service: The cellular concept," *Bell Syst. Tech. J.*, vol. 58, no. 1, pp. 15–41, 1979.

[49] J. Xu, J. Zhang, and J. G. Andrews, "On the accuracy of the Wyner model in cellular networks," *IEEE Trans. on Wireless Commun.*, vol. 10, no. 9, pp. 3098–3109, 2011.

[50] R. Jain, C. So-In *et al.*, "System-level modeling of IEEE 802.16 E mobile WiMAX networks: key issues," *IEEE Wireless Commun.*, vol. 15, no. 5, pp. 73–79, 2008.

[51] J. C. Ikuno, M. Wrulich, and M. Rupp, "System level simulation of LTE networks," in *Proc. IEEE 71st Veh. Techn. Conference (VTC)*, 2010, pp. 1–5.

[52] H. ElSawy, E. Hossain, and M. Haenggi, "Stochastic geometry for modeling, analysis, and design of multi-tier and cognitive cellular wireless networks: A survey," *IEEE Commun. Surveys & Tutorials*, vol. 15, no. 3, pp. 996–1019, 2013.

[53] M. Haenggi, J. G. Andrews, F. Baccelli, O. Dousse, and M. Franceschetti, "Stochastic geometry and random graphs for the analysis and design of wireless networks," *IEEE J. on Sel. Areas Commun.*, vol. 27, no. 7, 2009.

[54] M. Z. Win, P. C. Pinto, and L. A. Shepp, "A mathematical theory of network interference and its applications," *Proceedings of the IEEE*, vol. 97, no. 2, pp. 205–230, 2009.

[55] J. G. Andrews, R. K. Ganti, M. Haenggi, N. Jindal, and S. Weber, "A primer on spatial modeling and analysis in wireless networks," *IEEE Commun. Mag.*, vol. 48, no. 11, pp. 156–163, 2010.

[56] F. Baccelli, B. Błaszczyszyn *et al.*, *Stochastic geometry and wireless networks: Volume II Applications, Foundations and Trends® in Networking*. Now Publishers, Inc., 2010.

[57] H. ElSawy, A. Sultan-Salem, M.-S. Alouini, and M. Z. Win, "Modeling and analysis of cellular networks using stochastic geometry: A tutorial," *IEEE Commun. Surveys & Tutorials*, vol. 19, no. 1, pp. 167–203, 2017.

[58] V. Chandrasekhar and J. G. Andrews, "Uplink capacity and interference avoidance for two-tier femtocell networks," *IEEE Trans. on Wireless Commun.*, vol. 8, no. 7, pp. 3498–3509, 2009.

[59] V. Chandrasekhar, M. Kountouris, and J. G. Andrews, "Coverage in multi-antenna two-tier networks," *IEEE Trans. on Wireless Commun.*, vol. 8, no. 10, pp. pp–5314, 2009.

[60] V. Chandrasekhar and J. G. Andrews, "Spectrum allocation in tiered cellular networks," *IEEE Trans. on Commun.*, vol. 57, no. 10, pp. 3059–3068, 2009.

[61] W. C. Cheung, T. Q. Quek, and M. Kountouris, "Throughput optimization, spectrum allocation, and access control in two-tier femtocell networks," *IEEE J. on Sel. Areas in Commun.*, vol. 30, no. 3, pp. 561–574, 2012.

[62] F. Baccelli, M. Klein, M. Lebourges, and S. Zuyev, "Stochastic geometry and architecture of communication networks," *Telecommun. Syst.*, vol. 7, pp. 209–227, 1997.

[63] T. X. Brown, "Cellular performance bounds via shotgun cellular systems," *IEEE J. on Sel. Areas Commun.*, vol. 18, no. 11, pp. 2443–2455, 2000.

[64] J. G. Andrews, F. Baccelli, and R. K. Ganti, "A tractable approach to coverage and rate in cellular networks," *IEEE Trans. on Commun.*, vol. 59, no. 11, pp. 3122–3134, 2011.

[65] A. Guo and M. Haenggi, "Spatial stochastic models and metrics for the structure of base stations in cellular networks," *IEEE Trans. on Wireless Commun.*, vol. 12, no. 11, pp. 5800–5812, 2013.

[66] H. S. Dhillon, R. K. Ganti, F. Baccelli, and J. G. Andrews, "Modeling and analysis of K-tier downlink heterogeneous cellular networks," *IEEE J. on Sel. Areas Commun.*, vol. 30, no. 3, pp. 550–560, 2012.

[67] S. Mukherjee, "Distribution of downlink SINR in heterogeneous cellular networks," *IEEE J. on Sel. Areas in Commun.*, vol. 30, no. 3, pp. 575–585, 2012.

[68] H.-S. Jo, Y. J. Sang, P. Xia, and J. G. Andrews, "Heterogeneous cellular networks with flexible cell association: A comprehensive downlink SINR analysis," *IEEE Trans. on Wireless Commun.*, vol. 11, no. 10, pp. 3484–3495, 2012.

[69] S. Singh, H. S. Dhillon, and J. G. Andrews, "Offloading in heterogeneous networks: Modeling, analysis, and design insights," *IEEE Trans. on Wireless Commun.*, vol. 12, no. 5, pp. 2484–2497, 2013.

[70] S. Singh and J. G. Andrews, "Joint resource partitioning and offloading in heterogeneous cellular networks," *IEEE Trans. on Wireless Commun.*, vol. 13, no. 2, pp. 888–901, 2013.

[71] R. Trestian, O. Ormond, and G.-M. Muntean, "Game theory-based network selection: Solutions and challenges," *IEEE Commun. Surveys & Tutorials*, vol. 14, no. 4, pp. 1212–1231, 2012.

[72] H. S. Dhillon, R. K. Ganti, and J. G. Andrews, "Load-aware modeling and analysis of heterogeneous cellular networks," *IEEE Trans. on Wireless Commun.*, vol. 12, no. 4, pp. 1666–1677, 2013.

[73] H. ElSawy, E. Hossain, and S. Camorlinga, "Traffic offloading techniques in two-tier femtocell networks," in *Proc. IEEE International Conference on Commun. (ICC)*, 2013, pp. 6086–6090.

[74] H. Elshaer, F. Boccardi, M. Dohler, and R. Irmer, "Downlink and uplink decoupling: A disruptive architectural design for 5G networks," in *Proc. IEEE Global Commun. Conference*, 2014, pp. 1798–1803.

[75] K. Smiljkovikj, P. Popovski, and L. Gavrilovska, "Analysis of the decoupled access for downlink and uplink in wireless heterogeneous networks," *IEEE Wireless Commun. Letters*, vol. 4, no. 2, pp. 173–176, 2015.

[76] F. Boccardi, J. Andrews, H. Elshaer, M. Dohler, S. Parkvall, P. Popovski, and S. Singh, "Why to decouple the uplink and downlink in cellular networks and how to do it," *IEEE Commun. Mag.*, vol. 54, no. 3, pp. 110–117, 2016.

[77] N. Garg, S. Singh, and J. Andrews, "Impact of dual slope path loss on user association in Hetnets," in *Proc. IEEE Globecom Workshops (GC Wkshps)*, 2015, pp. 1–6.

[78] A. Simonsson and A. Furuskar, "Uplink power control in LTE-overview and performance, subtitle: principles and benefits of utilizing rather than compensating for SINR variations," in *Proc. IEEE 68th Veh. Techn. Conference*, 2008, pp. 1–5.

[79] Y. Wang and S. Venkatraman, "Uplink power control in LTE heterogeneous networks," in *Proc. IEEE Globecom Workshops*, 2012, pp. 592–597.

[80] H. Tabassum, F. Yilmaz, Z. Dawy, and M.-S. Alouini, "A statistical model of uplink inter-cell interference with slow and fast power control mechanisms," *IEEE Trans. on Commun.*, vol. 61, no. 9, pp. 3953–3966, 2013.

[81] V. N. Ha and L. B. Le, "Distributed base station association and power control for heterogeneous cellular networks," *IEEE Trans. on Veh. Tech.*, vol. 63, no. 1, pp. 282–296, 2013.

[82] T. D. Novlan, H. S. Dhillon, and J. G. Andrews, "Analytical modeling of uplink cellular networks," *IEEE Trans. on Wireless Commun.*, vol. 12, no. 6, pp. 2669–2679, 2013.

[83] S. Singh, X. Zhang, and J. G. Andrews, "Joint rate and SINR coverage analysis for decoupled uplink-downlink biased cell associations in hetnets," *IEEE Trans. on Wireless Commun.*, vol. 14, no. 10, pp. 5360–5373, 2015.

[84] D. Lopez-Perez, I. Guvenc, G. De la Roche, M. Kountouris, T. Q. Quek, and J. Zhang, "Enhanced inter-cell interference coordination challenges in heterogeneous networks," *IEEE Wireless Commun.*, vol. 18, no. 3, 2011.

[85] N. Saquib, E. Hossain, L. B. Le, and D. I. Kim, "Interference management in OFDMA femtocell networks: Issues and approaches," *IEEE Wireless Commun.*, vol. 19, no. 3, pp. 86–95, 2012.

[86] M. Fereydooni, M. Sabaei, M. Dehghan, M. Taranetz, and M. Rupp, "A mathematical framework to evaluate flexible outdoor user association in urban two-tier cellular networks," *IEEE Trans. on Wireless Commun.*, vol. 17, no. 3, pp. 1559–1573, 2017.

[87] G. Giambene *et al.*, "Analysis of LTE-A heterogeneous networks with SIR-based cell association and stochastic geometry," *J. of Commun. and Networks*, vol. 20, no. 2, pp. 129–143, 2018.

[88] N. Saquib, E. Hossain, and D. I. Kim, "Fractional frequency reuse for interference management in LTE-advanced hetnets," *IEEE Wireless Commun.*, vol. 20, no. 2, pp. 113–122, 2013.

[89] T. D. Novlan, R. K. Ganti, A. Ghosh, and J. G. Andrews, "Analytical evaluation of fractional frequency reuse for OFDMA cellular networks," *IEEE Trans. on Wireless Commun.*, vol. 10, no. 12, pp. 4294–4305, 2011.

[90] ——, "Analytical evaluation of fractional frequency reuse for heterogeneous cellular networks," *IEEE Trans. on Commun.*, vol. 60, no. 7, pp. 2029–2039, 2012.

[91] M. Fereydooni, M. Sabaei, M. Dehghan, G. B. Eslamlou, and M. Rupp, "Analytical evaluation of heterogeneous cellular networks under flexible user association and frequency reuse," *Computer Commun.*, vol. 116, pp. 147–158, 2018.

[92] A. Ijaz, S. A. Hassan, S. A. R. Zaidi, D. N. K. Jayakody, and S. M. H. Zaidi, "Coverage and rate analysis for downlink HetNets using modified reverse frequency allocation scheme," *IEEE Access*, vol. 5, pp. 2489–2502, 2017.

[93] X. Zhang and J. G. Andrews, "Downlink cellular network analysis with multi-slope path loss models," *IEEE Trans. on Commun.*, vol. 63, no. 5, pp. 1881–1894, 2015.

[94] M. Kountouris *et al.*, "Performance limits of network densification," *IEEE J. on Sel. Areas in Commun.*, vol. 35, no. 6, pp. 1294–1308, 2017.

[95] M. Ding, P. Wang, D. López-Pérez, G. Mao, and Z. Lin, "Performance impact of LoS and NLoS transmissions in dense cellular networks," *IEEE Trans. on Commun.*, vol. 15, no. 3, pp. 2365–2380, 2015.

[96] J. Liu, M. Sheng, L. Liu, and J. Li, "Effect of densification on cellular network performance with bounded pathloss model." *IEEE Commun. Letters*, vol. 21, no. 1, pp. 346–349, 2017.

[97] ——, "Performance of small cell networks under multislope bounded pathloss model: From sparse to ultradense deployment," *IEEE Trans. on Veh. Tech.*, vol. 67, no. 11, pp. 11 022–11 034, 2018.

[98] M. Ding and D. López-Pérez, "Performance impact of base station antenna heights in dense cellular networks," *IEEE Trans. on Wireless Commun.*, vol. 16, no. 12, pp. 8147–8161, 2017.

[99] H. Wang, X. Zhou, and M. C. Reed, "Analytical evaluation of coverage-oriented femtocell network deployment," in *Proc. IEEE International Conference on Communications (ICC)*, 2013, pp. 5974–5979.

[100] J. Weitzen and T. Grosch, "Comparing coverage quality for femtocell and macrocell broadband data services," *IEEE Commun. Mag.*, vol. 48, no. 1, pp. 40–44, 2010.

[101] H. Wang and M. C. Reed, "Tractable model for heterogeneous cellular networks with directional antennas," in *Proc. IEEE Australian Commun. Theory Workshop (AusCTW)*, 2012, pp. 61–65.

[102] M. Filo, C. H. Foh, S. Vahid, and R. Tafazolli, "Performance analysis of ultra-dense networks with regularly deployed base stations," *IEEE Trans. on Wireless Commun.*, vol. 19, no. 5, pp. 3530–3545, 2020.

[103] I. Nakata and N. Miyoshi, "Spatial stochastic models for analysis of heterogeneous cellular networks with repulsively deployed base stations," *Performance Evaluation*, vol. 78, pp. 7–17, 2014.

[104] N. Deng, W. Zhou, and M. Haenggi, "A heterogeneous cellular network model with inter-tier dependence," in *Proc. IEEE Global Commun. Conference*, 2014, pp. 1522–1527.

[105] N. Miyoshi and T. Shirai, "Spatial modeling and analysis of cellular networks using the Ginibre point process: A tutorial," *IEICE Trans. on Commun.*, vol. 99, no. 11, pp. 2247–2255, 2016.

[106] C.-S. Choi, J. O. Woo, and J. G. Andrews, "An analytical framework for modeling a spatially repulsive cellular network," *IEEE Trans. on Commun.*, vol. 66, no. 2, pp. 862–874, 2018.

[107] H. Wang, X. Zhou, and M. C. Reed, "Coverage and throughput analysis with a non-uniform small cell deployment," *IEEE Trans. on Wireless Commun.*, vol. 13, no. 4, pp. 2047–2059, 2014.

[108] C.-h. Lee and M. Haenggi, "Interference and outage in poisson cognitive networks," *IEEE Trans. on Wireless Commun.*, vol. 11, no. 4, pp. 1392–1401, 2012.

[109] H. ElSawy, E. Hossain, and M.-S. Alouini, "Analytical modeling of mode selection and power control for underlay D2D communication in cellular networks," *IEEE Trans. on Commun.*, vol. 62, no. 11, pp. 4147–4161, 2014.

[110] N. Deng, W. Zhou, and M. Haenggi, "Heterogeneous cellular network models with dependence," *IEEE J. on Sel. Areas in Commun.*, vol. 33, no. 10, pp. 2167–2181, 2015.

[111] H. Wei, N. Deng, W. Zhou, and M. Haenggi, "Approximate SIR analysis in general heterogeneous cellular networks," *IEEE Trans. on Commun.*, vol. 64, no. 3, pp. 1259–1273, 2016.

[112] Z. Yazdanshenasan, H. S. Dhillon, M. Afshang, and P. H. Chong, "Poisson hole process: Theory and applications to wireless networks," *IEEE Trans. on Wireless Commun.*, vol. 15, no. 11, pp. 7531–7546, 2016.

[113] V. Jungnickel, K. Manolakis, W. Zirwas, B. Panzner, V. Braun, M. Lossow, M. Sternad, R. Apelfrojd, and T. Svensson, "The role of small cells, coordinated multipoint, and massive MIMO in 5G," *IEEE Commun. Mag.*, vol. 52, no. 5, pp. 44–51, 2014.

[114] P. Xia, C.-H. Liu, and J. G. Andrews, "Downlink coordinated multi-point with overhead modeling in heterogeneous cellular networks," *IEEE Trans. on Wireless Commun.*, vol. 12, no. 8, pp. 4025–4037, 2013.

[115] L. Guo and S. Cong, "Coverage and rate analysis for location-aware cross-tier cooperation in two-tier HetNets," *Symmetry*, vol. 9, no. 8, p. 157, 2017.

[116] S. Bassoy, H. Farooq, M. A. Imran, and A. Imran, "Coordinated multi-point clustering schemes: A survey," *IEEE Commun. Surveys & Tutorials*, vol. 19, no. 2, pp. 743–764, 2017.

[117] F. Muhammad, Z. H. Abbas, and F. Y. Li, "Cell association with load balancing in nonuniform heterogeneous cellular networks: Coverage probability and rate analysis," *IEEE Trans. on Veh. Tech.*, vol. 66, no. 6, pp. 5241–5255, 2016.

[118] Z. H. Abbas, F. Muhammad, and L. Jiao, "Analysis of load balancing and interference management in heterogeneous cellular networks," *IEEE Access*, vol. 5, pp. 14 690–14 705, 2017.

[119] M. S. Haroon, Z. H. Abbas, G. Abbas, and F. Muhammad, "Coverage analysis of ultra-dense heterogeneous cellular networks with interference management," *Wireless Networks*, vol. 26, no. 3, pp. 2013–2025, 2020.

[120] R. Hernandez-Aquino, S. A. R. Zaidi, D. McLernon, and M. Ghogho, "Modelling and performance evaluation of non-uniform two-tier cellular networks through Stienen model," in *Proc. IEEE International Conference on Commun. (ICC)*, 2016, pp. 1–6.

[121] R. Hernandez-Aquino, S. A. R. Zaidi, M. Ghogho, D. McLernon, and A. Swami, "Stochastic geometric modeling and analysis of non-uniform two-tier networks: A Stienen's model-based approach," *IEEE Trans. on Wireless Commun.*, vol. 16, no. 6, pp. 3476–3491, 2017.

[122] M. S. Haroon, Z. H. Abbas, F. Muhammad, and G. Abbas, "Coverage analysis of cell-edge users in heterogeneous wireless networks using Stienen's model and RFA scheme," *International J. of Commun. Systems*, p. e4147, 2019.

[123] ——, "Analysis of coverage-oriented small base station deployment in heterogeneous cellular networks," *Physical Commun.*, vol. 38, p. 100908, 2020.

[124] T. Q. Duong, X. Chu, and H. A. Suraweera, *Ultra-dense networks for 5G and beyond: modelling, analysis, and applications.* Wiley, 2019.

[125] M. Ding and D. López-Pérez, "On the performance of practical ultra-dense networks: The major and minor factors," in *Proc. IEEE 15th International Symposium on Modeling and Optimization in Mobile, Ad Hoc, and Wireless Networks (WiOpt)*, 2017, pp. 1–8.

[126] J. Andrews, S. Singh, Q. YE, X. LIN, and H. Dhillon, "An overview of load balancing in hetnets: Old myths and open problems," *IEEE Wireless Commun.*, vol. 21, no. 2, pp. 18–25, 2014.

[127] M. Taranetz, R. W. Heath, and M. Rupp, "Analysis of urban two-tier heterogeneous mobile networks with small cell partitioning," *IEEE Trans. on Wireless Commun.*, vol. 15, no. 10, pp. 7044–7057, 2016.

[128] Z. Zhang and R. Q. Hu, "Dense cellular network analysis with LoS/NLoS propagation and bounded path loss model," *IEEE Commun. Letters*, vol. 22, no. 11, pp. 2386–2389, 2018.

[129] A. AlAmmouri, J. G. Andrews, and F. Baccelli, "A unified asymptotic analysis of area spectral efficiency in ultradense cellular networks," *IEEE Trans. on Inf. Theory*, vol. 65, no. 2, pp. 1236–1248, 2018.

[130] B. Yang, G. Mao, M. Ding, X. Ge, and X. Tao, "Dense small cell networks: From noise-limited to dense interference-limited," *IEEE Trans. on Veh. Tech.*, vol. 67, no. 5, pp. 4262–4277, 2018.

[131] C.-X. Wang, A. Ghazal, B. Ai, Y. Liu, and P. Fan, "Channel measurements and models for high-speed train communication systems: a survey," *IEEE Commun. Surveys & Tutorials*, vol. 18, no. 2, pp. 974–987, 2016.

[132] M. Ding and D. L. Pérez, "Please lower small cell antenna heights in 5G," in *Proc. IEEE Global Commun. Conferernce (Globecom)*, 2016, pp. 1–6.

[133] M. Filo, C. H. Foh, S. Vahid, and R. Tafazolli, "Performance impact of antenna height in ultra-dense cellular networks," in *Proc. IEEE International Conference on Commun. Workshops (ICC Workshops)*, 2017, pp. 429–434.

[134] I. Atzeni, J. Arnau, and M. Kountouris, "Downlink cellular network analysis with LOS/NLOS propagation and elevated base stations," *IEEE Trans. on Wireless Commun.*, vol. 17, no. 1, pp. 142–156, 2018.

[135] J. Venkataraman, M. Haenggi, and O. Collins, "Shot noise models for outage and throughput analyses in wireless ad hoc networks," in *Proc. IEEE Military Commun. Conference (MILCOM)*, 2006, pp. 1–7.

[136] R. K. Ganti and M. Haenggi, "Interference and outage in clustered wireless Ad Hoc networks," *IEEE Trans. on Inf. Theory*, vol. 55, no. 9, pp. 4067–4086, 2009.

[137] Z. Gong and M. Haenggi, "Interference and outage in mobile random networks: Expectation, distribution, and correlation," *IEEE Trans. on Mobile Computing*, vol. 13, no. 2, pp. 337–349, 2012.

[138] Q. Ye, B. Rong, Y. Chen, M. Al-Shalash, C. Caramanis, and J. G. Andrews, "User association for load balancing in heterogeneous cellular networks," *IEEE Trans. on Wireless Commun.*, vol. 12, no. 6, pp. 2706–2716, 2013.

[139] A. Shaverdian, J. Ghimire, and C. Rosenberg, "Simple and efficient network-aware user association rules for heterogeneous networks," *Computer Networks*, vol. 156, pp. 20–32, 2019.

[140] M. Zalghout, A. Khalil, M. Crussiére, S. Abdul-Nabi, and J.-F. Hélard, "Context-aware and priority-based user association and resource allocation in heterogeneous wireless networks," *Computer Networks*, vol. 149, pp. 76–92, 2019.

[141] W. U. Khan, Z. Ali, M. Waqas, and G. A. S. Sidhu, "Efficient power allocation with individual QoS guarantees in future small-cell networks," *AEU-International J. of Electronics and Commun.*, vol. 105, pp. 36–41, 2019.

[142] G. Giambene, T. Bourgeau, H. Chaouchi *et al.*, "Iterative multi-level soft frequency reuse with load balancing for heterogeneous LTE-A systems," *IEEE Trans. on Wireless Commun.*, vol. 16, no. 2, pp. 924–938, 2017.

[143] A. Mukherjee, D. De, and P. Deb, "Interference management in macro-femtocell and micro-femtocell cluster-based long-term evaluation-advanced green mobile network," *IET Commun.*, vol. 10, no. 5, pp. 468–478, 2016.

[144] M. Z. Chowdhury, M. T. Hossan, and Y. M. Jang, "Interference management based on RT/nRT traffic classification for FFR-aided small cell/macrocell heterogeneous networks," *IEEE Access*, vol. 6, pp. 31 340–31 358, 2018.

[145] A. Mukherjee, P. Deb, D. De, and M. S. Obaidat, "WmA-MiFN: A weighted majority and auction game based green ultra-dense micro-femtocell network system," *IEEE Systems J.*, vol. 14, no. 1, pp. 353–362, 2019.

[146] M. Ghadyani and A. Shahzadi, "Compressive sensing power control for interference management in D2D underlaid massive MIMO systems," *AEU-International J. of Electronics and Commun.*, vol. 90, pp. 79–87, 2018.

[147] E. Hossain, M. Rasti, H. Tabassum, and A. Abdelnasser, "Evolution toward 5G multi-tier cellular wireless networks: An interference management perspective," *IEEE Wireless Commun.*, vol. 21, no. 3, pp. 118–127, 2014.

[148] M. Mirahmadi, A. Al-Dweik, and A. Shami, "Interference modeling and performance evaluation of heterogeneous cellular networks," *IEEE Trans. on Commun.*, vol. 62, no. 6, pp. 2132–2144, 2014.

[149] S. Hamouda, M. Zitoun, and S. Tabbane, "Win–win relationship between macrocell and femtocells for spectrum sharing in LTE-A," *IET Commun.*, vol. 8, no. 7, pp. 1109–1116, 2014.

[150] H. Kour, R. K. Jha, and S. Jain, "A comprehensive survey on spectrum sharing: Architecture, energy efficiency and security issues," *J. of Network and Computer Applications*, vol. 103, pp. 29–57, 2018.

[151] Q. Deng, Z. Li, J. Chen, F. Zeng, H.-M. Wang, L. Zhou, and Y.-J. Choi, "Dynamic spectrum sharing for hybrid access in OFDMA-based cognitive femtocell networks," *IEEE Trans. on Veh. Tech.*, vol. 67, no. 11, pp. 10 830–10 840, 2018.

[152] A. S. Shafigh, S. Glisic, E. Hossain, B. Lorenzo, and L. A. DaSilva, "User-centric distributed spectrum sharing in dynamic network architectures," *IEEE/ACM Trans. on Networking (TON)*, vol. 27, no. 1, pp. 15–28, 2019.

[153] T. K. Sarkar, Z. Ji, K. Kim, A. Medouri, and M. Salazar-Palma, "A survey of various propagation models for mobile communication," *IEEE Antennas and Propagation Mag.*, vol. 45, no. 3, pp. 51–82, 2003.

[154] M. Hawasli and S. A. Çolak, "Toward green 5G heterogeneous small-cell networks: power optimization using load balancing technique," *AEU-International J. of Electronics and Commun.*, vol. 82, pp. 474–485, 2017.

[155] F. Qamar, M. N. Hindia, K. Dimyati, K. A. Noordin, and I. S. Amiri, "Interference management issues for the future 5G network: A review," *Telecom. Systems*, pp. 1–17, 2019.

[156] N. Hassan and X. Fernando, "Interference mitigation and dynamic user association for load balancing in heterogeneous networks," *IEEE Trans. on Veh. Tech.*, vol. 68, no. 8, pp. 7578–7592, 2019.

[157] X. Ge, X. Li, H. Jin, J. Cheng, and V. C. Leung, "Joint user association and user scheduling for load balancing in heterogeneous networks," *IEEE Trans. on Wireless Commun.*, vol. 17, no. 5, pp. 3211–3225, 2018.

[158] S. Lee and K. Huang, "Coverage and economy of cellular networks with many base stations," *IEEE Commun. Letters*, vol. 16, no. 7, pp. 1038–1040, 2012.

[159] P. D. Mankar, G. Das, and S. S. Pathak, "Load-aware performance analysis of cell center/edge users in random hetnets," *IEEE Trans. on Veh. Tech.*, vol. 67, no. 3, pp. 2476–2490, 2017.

[160] M. Ding, D. López-Pérez, G. Mao, and Z. Lin, "Performance impact of idle mode capability on dense small cell networks," *IEEE Trans. on Veh. Tech.*, vol. 66, no. 11, pp. 10 446–10 460, 2017.

[161] C. Galiotto, N. K. Pratas, L. Doyle, and N. Marchetti, "Effect of LOS/NLOS propagation on 5G ultra-dense networks," *Computer Networks*, vol. 120, pp. 126–140, 2017.

[162] A. Ullah, Z. H. Abbas, G. Abbas, F. Muhammad, and L. Jiao, "Performance analysis of user-centric SBS deployment with load balancing in heterogeneous cellular networks: A Thomas cluster process approach," *Computer Networks*, vol. 170, pp. 107–120, 2020.

[163] K. Shehzad, N. M. Khan, and J. Ahmed, "Impact of frequency reuse and flexible cell association on the performance of dense heterogeneous cellular networks using dual-slope path loss model," *IEEE Access*, vol. 7, pp. 166 214–166 234, 2019.

[164] M. Haenggi, "On distances in uniformly random networks," *IEEE Trans. on Inf. Theory*, vol. 51, no. 10, pp. 3584–3586, 2005.

Appendices

Appendix A

Proofs for Chapter No. 3

A.1 Proof of Macro T-AP in R-II

The probabilistic event defining joint association probability of T-UE with macro tier in R-II is given as

$$\mathcal{A}_{\mathcal{M},\text{R-II}} = \mathbb{P}\left[{P_r}^M > {P_r}^S, \text{R-II}\right], \tag{A.1}$$

where ${P_r}^M$ and ${P_r}^S$ are received powers from the closest macro and small tier BSs respectively. Similar to R-I, the received powers at T-UE using DS-PLM from nearest both tier BSs in R-II are ${P_r}^M = P_M \eta_M L_0 x_M^{-\alpha_{1M}}$ and ${P_r}^S = P_S B_S L_0 x_S^{-\alpha_{0S}}$ respectively. Inserting them in (A.1) to get

$$\mathcal{A}_{\mathcal{M},\text{R-II}} = \mathbb{P}\left[P_M B_M \eta_M L_0 x_M^{-\alpha_{1M}} > P_S B_S L_0 x_S^{-\alpha_{0S}},\ \text{R-II}\right], \tag{A.2}$$

rearranging the terms in (A.2) gives

$$\mathcal{A}_{\mathcal{M},\text{R-II}} = \mathbb{P}\left[x_S\ >\ \left(\frac{P_S B_S}{P_M \eta_M}\right)^{\frac{1}{\alpha_{0S}}} x_M^{\frac{\alpha_{1M}}{\alpha_{0S}}},\ \text{R-II}\right]. \tag{A.3}$$

From Table 3.1, we already know the constraints on X_M and X_S in region R-II. Now by conditioning on X_M, (A.3) takes the integral form

$$\mathcal{A}_{\mathcal{M},\text{R-II}} = \int_{R_{CM}}^{\infty} \mathbb{P}\left[(x_S > \gamma \ \cap \ x_S < R_{CS}), \text{R-II} | x_M\right] f_{X_M}(x_M) \, \mathrm{d}x_M, \tag{A.4}$$

where $\gamma = (P_S B_S / P_M \eta_M)^{1/\alpha_{0S}} \, x_M^{\alpha_{1M}} / \alpha_{0S}$ and $f_{X_M}(x_M)$ is already given in (3.3). The integration limits in (A.4) are from R_{CM} to ∞, as X_M is constrained over the same range as well. Now, simplifying (A.4) by using (3.2) gives the desired expression for association probability of T-UE with macro tier in R-II and completes the proof of (3.12).

A.2 Proof of Macro T-AP in R-III

The probabilistic event defining joint association probability of T-UE with macro tier in R-III is given as

$$\mathcal{A}_{\mathcal{M},\text{R-III}} = \mathbb{P}\left[{P_r}^M > {P_r}^S, \text{R-III}\right], \tag{A.5}$$

where ${P_r}^M$ and ${P_r}^S$ are received powers from the closest macro and small tier BSs respectively. Similar to R-I and R-II, the received powers at T-UE using DS-PLM from nearest both tier BSs in R-III are ${P_r}^M = P_M L_0 x_M^{-\alpha_{0M}}$ and ${P_r}^S = P_S B_S \eta_S L_0 x_S^{-\alpha_{1S}}$ respectively. Inserting them in (A.5) to get

$$\mathcal{A}_{\mathcal{M},\text{R-III}} = \mathbb{P}\left[P_M B_M L_0 x_M^{-\alpha_{0M}} > P_S B_S \eta_S L_0 x_S^{-\alpha_{1S}}, \ \text{R-III}\right], \tag{A.6}$$

rearranging the terms in (A.6) gives

$$\mathcal{A}_{\mathcal{M},\text{R-III}} = \mathbb{P}\left[x_S \ > \ \left(\frac{P_S B_S \eta_S}{P_M}\right)^{\frac{1}{\alpha_{1S}}} x_M^{\frac{\alpha_{0M}}{\alpha_{1S}}}, \ \text{R-III}\right]. \tag{A.7}$$

From Table 3.1, the constraints on X_M and X_S in region R-III are already known. Now by conditioning on X_M, (A.7) takes the integral form

$$\mathcal{A}_{\mathcal{M},\text{R-III}} = \int_0^{R_{CM}} \mathbb{P}\left[(x_S > \kappa \ \cap \ x_S > R_{CS}), \text{R-III} | x_M\right] f_{X_M}(x_M) \ \mathrm{d}x_M, \tag{A.8}$$

where $f_{X_M}(x_M)$ is already given in (3.3). The integration limits in (A.8) are from 0 to R_{CM}, as X_M is constrained over the same range as well. Now, simplifying (A.8) by using (3.2) gives the desired expression for association probability of T-UE with macro tier in R-III and completes the proof of (3.14).

A.3 Proof of Macro T-AP in R-IV

Similar to the proofs of macro tier association in R-I,R-II and R-III, we once again define a probabilistic event for defining joint association probability of T-UE with macro tier in R-IV as

$$\mathcal{A}_{\mathcal{M},\text{R-IV}} = \mathbb{P}\left[{P_r}^M > {P_r}^S, \text{R-IV}\right], \tag{A.9}$$

where ${P_r}^M$ and ${P_r}^S$ are received powers from the closest macro and small tier BSs respectively. The received powers at T-UE using DS-PLM from nearest both tier BSs in R-IV are ${P_r}^S = P_M L_0 x_M^{-\alpha_{0M}}$ and ${P_r}^S = P_S B_S L_0 x_S^{-\alpha_{0S}}$ respectively. Inserting them in (A.9) to get

$$\mathcal{A}_{\mathcal{M},\text{R-IV}} = \mathbb{P}\left[P_M L_0 x_M^{-\alpha_{0M}} > P_S B_S L_0 x_S^{-\alpha_{0S}}, \ \text{R-IV}\right], \tag{A.10}$$

rearranging the terms in (A.10) gives

$$\mathcal{A}_{\mathcal{M},\text{R-IV}} = \mathbb{P}\left[x_S \ > \ \left(\frac{P_S B_S}{P_M}\right)^{\frac{1}{\alpha_{0S}}} x_M^{\frac{\alpha_{0M}}{\alpha_{0S}}}, \ \text{R-IV}\right]. \tag{A.11}$$

From Table 3.1, we already know the constraints on X_M and X_S in region R-IV. Now by conditioning on X_M, (A.11) takes the integral form

$$\mathcal{A}_{\mathcal{M},\text{R-IV}} = \int_0^{R_{CM}} \mathbb{P}\left[\left(x_S > \left(\frac{P_S B_S}{P_M}\right)^{\frac{1}{\alpha_{0S}}} x_M^{\frac{\alpha_{0M}}{\alpha_{0S}}} \cap\ x_S < R_{CS}\right), \text{R-IV} | X_M\right] f_{X_M}(x_M)\ \mathrm{d}x_M, \tag{A.12}$$

where $f_{X_M}(x_M)$ is already given in (3.3). The integration limits in (A.12) are from 0 to R_{CM}, as X_M is constrained over the same range as well. Now, simplifying (A.12) by using (3.2) gives the desired expression for association probability of T-UE with macro tier in R-IV and completes the proof of (3.16).

A.4 Proof of the Distance PDF between T-UE and Nearest MBS when Distance is Smaller than R_{CM}

For a macro tier associated T-UE which is located at a distance smaller than R_{CM}, the likelihood of event $X_M > x_M$ is given as

$$\mathbb{P}\left[X_M > x_M\right] = \mathbb{P}\left[X_M > x_M | \left(\mathcal{A}_{\mathcal{M}}, X_M < R_{CM}\right)\right]. \tag{A.13}$$

By converting the right hand side (R.H.S) of (A.13) into joint probability, we get

$$\mathbb{P}\left[X_M > x_M\right] = \frac{\mathbb{P}\left[X_M > x_M, {P_r}^M > {P_r}^S, X_M < R_{CM}\right]}{\mathbb{P}\left[{P_r}^M > {P_r}^S, X_M < R_{CM}\right]}. \tag{A.14}$$

In (A.14), the sub-event $\left[{P_r}^M > {P_r}^S, X_M < R_{CM}\right]$ can be expanded based on the knowledge of association probability regions i.e., R-III and R-IV to get

$$\begin{aligned}\left[{P_r}^M > {P_r}^S, X_M < R_{CM}\right] = &\left[{P_r}^M > {P_r}^S, X_M < R_{CM}, X_S > R_{CS}\right] \\ &\cup \left[{P_r}^M > {P_r}^S, X_M < R_{CM}, X_S < R_{CS}\right]. \end{aligned} \tag{A.15}$$

The R.H.S of (A.15) refers to two disjoint events. By using (A.5) and (A.9), (A.15) can be rewritten as

$$\left[{P_r}^M > {P_r}^S, X_M < R_{CM}\right] = \mathcal{A}_{\mathcal{M},\text{R-III}} + \mathcal{A}_{\mathcal{M},\text{R-IV}}. \tag{A.16}$$

Now by inserting (A.16) into (A.14) and simplifying to get

$$\mathbb{P}\left[X_M > x_M\right] = \left(\frac{\begin{cases} \mathbb{P}\left[X_M > x_M, (X_S > \kappa, X_M < R_{CM})\right] & X_S \geq R_{CS} \\ \mathbb{P}\left[X_M > x_M, (X_S > g_A, X_M < R_{CM})\right] & X_S < R_{CS} \end{cases}}{\mathcal{A}_{\mathcal{M},\text{R-III}} + \mathcal{A}_{\mathcal{M},\text{R-IV}}} \right), \tag{A.17}$$

using PDF of X_M, (A.17) can be expressed as

$$\mathbb{P}\left[X_M > x_M\right] = \begin{cases} \dfrac{\int_{x_M}^{R_{CM}} \mathbb{P}\left[(X_S > \kappa, X_S \geq R_{CS})\right] f_{X_M}(x_M)\, \mathrm{d}x_M}{\mathcal{A}_{\mathcal{M},\text{R-III}} + \mathcal{A}_{\mathcal{M},\text{R-IV}}} & \kappa \geq R_{CS} \\ \dfrac{\int_{x_M}^{R_{CM}} \mathbb{P}\left[(X_S > g_A, X_S < R_{CS})\right] f_{X_M}(x_M)\, \mathrm{d}x_M}{\mathcal{A}_{\mathcal{M},\text{R-III}} + \mathcal{A}_{\mathcal{M},\text{R-IV}}} & \kappa < R_{CS} \end{cases}. \tag{A.18}$$

The desired PDF of X_M conditioned on distance between T-UE and associated MBS smaller than R_{CM} is obtained by simplification of A.18 to complete the proof of (3.26).

A.5 Proof of the Distance PDF between T-UE and Nearest SBS when Distance is Smaller than R_{CS}

When the T-UE is associated with smaller tier and its distance from the connected SBS is shorter than R_{CS}, then the likelihood of event $X_S > x_S$ is given as

$$\mathbb{P}\left[X_S > x_S\right] = \mathbb{P}\left[X_S > x_S | \left(\mathcal{A}_{\mathcal{S}}, X_S < R_{CS}\right)\right]. \tag{A.19}$$

By converting the right hand side (R.H.S) of (A.19) into joint probability, we get

$$\mathbb{P}\left[X_S > x_S\right] = \frac{\mathbb{P}\left[X_S > x_S, {P_r}^S > {P_r}^M, X_S < R_{CS}\right]}{\mathbb{P}\left[{P_r}^S > {P_r}^M, X_S < R_{CS}\right]}. \tag{A.20}$$

In (A.20), the sub-event $\left[{P_r}^S > {P_r}^M, X_S < R_{CS}\right]$ can be expanded based on the knowledge of association probability regions i.e., R-III and R-IV to get

$$\begin{aligned}\left[{P_r}^S > {P_r}^M, X_S < R_{CS}\right] = &\left[{P_r}^S > {P_r}^M, X_S < R_{CS}, X_M > R_{CM}\right] \\ &\cup \left[{P_r}^S > {P_r}^M, X_S < R_{CS}, X_M < R_{CM}\right]. \end{aligned} \tag{A.21}$$

The R.H.S of (A.21) refers to two mutually exclusive events that cannot occur at the same time and can be rewritten as

$$\left[{P_r}^S > {P_r}^M, X_S < R_{CS}\right] = \mathcal{A}_{\mathcal{S},\text{R-II}} + \mathcal{A}_{\mathcal{S},\text{R-IV}}. \tag{A.22}$$

Now by inserting (A.22) into (A.20) to get

$$\mathbb{P}\left[X_S > x_S\right] = \begin{cases} \frac{\mathbb{P}[X_S > x_S, (X_M > k_B, X_S < R_{CS})]}{\mathcal{A}_{\mathcal{S},\text{R-II}} + \mathcal{A}_{\mathcal{S},\text{R-IV}}} & k_B \geq R_{CM} \\ \frac{\mathbb{P}[X_S > x_S, (X_M > q_A, X_S < R_{CS})]}{\mathcal{A}_{\mathcal{S},\text{R-II}} + \mathcal{A}_{\mathcal{S},\text{R-IV}}} & k_B < R_{CM} \end{cases}, \tag{A.23}$$

using PDF of X_S, (A.23) can be expressed as

$$\mathbb{P}\left[X_S > x_S\right] = \begin{cases} \dfrac{\int_{x_S}^{R_{CS}} \mathbb{P}\left[(X_M > k_B, X_M > R_{CM})\right] f_{X_S}(x_S)\, \mathrm{d}x_S}{\mathcal{A}_{\mathcal{S},\text{R-II}} + \mathcal{A}_{\mathcal{S},\text{R-IV}}} & k_B \geq R_{CM} \\ \dfrac{\int_{x_S}^{R_{CS}} \mathbb{P}\left[(X_M > q_A, X_M < R_{CM})\right] f_{X_S}(x_S)\, \mathrm{d}x_S}{\mathcal{A}_{\mathcal{S},\text{R-II}} + \mathcal{A}_{\mathcal{S},\text{R-IV}}} & k_B < R_{CM} \end{cases}. \tag{A.24}$$

By simplifying (A.24), the desired PDF of X_S conditioned on the distance between T-UE and associated SBS shorter than R_{CS} is obtained to complete the proof of (3.34).

A.6 Proof of Macro Tier Coverage in Region $X_M < R_{CM}$

The integral form of macro tier coverage in the region $X_M < R_{CM}$ is given as

$$\mathrm{C}_{P_M|X_M<R_{CM}}(x_M) = \int_0^{R_{CM}} \mathbb{P}[\Gamma_{X_{M|X_M<R_{CM}}}(x_M) > \tau]\; f_{X_M|X_M<R_{CM}}(x_M)\, \mathrm{d}x_M, \tag{A.25}$$

where $f_{X_M|X_M<R_{CM}}(x_M)$ is already determined in section 3.3.2 and is given in (3.26), while $\mathbb{P}[\Gamma_{X_{M|X_M<R_{CM}}}(x_M) > \tau]$ is yet to be derived. The limits of integration in (A.25) are from 0 to R_{CM} as the T-UE lies within the R_{CM} of its closest MBS.

After substituting suitable parametric values in (3.38), the conditioned macro tier CCDF given x_M smaller than R_{CM} can be expressed as

$$\mathbb{P}[\Gamma_{X_{M|X_M<R_{CM}}}(x_M) > \tau] = \exp\left(\frac{-\tau\sigma^2}{P_M L_0 x_M^{-\alpha_{0M}}}\right)\mathcal{L}_{\mathcal{I}_\mathcal{M}}\left(\frac{-\tau\ x_M^{\alpha_{0M}}}{P_M}\right)\mathcal{L}_{\mathcal{I}_\mathcal{S}}\left(\frac{-\tau\ x_M^{\alpha_{0M}}}{P_M}\right). \tag{A.26}$$

In region x_M smaller than R_{CM}, the T-UE can possibly receive co-tier interference from MBSs operating at frequency channel N and located at distance both greater and smaller than R_{CM}. Therefore, $\mathcal{L}_{\mathcal{I}_\mathcal{M}}$ for x_M smaller than R_{CM} contains two integrals in its expression

$$\mathcal{L}_{\mathcal{I}_\mathcal{M}}\left(\frac{-\tau\ x_M^{\alpha_{0M}}}{P_M}\right) = \exp\left(\frac{-2\pi\lambda_M}{N}\left(\int_{x_M}^{R_{CM}}\frac{y}{1+\left(x_M^{\alpha_{0M}}\tau\right)^{-1}y^{\alpha_{0M}}}\mathrm{d}y + \int_{R_{CM}}^{\infty}\frac{y}{1+\left(x_M^{\alpha_{0M}}\eta_M\tau\right)^{-1}y^{\alpha_{1M}}}\mathrm{d}y\right)\right). \tag{A.27}$$

Solving the integrations in (A.27), we get

$$\mathcal{L}_{\mathcal{I}_\mathcal{M}}\left(\frac{-\tau\ x_M^{\alpha_{0M}}}{P_M}\right) = \exp\left[\frac{-2\pi\lambda_M}{N}\left(\left(-\frac{x_M^2}{2}\ {}_2F_1\left[1,\frac{2}{\alpha_{0M}};1+\frac{2}{\alpha_{0M}};-\frac{1}{\tau}\right]\right) + \frac{R_{CM}^2}{2}\ {}_2F_1\left[1,\frac{2}{\alpha_{0M}};1+\frac{2}{\alpha_{0M}};-\left(\frac{R_{CM}}{x_M}\right)^{\alpha_{0M}}\frac{1}{\tau}\right] + \frac{\eta_M\tau x_M^{\alpha_{0M}}(R_{CM})^{2-\alpha_{1M}}}{-2+\alpha_{1M}}{}_2F_1\left[1,1-\frac{2}{\alpha_{1M}};2-\frac{2}{\alpha_{1M}};-\frac{\eta_M\tau(x_M)^{\alpha_{0M}}}{(R_{CM})^{\alpha_{1M}}}\right]\right)\right]. \tag{A.28}$$

Similarly, the inter-tier interference in region x_M smaller than R_{CM} may also come from two distance ranges. Thus, resulting in two integrals for determining of $\mathcal{L}_{\mathcal{I}_\mathcal{S}}$ as well. The limits of integration for computing interference from SBSs lying at distance smaller than R_{CS} are g_A to R_{CS}, while for interferers lying at distance farther than R_{CS} are R_{CS} to ∞.

The integral form of inter-tier interference is given as

$$\mathcal{L}_{\mathcal{I}_S}\left(\frac{-\tau\ x_M^{\alpha_{0M}}}{P_M}\right) = \exp\left(\frac{-2\pi\lambda_S}{N}\left(\int_{g_A}^{R_{CS}} \frac{y}{1+\left(x_M^{\alpha_{0M}}\frac{P_S}{P_M}\tau\right)^{-1} y^{\alpha_{0S}}}\mathrm{d}y\right)\right) + \exp\left(\frac{-2\pi\lambda_S}{N}\left(\int_{R_{CS}}^{\infty} \frac{y}{1+\left(x_M^{\alpha_{0M}}\frac{P_S\eta_S}{P_M}\tau\right)^{-1} y^{\alpha_{1S}}}\mathrm{d}y\right)\right), \quad \text{(A.29)}$$

solving integrations in (A.29) gives

$$\mathcal{L}_{\mathcal{I}_S}\left(\frac{-\tau\ x_M^{\alpha_{0M}}}{P_M}\right) = \exp\left[\frac{-2\pi\lambda_S}{N}\left(-\frac{g_A^2}{2}{}_2F_1\left[1,\frac{2}{\alpha_{0S}};1+\frac{2}{\alpha_{0S}};-\frac{B_S}{\tau}\right] + \frac{R_{CS}^2}{2}{}_2F_1\left[1,\frac{2}{\alpha_{0S}};1+\frac{2}{\alpha_{0S}};-\frac{P_M R_{CS}^{\alpha_{0S}}}{P_S x_M^{\alpha_{0M}}\tau}\right] + \frac{P_S\eta_S\tau x_M^{\alpha_{0M}} R_{CS}^{2-\alpha_{1S}}}{P_M\left(-2+\alpha_{1S}\right)}{}_2F_1\left[1,1-\frac{2}{\alpha_{1S}};2-\frac{2}{\alpha_{1S}};-\frac{P_S\eta_S x_M^{\alpha_{0M}}\tau}{P_M R_{CS}^{\alpha_{1S}}}\right]\right)\right], \quad \text{(A.30)}$$

The resultant expression for macro tier contribution in CCDF of received SINR for x_M smaller than R_{CM} is obtained by inserting (A.28) and (A.30) in (A.26) to get

$$\mathbb{P}[\Gamma_{X_{M|X_M<R_{CM}}}(x_M) > \tau] = \exp\left(\frac{-\tau\sigma^2}{P_M L_0 x_M^{-\alpha_{0M}}}\right)\exp\left[\frac{-2\pi\lambda_S}{N}\left(-\frac{g_A^2}{2} \times {}_2F_1\left[1,\frac{2}{\alpha_{0S}};1+\frac{2}{\alpha_{0S}};-\frac{B_S}{\tau}\right] + \frac{R_{CS}^2}{2}{}_2F_1\left[1,\frac{2}{\alpha_{0S}};1+\frac{2}{\alpha_{0S}};-\frac{P_M R_{CS}^{\alpha_{0S}}}{P_S x_M^{\alpha_{1M}}\tau}\right] + \frac{P_S\eta_S\tau x_M^{\alpha_{0M}} R_{CS}^{2-\alpha_{1S}}}{P_M\left(-2+\alpha_{1S}\right)}{}_2F_1\left[1,1-\frac{2}{\alpha_{1S}};2-\frac{2}{\alpha_{1S}};-\frac{P_S\eta_S x_M^{\alpha_{0M}}\tau}{P_M R_{CS}^{\alpha_{1S}}}\right]\right)\right] \times \exp\left[-\frac{2\pi\lambda_M}{N}\left(\left(-\frac{x_M^2}{2}\ {}_2F_1\left[1,\frac{2}{\alpha_{0M}};1+\frac{2}{\alpha_{0M}};-\frac{1}{\tau}\right]\right) + \frac{R_{CM}^2}{2}\ {}_2F_1\left[1,\frac{2}{\alpha_{0M}};1+\frac{2}{\alpha_{0M}};-\left(\frac{R_{CM}}{x_M}\right)^{\alpha_{0M}}\frac{1}{\tau}\right] + \frac{\eta_M\tau x_M^{\alpha_{0M}} R_{CM}^{2-\alpha_{1M}}}{-2+\alpha_{1M}}{}_2F_1\left[1,1-\frac{2}{\alpha_{1M}};2-\frac{2}{\alpha_{1M}};-\frac{\eta_M x_M^{\alpha_{0M}}\tau}{R_{CM}^{\alpha_{1M}}}\right]\right)\right]. \quad \text{(A.31)}$$

Finally by inserting (A.31) into (A.25), we get the desired expression for macro tier coverage in R_2 to complete the proof of (3.47).

Appendix B

Proofs for Chapter No. 4

B.1 Proof of T-UE Association with Macro-tier in R-III

The joint association probability of T-UE with macro tier in R-III is given by the following probabilistic event

$$\mathcal{A}_{\mathcal{M},\text{R-III}} = \mathbb{P}\left[{P_r}^{M} > {P_r}^{S}, \text{R-III}\right], \tag{B.1}$$

where ${P_r}^{M}$ and ${P_r}^{S}$ are received powers from the nearest macro and small tier BSs respectively. By using DS-PLM, the averaged received powers from the respective nearest BSs of both tiers in R-III are ${P_r}^{M} = P_M \eta_M L_0 x_M^{-\alpha_{1M}}$ and ${P_r}^{S} = P_S B_S L_0 x_S^{-\alpha_{0S}}$ respectively. Inserting them in (B.1) to get

$$\mathcal{A}_{\mathcal{M},\text{R-III}} = \mathbb{P}\left[P_M \eta_M L_0 x_M^{-\alpha_{1M}} > P_S B_S L_0 x_S^{-\alpha_{0S}},\ \text{R-III}\right], \tag{B.2}$$

rearranging the terms in (B.2) gives

$$\mathcal{A}_{\mathcal{M},\text{R-III}} = \mathbb{P}\left[x_S\ >\ \left(\frac{P_S B_S}{P_M \eta_M}\right)^{\frac{1}{\alpha_{0S}}} x_M^{\frac{\alpha_{1M}}{\alpha_{0S}}},\ \text{R-III}\right]. \tag{B.3}$$

From Table 4.1, we already know the constraints on X_M and X_S in R-III, and based on those (B.3) takes the integral form as

$$\mathcal{A}_{\mathcal{M},\text{R-III}} = \int_{R_{CM}}^{\infty} \mathbb{P}\left[(x_S > \left(\frac{P_S B_S}{P_M \eta_M}\right)^{\frac{1}{\alpha_{0S}}} x_M^{\frac{\alpha_{1M}}{\alpha_{0S}}} \cap\ x_S > R_{CS}), \text{R-III}\right] f_{X_M}(x_M)\, \mathrm{d}x_M, \tag{B.4}$$

where $f_{X_M}(x_M)$ is already given in (4.4). The integration limits in (B.4) are from R_{CM} to ∞, as X_M is constrained over the same range as well. Now, simplifying (B.4) by using (4.3) gives the desired expression for association probability of T-UE with macro tier in R-III and completes the proof of (4.13).

B.2 Proof of the Macro Tier Coverage when the Distance between T-UE and its Associated MBS is Smaller than R_{CM}

The integral form of the macro tier coverage in region R-I is given as

$$\mathrm{C}_{P_M|X_M<R_{CM}}(x_M) = \int_{0}^{R_{CM}} \mathbb{P}[\Gamma_{X_{M|X_M<R_{CM}}}(x_M) > \tau]\, f_{X_M|X_M<R_{CM}}(x_M)\, \mathrm{d}x_M, \tag{B.5}$$

where $f_{X_M|X_M<R_{CM}}(x_M)$ is already determined in section 4.3.2 and is given in (4.20), while $\mathbb{P}[\Gamma_{X_{M|X_M<R_{CM}}}(x_M) > \tau]$ is yet to be derived. The limits of integration in (B.5) are from 0 to R_{CM} as the T-UE lies at distances smaller than R_{CM} of its closest MBS.

The conditioned macro tier CCDF given x_M smaller than R_{CM} can be expressed with the help of (4.25) as

$$\mathbb{P}[\Gamma_{X_{M|X_M<R_{CM}}}(x_M) > \tau] = \exp\left(\frac{-\tau\sigma^2}{P_M L_0 x_M^{-\alpha_{0M}}}\right) \mathcal{L}_{\mathcal{I}_\mathcal{M}}\left(\frac{-\tau\ x_M^{\alpha_{0M}}}{P_M}\right) \mathcal{L}_{\mathcal{I}_\mathcal{S}}\left(\frac{-\tau\ x_M^{\alpha_{0M}}}{P_M}\right). \tag{B.6}$$

In region x_M smaller than R_{CM}, the T-UE can possibly receive co-tier interference from MBSs operating at frequency channel N and located at distances both greater and smaller than R_{CM}. Therefore, $\mathcal{L}_{\mathcal{I}_\mathcal{M}}$ for x_M smaller than R_{CM} contains two integrals in its expression

$$\mathcal{L}_{\mathcal{I}_\mathcal{M}}\left(\frac{-\tau\ x_M^{\alpha_{0M}}}{P_M}\right) = \exp\left(\frac{-2\pi\lambda_M}{N}\left(\int_{x_M}^{R_{CM}} \frac{y}{1+\left(x_M^{\alpha_{0M}}\tau\right)^{-1} y^{\alpha_{0M}}}\mathrm{d}y + \int_{R_{CM}}^{\infty} \frac{y}{1+\left(x_M^{\alpha_{0M}}\eta_M\tau\right)^{-1} y^{\alpha_{1M}}}\mathrm{d}y\right)\right). \quad \text{(B.7)}$$

Solving the integration in (B.7), we get

$$\mathcal{L}_{\mathcal{I}_\mathcal{M}}\left(\frac{-\tau\ x_M^{\alpha_{0M}}}{P_M}\right) = \exp\left[\frac{-2\pi\lambda_M}{N}\left(\left(-\frac{x_M^2}{2}\ {}_2F_1\left[1,\frac{2}{\alpha_{0M}};1+\frac{2}{\alpha_{0M}};-\frac{1}{\tau}\right]\right) + \frac{R_{CM}^2}{2}\ {}_2F_1\left[1,\frac{2}{\alpha_{0M}};1+\frac{2}{\alpha_{0M}};-\left(\frac{R_{CM}}{x_M}\right)^{\alpha_{0M}}\frac{1}{\tau}\right] + \frac{\eta_M\tau x_M^{\alpha_{0M}}(R_{CM})^{2-\alpha_{1M}}}{-2+\alpha_{1M}}{}_2F_1\left[1,1-\frac{2}{\alpha_{1M}};2-\frac{2}{\alpha_{1M}};-\frac{\eta_M\tau(x_M)^{\alpha_{0M}}}{(R_{CM})^{\alpha_{1M}}}\right]\right)\right]. \quad \text{(B.8)}$$

The integration limits for determining the inter-tier interference in region x_M smaller than R_{CM} is a little tricky. This is because, we need to ensure that the T-UE associates with MBS when it lies inside the R_{CM} of its closest MBS. Moreover, given $x_M < R_{CM}$, there is a very little likelihood that the T-UE may still receive better signal strength from SBSs residing near the R_{CM} boundary of MBS. Therefore, to avoid such a scenario, we take small tier interference with reference to x_M, i.e., $x_M \leq (R_{CM} - R_{CS})$ or $x_M > (R_{CM} - R_{CS})$.

The integral form of inter-tier interference is given as

$$\mathcal{L}_{\mathcal{I}_S}\left(\frac{-\tau\ x_M^{\alpha_{0M}}}{P_M}\right) = \exp\left(\frac{-2\pi\lambda_S}{N}\right.$$
$$\left.\times\begin{cases}\left(\int\limits_{(R_{CM}-x_M)}^{\infty}\frac{y}{1+\left(x_M^{\alpha_{0M}}\frac{P_S\eta_S}{P_M}\tau\right)^{-1}y^{\alpha_{1S}}}\mathrm{d}y\right) & x_M \leq\ R_{CM}-R_{CS}\\ \left(\int\limits_{(R_{CM}+R_{CS}-x_M)}^{\infty}\frac{y}{1+\left(x_M^{\alpha_{0M}}\frac{P_S\eta_S}{P_M}\tau\right)^{-1}y^{\alpha_{1S}}}\mathrm{d}y\right) & x_M >\ R_{CM}-R_{CS}\end{cases}\right). \tag{B.9}$$

Simplifying (B.9) by using appropriate substitution to get

$$\mathcal{L}_{\mathcal{I}_S}\left(\frac{-x_M^{\alpha_{0M}}\tau}{P_M}\right) = \exp\left(\frac{-2\pi\lambda_S}{N(-2+\alpha_{1S})}\right.$$
$$\left.\times\begin{cases}\left(-\frac{P_S\tau\eta_S x_M^{\alpha_0 M}(R_{CM}-x_M)^{-2+\alpha_{1S}}}{P_M}\right. & \\ \left.\times\ {}_2F_1\left[1,1-\frac{2}{\alpha_{1S}};2-\frac{2}{\alpha_{1S}};-\frac{P_S\eta_S x_M^{\alpha_{0M}}\tau}{P_M(R_{CM}-x_M)^{\alpha_{1S}}}\right]\right) & x_M \leq\ R_{CM}-R_{CS}\\ \left(-\frac{P_S\tau\eta_S x_M^{\alpha_0 M}(R_{CM}+R_{CS}-x_M)^{-2+\alpha_{1S}}}{P_M}\right. & \\ \left.\times\ {}_2F_1\left[1,1-\frac{2}{\alpha_{1S}};2-\frac{2}{\alpha_{1S}};-\frac{P_S\eta_S x_M^{\alpha_{0M}}\tau}{P_M(R_{CM}+R_{CS}-x_M)^{\alpha_{1S}}}\right]\right) & x_M >\ R_{CM}-R_{CS}\end{cases}\right). \tag{B.10}$$

The resultant expression for macro tier contribution in CCDF of received SINR for x_M smaller than R_{CM} is obtained by inserting (B.8) and (B.10) in (B.6) to get

$$\mathbb{P}[\Gamma_{X_{M|X_M<R_{CM}}}(x_M) > \tau] = \exp\left(\frac{-\tau\sigma^2}{P_M L_0 x_M^{-\alpha_{0M}}}\right)\exp\left(\frac{-2\pi\lambda_S}{N(-2+\alpha_{1S})}\right.$$

$$\times \begin{cases} \left(-\frac{P_S \tau \eta_S x_M^{\alpha_{0M}} (R_{CM}-x_M)^{-2+\alpha_{1S}}}{P_M} \right. \\ \left. \times \, {}_2F_1\left[1, 1-\frac{2}{\alpha_{1S}}; 2-\frac{2}{\alpha_{1S}}; -\frac{P_S \eta_S x_M^{\alpha_{0M}} \tau}{P_M (R_{CM}-x_M)^{\alpha_{1S}}}\right] \right) & x_M \leq R_{CM} - R_{CS} \\ \left(-\frac{P_S \tau \eta_S x_M^{\alpha_{0M}} (R_{CM}+R_{CS}-x_M)^{-2+\alpha_{1S}}}{P_M} \right. \\ \left. \times \, {}_2F_1\left[1, 1-\frac{2}{\alpha_{1S}}; 2-\frac{2}{\alpha_{1S}}; -\frac{P_S \eta_S x_M^{\alpha_{0M}} \tau}{P_M (R_{CM}+R_{CS}-x_M)^{\alpha_{1S}}}\right] \right) & x_M > R_{CM} - R_{CS} \end{cases}$$

$$\times \exp\left[\frac{-2\pi\lambda_M}{N}\left(\left(-\frac{x_M^2}{2}\, {}_2F_1\left[1, \frac{2}{\alpha_{0M}}; 1+\frac{2}{\alpha_{0M}}; -\frac{1}{\tau}\right]\right)\right.\right.$$

$$+ \frac{R_{CM}^2}{2}\, {}_2F_1\left[1, \frac{2}{\alpha_{0M}}; 1+\frac{2}{\alpha_{0M}}; -\left(\frac{R_{CM}}{x_M}\right)^{\alpha_{0M}} \frac{1}{\tau}\right]$$

$$\left.\left. + \frac{\eta_M \tau x_M^{\alpha_{0M}} (R_{CM})^{2-\alpha_{1M}}}{-2+\alpha_{1M}} {}_2F_1\left[1, 1-\frac{2}{\alpha_{1M}}; 2-\frac{2}{\alpha_{1M}}; -\frac{\eta_M \tau (x_M)^{\alpha_{0M}}}{(R_{CM})^{\alpha_{1M}}}\right]\right)\right]. \quad \text{(B.11)}$$

Lastly by inserting (B.11) into (B.5), we get the desired expression for macro tier coverage in R-I to complete the proof of (4.33).